DOT/FAA/AR-xx/xx

Air Traffic Organization
Operations Planning
Office of Aviation Research
Washington, D.C. 20591

PILOTED SIMULATION STUDY TO DEVELOP TRANSPORT AIRCRAFT RUDDER CONTROL SYSTEM REQUIREMENTS

Phase 2 – Develop Criteria for Rudder Overcontrol

DRAFT

Date July 7, 2009

Final Report

U.S. Department of Transportation
Federal Aviation Administration

NOTICE

This document is disseminated under the sponsorship of the U.S. Department of Transportation in the interest of information exchange. The United States Government assumes no liability for the contents or use thereof. The United States Government does not endorse products or manufacturers. Trade or manufacturer's names appear herein solely because they are considered essential to the objective of this report. This document does not constitute FAA certification policy. Consult your local FAA aircraft certification office as to its use.

This report is available at the Federal Aviation Administration William J. Hughes Technical Center's Full-Text Technical Reports page: actlibrary.act.faa.gov in Adobe Acrobat portable document format (PDF).

Technical Report Documentation Page

1. Report No. DOT/FAA/(AR or CT)-xx/xx	2. Government Accession No.	3. Recipient's Catalog No.
4. Title and Subtitle PILOTED SIMULATION STUDY TO DEVELOP TRANSPORT AIRCRAFT RUDDER CONTROL SYSTEM REQUIREMENTS - Phase 2 - Develop Criteria for Rudder Overcontrol **DRAFT**		5. Report Date (month and year printed) 6. Performing Organization Code
7. Author(s) Roger H. Hoh, Thomas K Nicoll, Paul Desrochers		8. Performing Organization Report No.
9. Performing Organization Name and Address Hoh Aeronautics, Inc 2075 Palos Verdes Dr. North Suite 217 Lomita, CA 90717		10. Work Unit No. (TRAIS) 11. Contract or Grant No.
12. Sponsoring Agency Name and Address		13. Type of Report and Period Covered 14. Sponsoring Agency Code
15. Supplementary Notes .		

16. Abstract

This report presents the results of Phase 2 of a three phase study to identify criteria to minimize the potential for rudder overcontrol leading to structural failure of the vertical stabilizer in transport aircraft in up-and-away flight.

Rudder sizing and travel are typically defined by requirements for minimum controllable airspeeds following an engine failure (V_{MC}), and crosswind limits for takeoff and landing. The rudder authority that results from these requirements can impose excessive loads on the vertical stabilizer at high airspeeds. Therefore, rudder travel is limited as airspeed increases. The method used to limit rudder travel, can have an impact on the tendency to overcontrol, and varies significantly among and within manufacturers. The objective of this program is to develop data to allow the FAA to develop criteria for rudder flight control systems that ensure safe handling qualities by minimizing the tendency for overcontrol.

A piloted simulation was conducted on the NASA Ames Vertical Motion Simulator. The results of that simulation showed that the primary factor leading to a tendency for rudder overcontrol was short pedal-throw. All other factors were found to be of less significance. Specifically, it was found that increasing the pedal force did not compensate for short pedal-throw, and nonlinearity in the load-feel curve such as would result from high breakout and low maximum pedal force was not found to be a significant factor for overcontrol.

Rudder overcontrol results in very high vertical stabilizer loads only if accompanied by a large sideslip angle. This piloted simulation showed that there is a tendency to achieve slightly higher sideslip angles for configurations with short pedal-throw, but that other factors must be in play to accomplish the magnitude of sideslip that could cause failure of the vertical stabilizer. Preliminary analysis suggests that these factors consist of complete loss of yaw damper functionality when saturated and high rudder control power in combination with low effective dihedral.

The Phase 3 portion of this study will be focused on quantifying these factors to complete the development of criteria to prevent overcontrol and consequent overstressing of the vertical stabilizer.

17. Key Words	18. Distribution Statement
	This document is available to the U.S. public through the National Technical Information Service Springfield, VA 22161.

19. Security Classif. (of this report)	20. Security Classif. (of this page)	21. No. of Pages	22. Price
Unclassified	Unclassified		

Form DOT F 1700.7 (8-72) Reproduction of completed page authorized

TABLE OF CONTENTS

LIST OF FIGURES

LIST OF TABLES

SYMBOLS

A_i	Sum of sine wave amplitude component (ft/s)
$a_{y\,cab}$	Measured lateral simulator cab acceleration (ft/s^2 or gs)
$a_{y\,EOM}$	Lateral acceleration of the pilots station as calculated in the vehicle equations of motion (ft/s^2 or gs)
$ay_{c.g.}$	lateral acceleration of vehicle at center of gravity (ft/s^2 or gs)
$C_{Y-\beta}$	Non-dimensional Change in vehicle side force due to change in sideslip (deg^{-1})
$C_{Y-\delta r}$	Non-dimensional Change in vehicle side force due rudder deflection (deg^{-1})
$F_{3\sigma\,peak}$	Largest expected vertical stabilizer force from simulation trials (lbs)
F_{bo}	Force of pilot input measured at the pedal due to pedal breakout (lbs)
F_{bofs}	Force of pilot input measured at the pedal due to the breakout feel spring (lbs)
F_{cf}	Force of pilot input measured at the pedal due to Coloumb friction (lbs)
F_{hb}	Force of pilot input measured at the pedal while returning the pedal to zero displacement (lbs)
F_{lim}	Force of pilot input measured at the pedal at maximum pedal displacement (lbs)
F_{ped}	Force of pilot input measured at the pedal (lbs)
F_v	Force on the vertical stabilizer (lbs)
$F_{\beta\text{-}max}$	Maximum force imparted on the vertical stabilizer in accordance with CFR 14 part 25.351(d) (lbs)
G_{yf}	Vertical Motion Simulation lateral cab motion gain (g/g)
H_{M-r}	Rudder hinge moment (ft-lb)
K_{bofs}	Breakout feel spring constant (lb/in)
K_{ped}	Rudder to pedal deflection gearing (deg/in)
K_{SF}	Sum of sine wave gust gain (na)
LI	Linearity Index (na)
L_β	Change in vehicle rolling moment due to sideslip (ft-lbs/deg)
N_i	Sum of sine wave number of cycles (cycles)
p	Body axis roll rate (deg/s)
p_{gust}	Sum of sine wave rolling gust (ft/s)
PCU	Power control unit – drives rudder actuator
ROP	Rudder overcontrol parameter (na)
r	Body axis yaw rate (deg/s)
r_{stab}	Stability axis yaw rate (deg/s)
S	Wing planform area (ft^2)

T_S	Sum of sine wave scoring time (sec)
V_{CAS}	Calibrated vehicle airspeed (ft/s or kts)
V_{MC}	Minimum Controllable Airspeed (ft/s or kts)
V_T	True vehicle airspeed (ft/s or kts)
X_C	Sum of sine wave gust (ft/s)
YD A	Yaw damper implementation A (na)
YD B	Yaw damper implementation B (na)
YD_{LIM}	Yaw damper authority (deg)
Y_β	Change in vehicle side force due to change in sideslip (lbs/deg)
$Y_{\delta r}$	Change in vehicle side force due to rudder deflection (lbs/deg)
α	Angle of attack (deg)
β	Vehicle sideslip (deg)
$\beta_{ss\text{-}max}$	Static equilibrium sideslip angle in accordance with CFR 14 part 25.351(d) (deg)
ΔF_{EF}	Relative difference between simulation results for statistical maximum vertical
$\delta_{p\text{-}lim}$	Maximum pedal travel measured from detent to pedal stop (in)
δ_{ped}	Pedal deflection (in)
$\delta_{r\text{-}YD}$	Rudder deflection commanded by the yaw damper (deg)
ρ_0	Reference free-stream air density (slug/ft^3)
φ_o	Sum of sine wave phase component (rad or deg)
ω_i	Sum of sine wave frequency component (rad/s or deg/s)

1 INTRODUCTION

This report describes the results of the second phase of piloted simulator evaluations to develop rudder flight control system requirements for up-and-away flight.

Rudder sizing and travel are typically defined by requirements for minimum controllable airspeeds following an engine failure (V_{MC}), and crosswind limits for takeoff and landing. The rudder authority that results from these requirements can impose excessive loads on the vertical stabilizer at high airspeeds. Therefore, rudder travel is limited as airspeed increases. The method used to limit rudder travel, can have an impact on handling qualities and tendency to overcontrol, and varies significantly among and within manufacturers. The objective of this program is to develop data to allow the FAA to develop criteria for rudder flight control systems that ensure safe handling qualities by minimizing the tendency for overcontrol.

Three phases of testing have been developed to accomplish the program objective as follows.

Phase 1 Determine the required lateral motion of the simulator necessary to obtain valid pilot opinion for aggressive rudder control, and obtain initial results for Variable-Gearing, Variable Stop, and Force Limit rudder control system designs. Piloting tasks for this phase of testing are designed to guarantee aggressive use of rudder.

Phase 2 Using a simulator that meets the requirements defined in Phase 1, conduct detailed experiments to determine criteria for transport aircraft rudder control systems. Piloting tasks for this phase are designed to guarantee aggressive use of rudder. Analyze the results to formulate tentative criteria for rudder flight control systems in transport aircraft.

Phase 3 Validate the Phase 2 results using more realistic piloting tasks where rudder use is based on pilot judgment and technique. Results used to validate, and if necessary refine the criteria developed in Phase 2.

The Phase 1 final report is given in reference 1 and recommends the use of the NASA Ames Vertical Motion Simulator (VMS) to take advantage of the large lateral cab travel. On that basis, this Phase 2 study was accomplished on the VMS. The Phase 2 Test Plan is given in Reference 2.

The ultimate goal of this work is to develop criteria for rudder control system design that minimize the likelihood that a pilot would overcontrol in the directional axis. There have been a number of accidents/incidents where pilots misused the rudder control, most notably an Airbus A300-600 accident where the vertical stabilizer failed as a result of excessive rudder inputs in a wake vortex encounter (reference 3).

No attempt is made at optimizing rudder flight control system design as it is felt that manufacturers have a good understanding of what is required for good directional handling qualities for takeoff and landing (e.g. reference 4). Given that the rudder control on transport aircraft is used almost exclusively for takeoff and landing tasks, the rudder

control system parameters are optimized for that flight regime. In most cases the rudder size and deflection is based on providing sufficient control power to handle engine-out conditions as well as setting limits on crosswinds for landing.

At the low airspeeds used for takeoff and landing, there is no danger of overstressing the vertical stabilizer with excessive rudder use, and full deflection is provided to achieve the necessary control power. At higher airspeeds, this control power is no longer required, and rudder travel is limited to reduce the possibility of overstressing the vertical stabilizer. Based on the Phase 1 results, there is evidence that the method used to limit rudder travel can have an impact on the tendency to overcontrol. The present research is aimed at providing the data to allow the development of criteria for methods to limit rudder travel at high airspeeds.

A detailed analysis of the different types of rudder control system designs that reduce rudder travel with increasing airspeed is given in Appendix A.

2 DESCRIPTION OF EXPERIMENT

2.1 SIMULATION MATH MODEL

The simulated aircraft consisted of a generic transport model that existed at the NASA Ames Research Center simulation facility. That model was used in the Phase 1 testing and was previously used in research studies involving transport aircraft in the past, and was well accepted by the subject pilots as a realistic simulation. Several pilots with transport aircraft experience flew the model during checkout for the present study, and all agreed that it was representative of a medium sized twin engine transport aircraft at the test flight condition. The test flight condition consisted of cruise flight at 250 KIAS at 2000 ft altitude. This flight condition was similar to what existed in an Airbus A-300-600 accident wherein the vertical stabilizer failed. The NTSB accident report of that accident (Reference 3) indicated that pilot overcontrol of the rudder was a primary cause of the accident.

All aspects of the simulator math model were held constant during the experiment except for the rudder flight control system. As described in detail in Appendix A, the rudder flight control system was systematically varied, while the available rudder control power was constrained to be constant, to the extent that was possible with differing control systems.

The simulation math model used for the Phase 2 testing was identical to that used in Phase 1 except for some minor variations that are described in Appendix A.

2.2 SIMULATOR MOTION SYSTEM

The piloted simulation was accomplished on the NASA Ames Research Center Vertical Motion Simulator (VMS). This facility was used based on the results of the Phase 1 study (reference 1) that showed better correlation with pilot opinion with increased lateral motion. The VMS is a six degree of freedom motion base simulator with a lateral travel of 40 ft. For this simulation, the cab initial condition was close to the center of the lateral travel thereby providing ± 20 ft of travel during the runs. Vertical travel was ± 30 ft. and longitudinal travel was ± 4 ft.

Considerable effort was expended to maximize the travel of the lateral motion system without hitting motion stops. This was done in recognition of the fact that lateral motion cues are an important element of this study. Frequency response plots of the response of the lateral acceleration of the simulator cab to the lateral acceleration from the equations of motion ($a_{y\,cab} / a_{y\,EOM}$) are given in Appendix B. It was necessary to reduce the lateral motion gain slightly after a short period of testing because the cab was hitting lateral software stops. This was done when one pilot noted that his concern for hitting a stop was affecting his control technique.

A short exercise was accomplished at the end of the simulation trials to investigate the use of a higher motion gains and those results are discussed in Section 6.

2.3 SIMULATION ENVIORNMENT

Standard transport cockpit flight controls were provided in the simulator cab, consisting of a transport style yoke with maximum travel of ± 90 deg and rudder pedals with a maximum travel of ± 3.5 inches. Throttles were consistent with a twin–engine transport aircraft.

The primary flight display (PFD) that was provided in the simulated generic transport cockpit is shown in Figure **1**. This display was also provided to the experimenters in the control room.

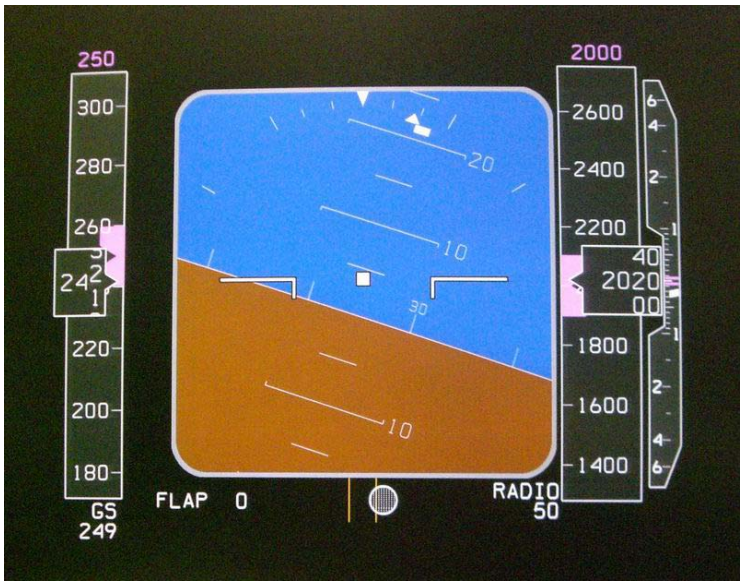

Figure **1** PFD Used in Rudder Simulation

Sideslip was displayed in the usual way with the “doghouse” symbol at the top of the display. It was also displayed with the more compelling sideslip ball at the bottom of the display. One ball deflection was scaled to 0.10 lateral g’s, which is the conventional scaling for this type of display. The top indicator was scaled so that 0.10 lateral g corresponded to a rectangle edge being aligned with one of the lower corners of the triangle. The displayed lateral accelerations were referenced to a point slightly aft of the

cockpit and 58 ft in front of the center of gravity (i.e., location of the inertial reference system in the EE bay). The acceleration displays were lagged by a first order filter with a 0.5 second time constant.

The magenta airspeed and altitude bugs were tailored so that the edge of desired performance existed when one edge of the square bug was aligned with the opposite edge of the white box surrounding the digital airspeed or altitude display. This made it easy for pilots to determine if they were within the specified desired airspeed and altitude performance during the task. Desired performance was specified as maintain airspeed at 250 kts $\pm$ 10 kts, and altitude at 2000 ft $\pm$ 100 ft.

The outside visual scene consisted of an airport and buildings as shown in Figure **2**.

Figure **2** Outside Visual Scene

It was found that having the aircraft lined up with a runway was useful for holding heading during the large rolling gust inputs. However, there was no task that related to use of the runway for landing, and runway alignment was not part of the task.

The display in Figure **2** was available to the experimenters along with several other displays that provided excellent situational awareness in the control room.

The display of cockpit controls shown in Figure **3** provided the experimenters with online information regarding the evaluation pilot's control activity during the tasks. Telltale pointers were incorporated to display the maximum rudder deflections during the run.

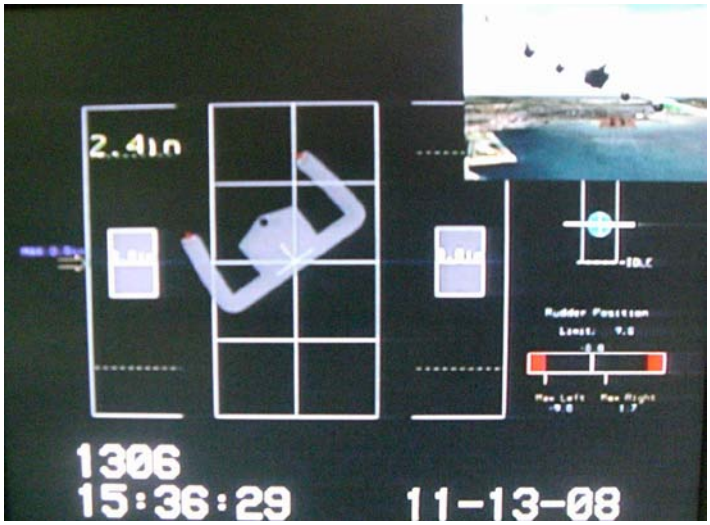

Figure **3** VMS Experimenter Displays for Rudder Study

2.4 PILOTING TASK

Current training protocol for transport aircraft training is to use rudders for crosswind landings and engine-out on takeoff and landing, and to not use rudder up-and-away. One exception is that pilots are allowed to use rudder up-and-away to assist in controlling the aircraft if out of aileron control power following a gust or wake vortex upset.

This training has been strongly reinforced following the A300-600 vertical stabilizer failure on AA flight 587. Nonetheless, some pilots are more prone to using rudders aggressively than others. In this study, we have taken the position that in the unlikely event the rudder is used in an aggressive manner while in up-and-away flight, it should result in predictable aircraft response with no tendency for overcontrol.

A lateral disturbance profile was developed that required the pilot to use rudder to augment aileron in order to keep the wings near level and the aircraft on a constant heading $\pm 10^{o}$. The disturbance consisted of a random appearing sum of sine waves that had the appearance of rolling gusts such as might occur in a wake vortex upset. The magnitude of the inputs was set to momentarily exceed the lateral control power during the peaks of the disturbance. This was done to require the subject pilots to use rudder to compensate for the lack of aileron control power. One subject pilot attempted to fly the task with aileron alone in accordance with currently accepted pilot technique, and noted that this was not possible. He noted that his technique was to avoid use of rudder until absolutely necessary. Most pilots noted that the disturbance input had the appearance of rolling gusts such as might occur in a wake vortex upset, except that it lasted longer than a typical wake vortex encounter (approximately one minute).

The task is illustrated by the diagram in Figure **4**

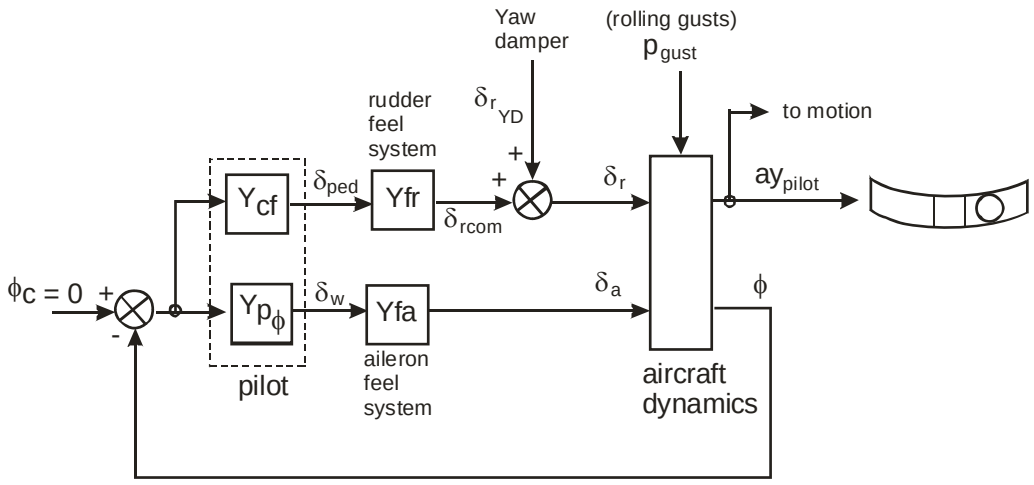

Figure **4** Pilot-in-the-Loop Representation of Roll Task

There was no attempt to simulate an actual wake vortex encounter with the roll tracking task. However, all pilots agreed that the task was a realistic simulation of a wake vortex upset. The pilots were briefed that this was not a roll control study, and that the focus was on rudder control. They were asked to focus on the use of rudder to augment roll control when assigning subjective pilot ratings.

All runs were made at a nominal airspeed of 250 KIAS and an altitude of 2000 ft in VMC conditions.

Desired and adequate performance standards used in the task are given in the pilot briefing in Appendix C.

Some thrust lever activity was required to keep airspeed in the desired range, which was ± 10 kt about the 250 KIAS target speed. The increased thrust requirement during the runs was a result of the increased drag that resulted from large control inputs required to accomplish the task.

2.4.1 Sum of Sine-wave Inputs

The governing equation for the sum of sine-wave inputs used in the simulation was identical to that used in the Phase 1 tests and is given as follows.

$$X_C = \sum_{i=1}^{n} K_{SF} A_i \sin(\omega_i t + \phi_0) \qquad (1)$$

Where n = 7 and the values for frequency and amplitude of the input sine-waves for each of the tasks are given in Table **1**.

K_{SF} is a scale factor to allow adjustment of the magnitude of all the input sine-waves simultaneously. This was varied empirically during the simulator checkout with the result that the scale factor for the roll task was set to 1.0. For the yaw task it was necessary to reduce the scale factor to 0.55 to avoid overdriving the motion system. All efforts were made to keep the motion gains as high as possible.

ϕ_0 is the initial phase angle, which was changed in increments of 60 degrees to make the sequence appear more random to the pilots. Each configuration was evaluated three times by most of the evaluation pilots. Each evaluation was accomplished with a different initial phase angle of 0, 60 and 120 deg. In that way, each configuration was evaluated with identical disturbance inputs. This was done when it was found that some initial phase angles produced more a more severe environment than others. The same initial phase angle was used for each of the 7 sine waves in Table **1**.

The sum-of-sines input lasted 69.25 seconds for each run. The first 5 seconds was for warm-up (non-scored time) followed by data taking during the following 63 seconds, and the inputs were terminated 1.25 seconds later.

As a side note, the frequencies in Table 1 are calculated as a function of the number of cycles (N_i), and the scoring time (T_s = 63 sec) - $\omega_i = \frac{2\pi N_i}{T_s}$

Sine wave No.	Roll Axis (roll gust inputs)		
	Ai (p_{gust}) deg/sec	No. Cycles	ω_i rad/sec
1	-9	3	0.2992
2	-9	4	0.39893
3	9	7	0.69813
4	4.5	18	1.79519
5	-1.8	30	2.99199
6	-1.8	40	3.98932
7	0.72	70	6.98131

Table **1** Sum-of-Sines Parameters

2.4.2 Evaluation Scenario

Test configurations were presented to the evaluation pilots in random order, and in the blind. As a result, each evaluation pilot saw the configurations in a different order.

It was decided that the first run with a new configuration was more representative of the real world because the need to augment aileron with rudder is extremely rare and represents unknown territory for the large majority of airline pilots. Therefore the experiment was conducted so that the pilot was allowed to move the rudders prior to the run to get a feel for pedal throw and forces, and then to make one run. This was followed by comments and assignment of pilot ratings.

Configuration evaluations were repeated at random times during the experiment and in most cases each evaluator saw each configuration three times. Additional runs were made when unexpected trends in the data were obtained for a given configuration.

The scenario for each evaluation was as follows.

1. Simulator put in Operate mode with no disturbance inputs
2. Data taking initiated 5 seconds after beginning of run
3. Disturbance injected 10 seconds after beginning of run
4. Data taking terminated 63 seconds after being initiated and disturbances removed. Simulator was put into IC by the pilot after disturbances were removed.
5. Pilot made comments and ratings per the scales and questionnaires shown below.

The pilots were requested to issue ratings from the Figure 5and Figure 6 scales, respond

to a questionnaire, and finally to issue Cooper-Harper handling Qualities Ratings (HQRs).

2.4.3 Pilot Rating Card

The purpose of these tests is to evaluate the rudder flight control system. The aileron control power is intentionally not adequate to regulate against the roll disturbances. This is done so that the pilot is forced to use rudder. Please focus your ratings and comments on the ability to use rudder to augment roll control in these severe disturbances.

RATINGS

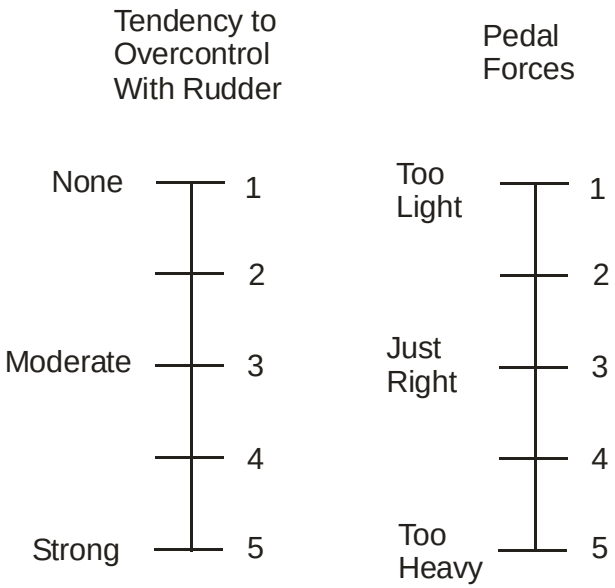

Figure 5 Subjective Rating Scales

When rating pedal forces, consider both the ability to augment aileron and mitigation of overcontrol.

QUESTIONNAIRE

1. Assign Cooper-Harper Pilot Rating

2. **Briefly** describe any unusual rudder feel system characteristics and any other information that you consider necessary to support your ratings

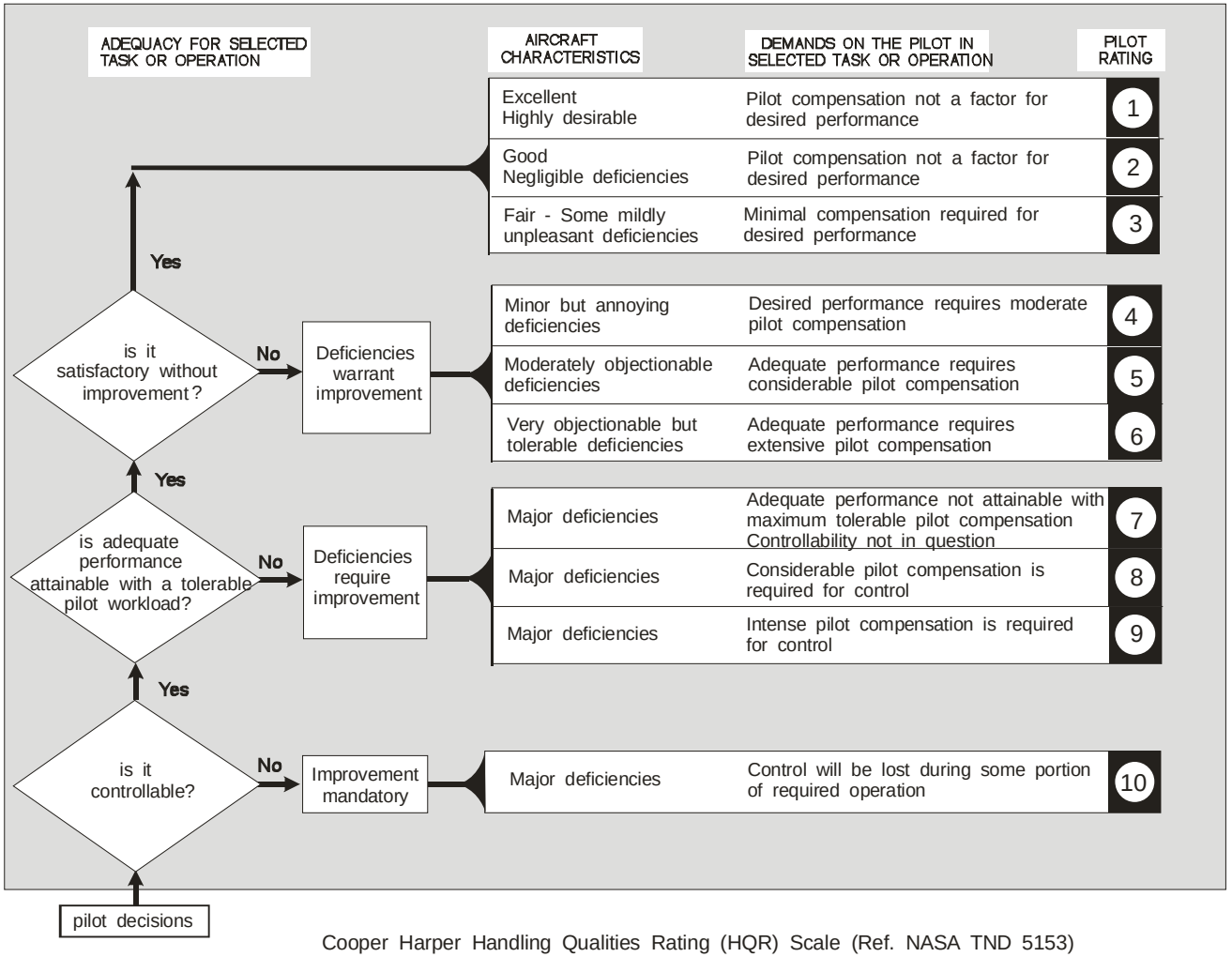

Cooper Harper Handling Qualities Rating (HQR) Scale (Ref. NASA TND 5153)

Figure 6 Cooper Harper Rating Scale

3 TEST CONFIGURATIONS

3.1 FEEL SYSTEM DEFINITIONS

Rudder flight control system definitions used in this study are shown in Figure **7**

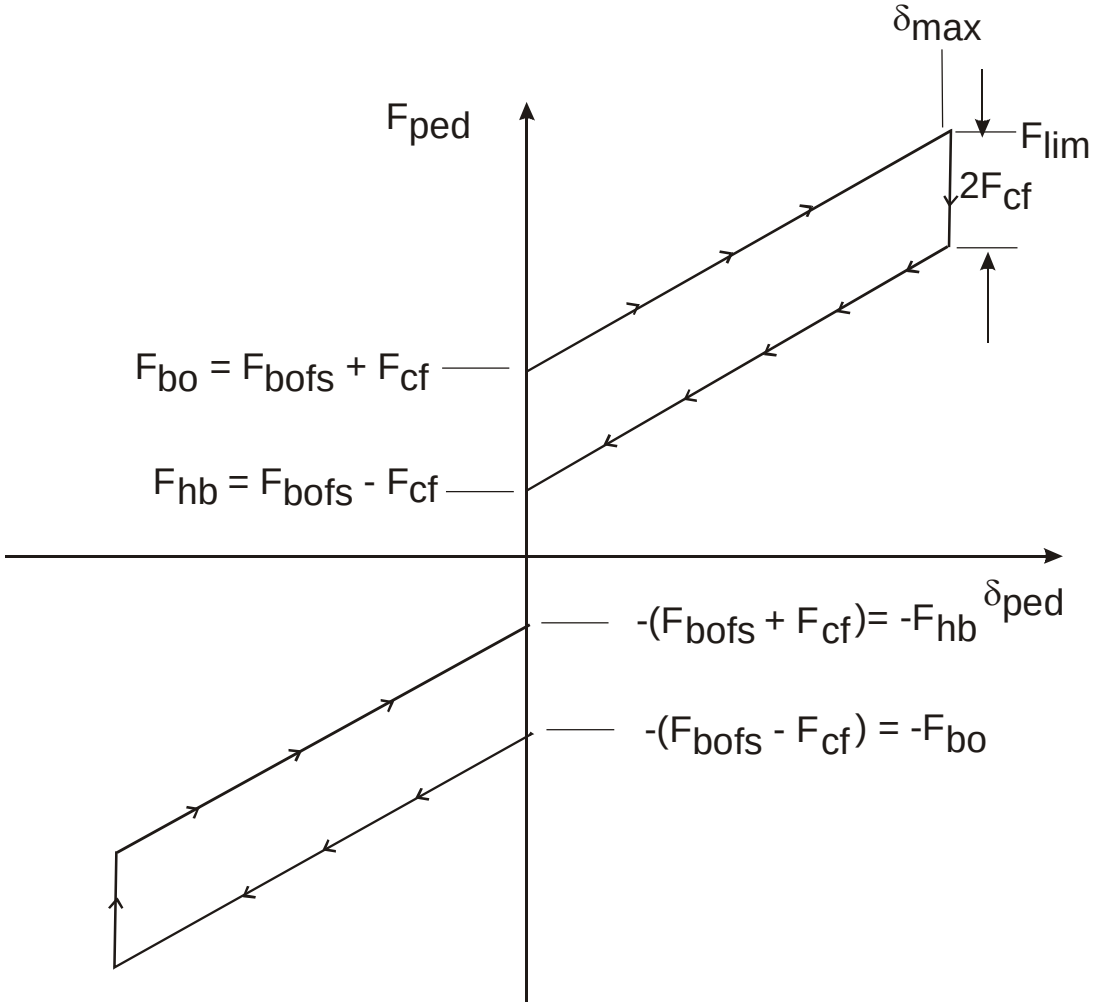

Figure **7** Definitions for Rudder Flight Control System

For the purpose of this simulation the following definitions from Figure **7** will apply.

Feel Spring Breakout (F_{bofs}) – A constant force in a direction to return the rudder control to trim regardless of displacement. This is simulated with a large spring gradient over a small deflection, with the force held constant once that deflection is exceeded.

Coloumb Friction (F_{cf}) – A constant force that is independent of displacement and in a direction opposite to the motion of the pedals.

Breakout Force (F_{bo}) – The force required to initiate pedal motion. This is the sum of the feel spring breakout and Coulomb friction: $F_{bo} = F_{bofs} + F_{cf}$

Holdback (F_{hb}) – The force required to hold pedal deflection just prior to zero pedal deflection when moving towards center. $F_{hb} = F_{bofs} - F_{cf}$

Load-Feel Curve – Pedal force as a function of pedal displacement – may be linear or nonlinear as shown in Appendix D. A nonlinear load-feel gradient is typically used to provide good force cues for small pedal deflections in Variable Stop systems without requiring excessive forces to achieve large rudder deflections during engine out or crosswind landing operations. Load feel curves are typically achieved with one or more centering springs and, where necessary, cams to achieve the nonlinear gradient. Both linear and nonlinear load-feel curves were included in this experiment. The linear load-feel curves result when the breakout force is close in value to F_{lim}, and the only way to practically connect the two points is a straight line.

Viscous Friction (F_{vf}) – Force that is proportional to pedal velocity in a direction to resist pedal motion, i.e., the feel system damping. The work in Reference 4 did not indicate a strong sensitivity in pilot opinion with respect to rudder feel system damping. The subject pilots in that experiment found that the response was satisfactory without improvement (Cooper Harper Handling Qualities (HQRs) ratings equal to or less than 3.5) for feel system damping ratios greater than 0.3. Tests with damping ratio of zero resulted in HQRs of no worse than 4.2. In this experiment, the damping ratio was held at approximately 0.5.

Stop – A force that simulates the mechanical limit of travel. The stop is a constant for Variable Gearing systems and is varies with airspeed in Variable Stop systems. The VMS control loaders created a stop in this experiment by increasing the force gradient to 400 lbs/in.

Flim – The pedal force necessary to move the pedals from trim to the stop. Trim was always zero pedal deflection for this experiment.

The pilot must input a force greater than the feel spring breakout force plus the Coulomb friction force ($F_{bofs} + F_{cf}$) before the rudder pedals move. The force required to keep the rudder pedals from returning to center is equal to or greater than ($F_{bofs} - F_{cf}$). These parameters have been studied in Reference 4 for landing tasks.

3.2 CONFIGURATIONS

The objective of the Phase 2 testing was to accomplish a systematic variation of the key parameters identified in Phase 1: limit force, breakout force, and maximum pedal-throw (F_{lim}, F_{bo}, and $\delta_{p\text{-}lim}$). The baseline testing consisted of three values of pedal travel (1.2, 2.4, and 3.5 inches), two values of limit force (35 lbs and 60 lbs) and 7 values of breakout between 4 and 45 lbs.

The effects of increased rudder travel (control power) and implementation of the yaw damper were also studied.

The parameter F_{bo} / F_{lim} was systematically varied from low to high values within the constraint that the rudder system is designed primarily to provide acceptable handling qualities for tasks such as crosswind landings and engine-out yaw control.

The achievable values of $F_{bo} / F_{\lim}$ are limited by the holdback force, F_{hb}, which is calculated as: $F_{hb} = F_{bo} - 2F_{cf}$, where F_{cf} is the coulomb friction force. A holdback force of 2 lbs was used for most of the configurations, because it allowed the maximum variation in $F_{bo} / F_{\lim}$ for a given $F_{\lim}$. Physically, the holdback force is the force that exists when returning the pedals to neutral, just prior to the pedals being centered.

The reference 4 rudder study showed that values of holdback between 0 and 8 lbs were acceptable. A brief study of the effect of holdback was conducted with some of the subject pilots. Those pilots did not feel that the difference between 2 lbs and 8 lbs of holdback was significant (see Section 5.6).

The coulomb friction force (F_{cf}) and the feel spring breakout force (F_{fsbo}) were calculated as a function of the total breakout force (F_{bo}) and the holdback force (F_{hb}) as follows.

$$F_{cf} = \frac{F_{bo} - F_{hb}}{2} \qquad F_{fsbo} = \frac{F_{bo} + F_{hb}}{2} \tag{2}$$

The holdback force was set to 2 lbs unless otherwise noted.

The breakout force was varied to values as high as 45 lbs. This was done to achieve large values of $F_{bo} / F_{\lim}$ when the limit force was 60 lbs. Values of breakout above 28 lbs may not be certifiable for precision rudder tasks such as crosswind landings based on the results of the reference 4 rudder study that showed Cooper-Harper handling qualities ratings (HQR) of greater than 5 when breakout was above 28 lbs[1]. Nonetheless, the test matrix included breakout values of 35 lbs and 45 lbs as a means to investigate trends for all combinations of limit force and maximum pedal travel.

The full test matrix used in the Phase 2 simulation is given in Figure 8. The configuration designation is (F_{lim}-F_{bo}-$\delta_{p\text{-}lim}$), where maximum pedal deflection is rounded off. For example, a configuration with a limit force of 35 lbs, a breakout of 10 lbs, and a maximum pedal travel of 1.2 inches is indicated by (35-10-1). The three major areas of study were baseline configurations, control power variation, and yaw damper variation. Most of the runs were made to populate the baseline configurations.

[1] The results of the Phase 1 simulation (reference 1) showed that the probability of certification is less than 50% for HQR > 5.

	Baseline Configurations						Effect of Control Power						Effect of Yaw Damper - YD B						
Case	Config	max rud	Flim	Fbo	max ped		Case	Config	max rud	Flim	Fbo	max ped		Case	Config	max rud	Flim	Fbo	max ped	Flim-Fbo
1	35-4-1	9	35	4	1.2		40	35-4-1-R12	12	35	4	1.2		70	35-4-1-YDB	9	35	4	1.2	31
2	35-10-1	9	35	10	1.2		41	35-10-1-R12	12	35	10	1.2		71	35-10-1-YDB	9	35	10	1.2	25
3	35-20-1	9	35	20	1.2		42	35-20-1-R12	12	35	20	1.2		72*	35-20-1-YDB	9	35	20	1.2	15
4	35-25-1	9	35	25	1.2		43	35-28-1-R12	12	35	25	1.2		73	35-25-1-YDB	9	35	25	1.2	10
4a	3VP	8.5	32	22	1.15		44	35-4-3-R12	12	35	4	3.5		74	60-15-1-YDB	9	60	15	1.2	45
5	35-4-2	9	35	4	2.4		45	35-10-3-R12	12	35	10	3.5		75	60-25-1-YDB	9	60	25	1.2	35
6	35-10-2	9	35	10	2.4		46	35-20-3-R12	12	35	20	3.5		76*	60-35-1-YDB	9	60	35	1.2	25
7	35-20-2	9	35	20	2.4		47	35-28-3-R12	12	35	25	3.5		77	60-45-1-YDB	9	60	45	1.2	15
8	35-25-2	9	35	25	2.4		48	60-15-1-R12	12	60	15	1.2		78	35-4-2-YDB	9	35	4	2.4	31
9	35-4-3	9	35	4	3.5		49	60-25-1-R12	12	60	25	1.2		79	35-10-2-YDB	9	35	10	2.4	25
10	35-10-3	9	35	10	3.5		50	60-35-1-R12	12	60	35	1.2		80	35-20-2-YDB	9	35	20	2.4	15
11	35-20-3	9	35	20	3.5		51	60-45-1-R12	12	60	45	1.2		81	35-25-2-YDB	9	35	25	2.4	10
12	35-25-3	9	35	25	3.5									82	35-4-1-R12-YDB	12	35	4	1.2	31
13	60-15-1	9	60	15	1.2									83	35-10-1-R12-YDB	12	35	10	1.2	25
14	60-25-1	9	60	25	1.2									84	35-20-1-R12-YDB	12	35	20	1.2	15
15	60-35-1	9	60	35	1.2									85	35-25-1-R12-YDB	12	35	25	1.2	10
16	60-45-1	9	60	45	1.2									86	60-15-2-YDB	9	60	15	2.4	45
17	60-15-2	9	60	15	2.4									87	60-25-2-YDB	9	60	25	2.4	35
18	60-25-2	9	60	25	2.4									88	60-35-2-YDB	9	60	35	2.4	25
19	60-35-2	9	60	35	2.4									89	60-45-2-YDB	9	60	45	2.4	15
20	60-45-2	9	60	45	2.4															
21	60-15-3	9	60	15	3.5															
22	60-25-3	9	60	25	3.5										For all cases except holdback variation: Fcf = (Fbo-2)/2 and Fbosp = (Fbo +					
23	60-35-3	9	60	35	3.5											Fbo	Fhb	Fcf	Fbosp	
24	60-45-3	9	60	45	3.5											4	2	1	3	
25	35-4-1-FL	f(HMr)	35	4	f(HMr)											10	2	4	6	
26	35-10-1-FL	f(HMr)	35	10	f(HMr)			Effect of Holdback								20	2	9	11	
27	35-20-1-FL	f(HMr)	35	20	f(HMr)											25	2	11.5	13.5	
28	35-25-1-FL	f(HMr)	35	25	f(HMr)			Config	max rud	Flim	Fbo	max ped	Fhb			15	2	6.5	8.5	
29	60-15-1-FL	f(HMr)	60	15	f(HMr)		4	35-25-1	9	35	25	1.2	2			35	2	16.5	18.5	
30	60-25-1-FL	f(HMr)	60	25	f(HMr)		61	35-25-1-HB5	9	35	25	1.2	5			45	2	21.5	23.5	
31	60-35-1-FL	f(HMr)	60	35	f(HMr)		62	35-25-1-HB8	9	35	25	1.2	8							
32	60-45-1-FL	f(HMr)	60	45	f(HMr)															
33	60-5-1	9	60	5	1.2			For these cases Fcf = (Fbo-Fhb)/2 and Fbosp = (Fbo + Fhb)/2												
34	60-5-2	9	60	5	2.4															
35	60-5-3	9	60	5	3.5															

Figure 8 Phase 2 Test Matrix

Each of the baseline configurations had a separate load-feel curve (pedal force vs. pedal displacement). The shapes of the load feel curve were dictated by the difference between breakout and limit force. When this difference was large, a nonlinear shape was used in accordance with standard practice (higher force gradient at lower deflection). When the difference was small, a linear load-feel curve is the only realistic way to connect the endpoints. The load-feel curves for each configuration are shown in Appendix D.

Based on analysis of the Phase 1 data, it was determined that the rudder control power must be held constant to isolate the effect of the rudder control system design parameters (F_{lim}-F_{bo}-$\delta_{p\text{-}lim}$),. Control power was held constant by holding the rudder limit constant with airspeed changes, and eliminating the effect of cable stretch (see Appendix A for details).

Configurations with 1.2 and 2.4 inch pedal travel were implemented as Variable Stop configurations (see Appendix A). The configurations with 3.5 inch pedal throw are by implemented as a variable gearing design.

It was found in Phase 1, that systems with high pedal forces had less control power because cable stretch reduced the rudder deflection at maximum pedal. Systems with low pedal forces had less cable stretch and therefore more control power. One approach would have been to vary the maximum rudder deflection as a function of limit force. However, the same effect was achieved by simply eliminating cable stretch.

The schedule of maximum rudder deflection as a function of airspeed results in a change in rudder control power if the subject pilot allows airspeed to vary significantly away from the target of 250 KIAS. Therefore, the input to the rudder deflection vs. airspeed schedule was held constant at 250 kts, regardless of the actual airspeed.

The maximum achievable sideslip was found to be constant over the airspeed variations encountered in the experiment ($\pm$ 10 kts or less).

3.3 YAW DAMPER

A block diagram of the representative generic yaw damper used in this simulation is shown in Appendix A. The yaw damper was implemented in two different ways and labeled YD A and YD B as described below.

3.3.1 Yaw Damper A Operation

The YD A output was limited to $\pm 3^o$ and summed with the rudder deflection commanded by the pedals, and that value was passed to the rudder limiter. This is illustrated in Figure **9**.

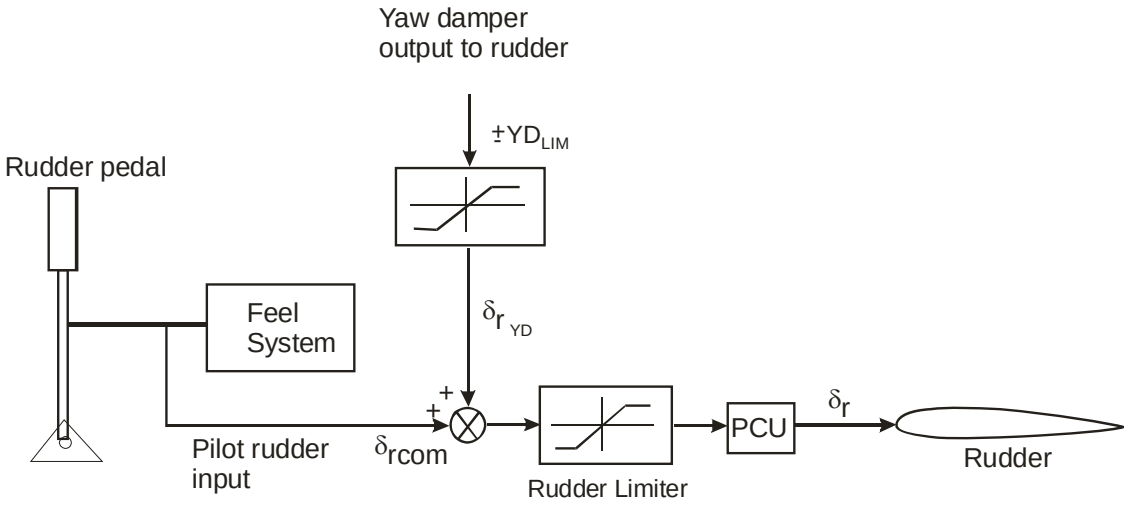

Note: Yaw damper input to rudder is restricted by magnitude of pilot input

Figure **9** Implementation of Version A Yaw Damper (YD A)

The pilot input pedal gearing was set so that maximum pedal deflection commanded the rudder limit. For baseline cases, this was set to 9^o. With this implementation, if the pilot applied full rudder pedal, the yaw damper decreased rudder by as much as 3^o, so that only 6^o of deflection was available. This occurred because the yaw damper functioned to decrease the yaw rate and sideslip that resulted from a large rudder pedal inputs.

For large pedal deflections YD A operation was essentially one-sided in that it could decrease rudder deflection, but could not increase rudder deflection. This had the effect of decreasing rudder control power in a favorable way so as to limit undesirable sideslip excursions if the rudder was over-controlled.

An alternative mechanization would be to set the pedal-to-rudder gearing so that a full pedal input results in a command equal to the value of the rudder limit plus the yaw damper authority. If that is done, the above described decrease in control power is eliminated. For example, if the rudder pedal gearing is set so that the pilot can command 12^o of rudder and the rudder is limited to 9^o, then the rudder response to large pedal inputs will be to drive to and remain on the 9^olimit. It will be shown in Section 5.5 that this can have a significant effect on sideslip excursions and vertical stabilizer loads. This was not tested in Phase 2, but should be planned for Phase 3.

3.3.2 Yaw Damper B Operation

Yaw damper B (YD B) was implemented to investigate the effect of summing the yaw damper command downstream of the rudder limiter as illustrated in Figure **10**.

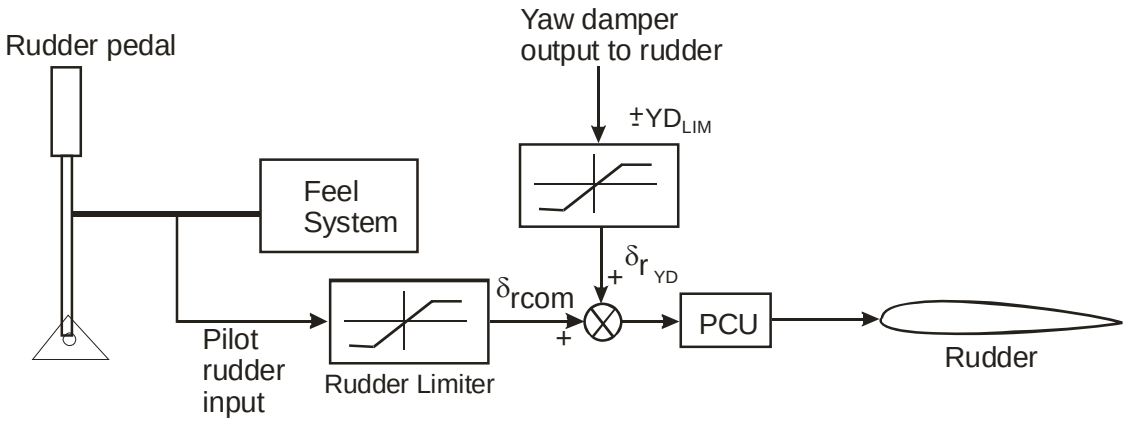

Note: Yaw damper input to rudder is not restricted by magnitude of pilot input

Figure **10** Implementation of Version B Yaw Damper (YD B)

The YD B input to the rudder differs from YD A in that it is possible for the yaw damper to add to and subtract from the limited rudder. For example, if the rudder limit is 9° and the yaw damper is limited to 3°, then it is possible to achieve rudder deflections between 6° and 12°.

The Variable Gearing design was used to implement the long pedal-throw configurations (see Appendix A). This design implicitly limits rudder deflection by varying the pedal-to-rudder gearing as a function of airspeed. The rudder limiter was set to 30° and therefore had no effect. For this simulation the rudder gearing was set so that full pedal (3.5 inches) resulted in 9° of rudder deflection. The yaw damper can add or subtract 3° so in effect this is the same as YD B.

3.4 EVALUATION PILOTS

Twelve evaluation pilots performed formal evaluations in this program. The names and background of each of the pilots is as follows. The number next to each pilot corresponds to the labels used in the data analysis when referring to the pilot subjects.

1 Paul Desrochers	Airline pilot, ex Boeing Test pilot, FAA DER Test Pilot, Type rated in most Boeing transport aircraft. FAA DER test pilot.
2 Roger Hoh	FAA DER Test Pilot, Type rated Boeing 737,
3 Troy Zwicke	FAA AEG pilot (Seattle ACO)
4 Mike Garrett	FAA AEG pilot (Seattle ACO)
5 Pat Morris	FAA Test Pilot (Ft. Worth ACO)
6 Jim Webre	FAA Test Pilot (Los Angeles ACO)
7 Guy Thiel	FAA Test Pilot (Los Angeles ACO)
8 Kevin Green	FAA Test Pilot
9 Al Wilson	FAA Test Pilot (Seattle ACO)

10 Rick Simmons FAA Test Pilot (Seattle ACO)

11 Armand Jacob Airbus Test Pilot

12 Mark Feurstein Boeing Test Pilot

4 FORCE ON VERTICAL STABILIZER

4.1 REPRESENTATIVE FORCE CALCULATION

The calculation of the loads on the vertical stabilizer used in the Phase 1 simulation was also used for the Phase 2 tests. This calculation was based on the fact that the lateral force on the vertical stabilizer is a result of sideslip and rudder deflection.

$$F_v \approx Y_\beta \beta + Y_{\delta_r} \delta_r = \left(C_{Y_\beta} \beta + C_{Y_{\delta r}} \delta_r \right) \frac{S \rho_o V_{CAS}^2}{2} \qquad (3)$$

This expression assumes that all of the sideforce due to sideslip is due to the vertical stabilizer. This is a reasonable approximation for the purpose of this study.

Generic values of aircraft derivatives that are representative of large transport aircraft and a representative wing area (S) was used in equation 3 as follows:

$$C_{Y_\beta} \approx -.0211/\deg \; and \; C_{Y_{\delta r}} = .00651/\deg$$

$$F_v = \left(-0.034\beta + .01\delta_r \right) V_{CAS}^2 \qquad (4)$$

Where sideslip and rudder deflection are in degrees, airspeed is in ft/sec, F_v is in lbs, and sideslip is positive with wind from the right, and rudder deflection is positive trailing edge left (standard NASA sign conventions).

Equation 4 does not provide values for any single aircraft, but does give the correct proportions of force due to sideslip and force due to rudder deflection for a typical transport aircraft. By using this same expression for all the tested configurations, it is possible to compare the forces on the vertical stabilizer that result from different rudder flight control system mechanizations.

As a sanity check, the sideslip (10^o) and rudder deflection (-11^o) for AA 587 at the time of failure at 250 kts, were input to equation 4, resulting in a force of 80,327 lbs on the vertical stabilizer. At a near maximum takeoff weight for the simulated generic transport aircraft of 175,000 lbs, this results in a lateral acceleration of 0.46g. The NTSB data indicated a lateral acceleration of 0.5g, indicating that equation 4 is a reasonable estimate of sideforce due to sideslip and rudder deflection.

4.2 VERTICAL STABILIZER LOADS

The loads on the vertical stabilizer result from a combination of sideslip and rudder deflection as illustrated in Figure 11.

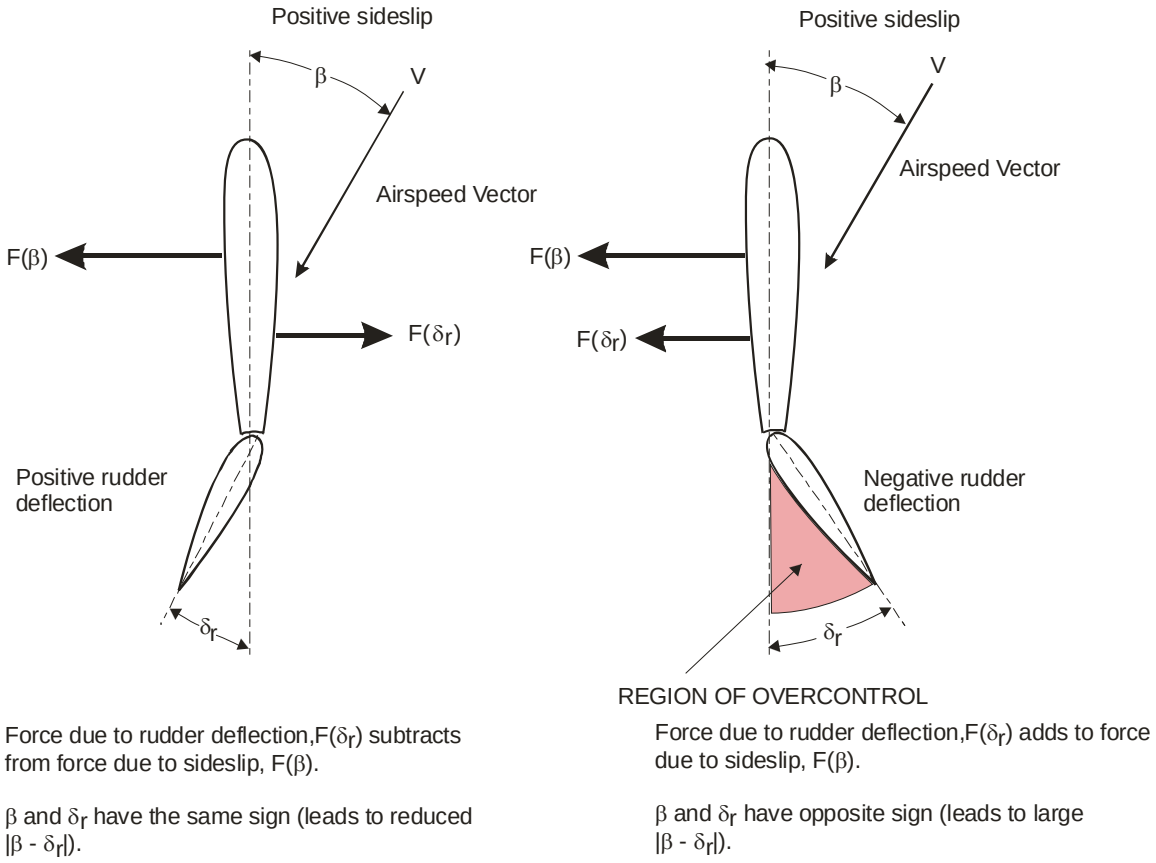

Figure 11 Illustration of Region of Overcontrol

The illustrations in Figure 11 show that the force on the vertical stabilizer is maximized when sideslip and rudder deflection are of opposite sign. For sideslip and rudder deflection to be of opposite sign, it is necessary for the pilot to apply rudder in a direction to reduce sideslip. This puts the rudder in the shaded red "overcontrol" region in Figure 11.

When rudder is used to augment aileron (as was required to accomplish the task), the pilot intentionally sideslips in a direction to cause the effective dihedral (L_β) to add to the rolling moment due to aileron. When this is done rudder deflection and sideslip have the same sign and the force on the vertical stabilizer due to rudder deflection subtracts from the force due to sideslip. It is only when the pilot reverses the rudder in the presence of large sideslip that the forces add as defined by the shaded region in Figure 11.

Analysis of the simulation data indicated that significant rudder deflections into the overcontrol region occurred as a result of two distinct pilot techniques when regulating against large rolling disturbances.

Pilot Technique A Pilot does not use rudder until full aileron is applied and the aircraft is still rolling away from the applied aileron. At that point a rudder input is made to augment the aileron. This tends to result in excursions into the overcontrol region because there is some sideslip due to the adverse yaw that develops with full aileron deflection. The avoidance of rudder to augment aileron until it is absolutely necessary is consistent with current training.

Pilot Technique B Pilot uses rudder continuously to augment roll control with aileron.

An example of Technique A from the simulation experiment is shown in Figure 12. Here it is seen that the pilot inputs full aileron to counter a large rolling gust with essentially no rudder input. The yaw damper cannot quite keep up with the large aileron input resulting in a small positive sideslip (adverse yaw). When the pilot finally decides that rudder is necessary, he abruptly puts in full control. The rudder enters the overcontrol region resulting in a peak in the force on the vertical stabilizer. As long as the yaw damper minimizes the adverse yaw due to a full aileron input, the sideslip will remain small and forces on the vertical stabilizer should not be excessive.

Pilot technique B is shown in Figure 13 where the pilot is seen to be using rudder in a continuous manner. The sign of rudder and sideslip are seen to be the same as expected when rudder is used to augment aileron. However, if the pilot gets out of phase with aileron or momentarily misapplies the rudder the forces on the vertical stabilizer due to rudder and sideslip add. This is seen to occur at 75.8 seconds in Figure 13, and a peak in the force on the vertical stabilizer is observed. This is similar to the scenario that resulted in failure of the vertical stabilizer in the reference 3 NTSB report (albeit, with a much greater magnitude of sideslip). The time histories in Figure 13 are from the simulation run that produced the highest vertical stabilizer that was encountered in Phase 2.

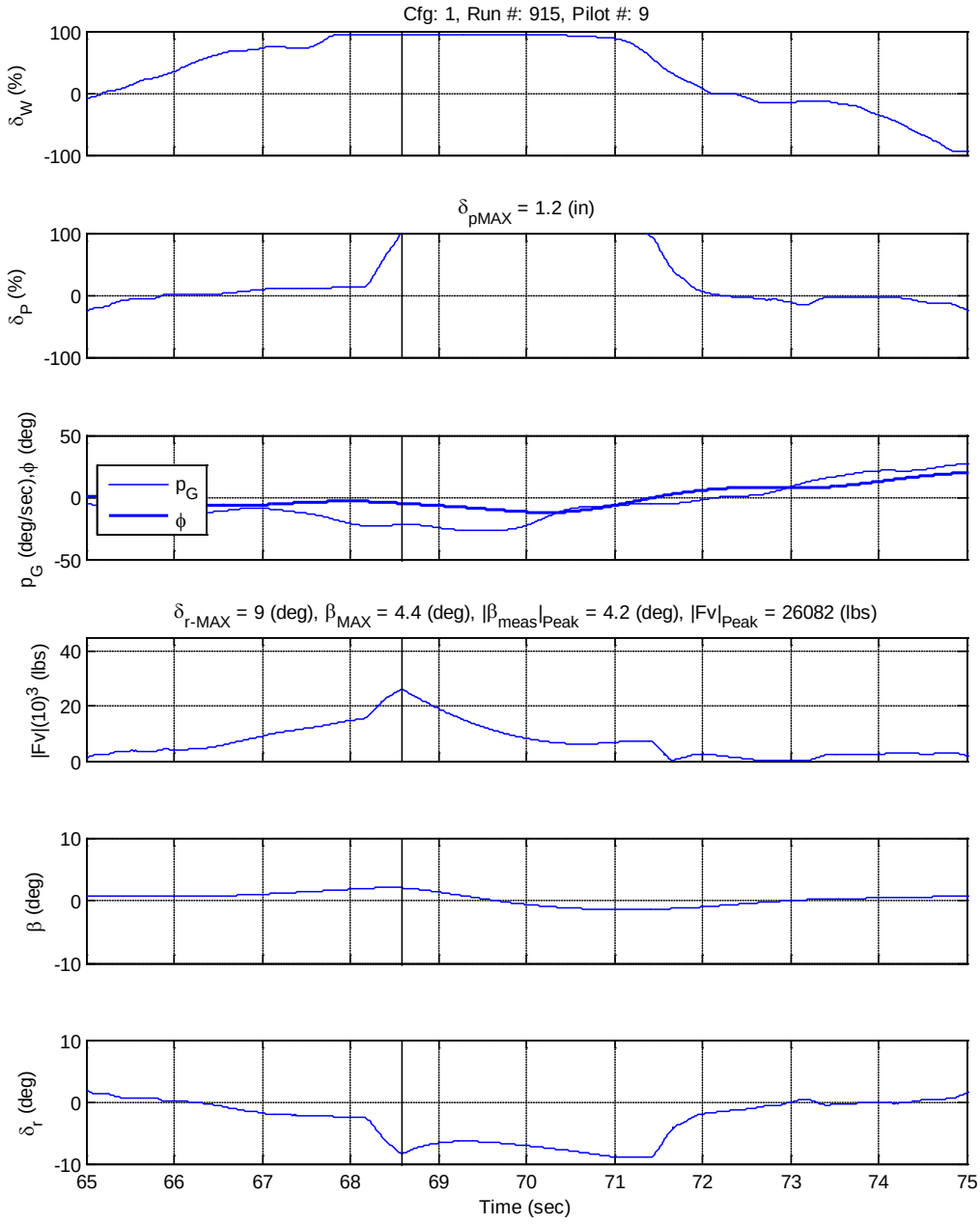

Figure 12 Example of Pilot Technique A

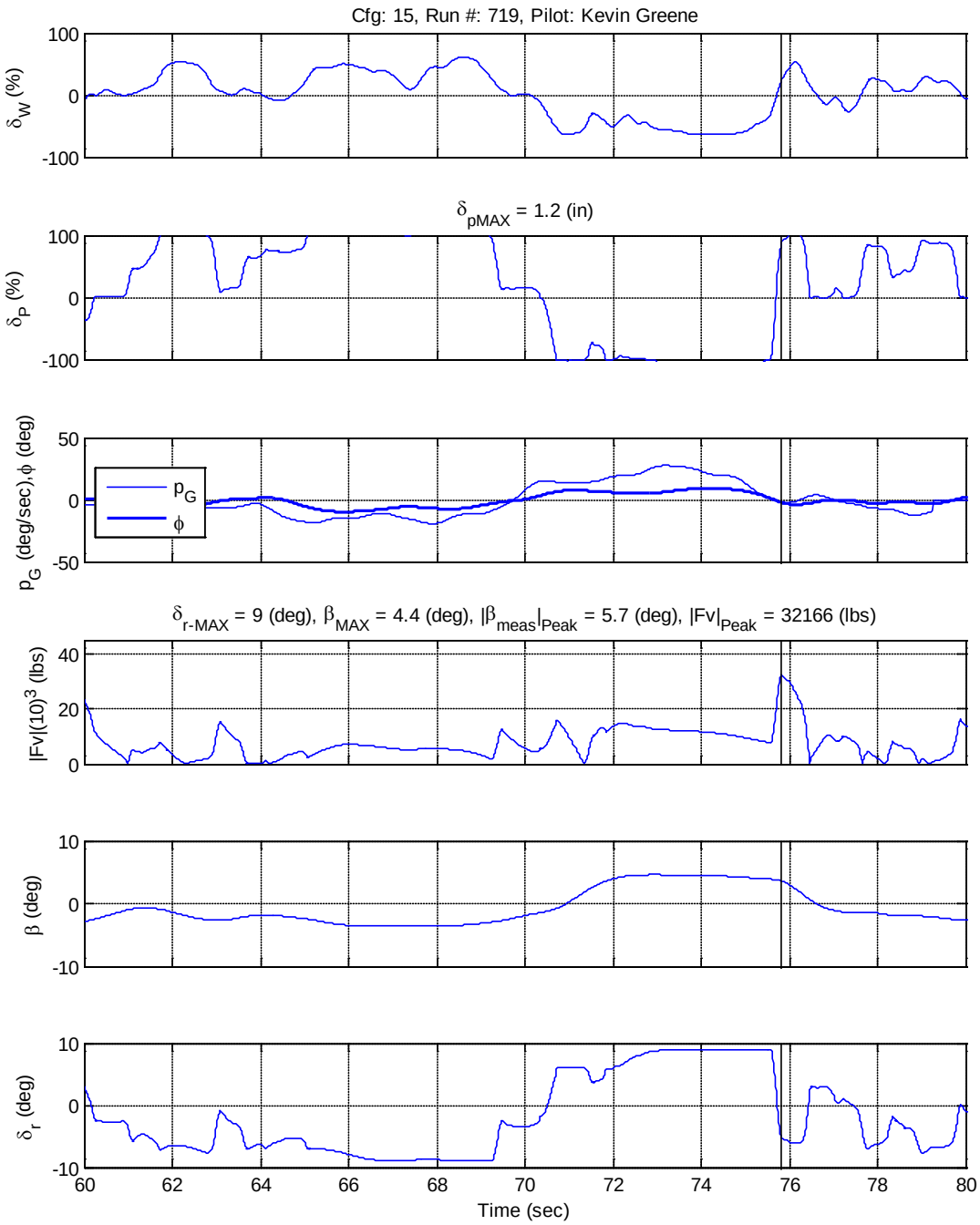

Figure 13 Example of Pilot Technique B

While it is not the intent of this work to reconstruct the accident that led to failure of the vertical

stabilizer reported in reference 3, it is illustrative to review the data from that accident in terms of the above discussion. The time histories in Figure 14 were derived from the data in reference 5.

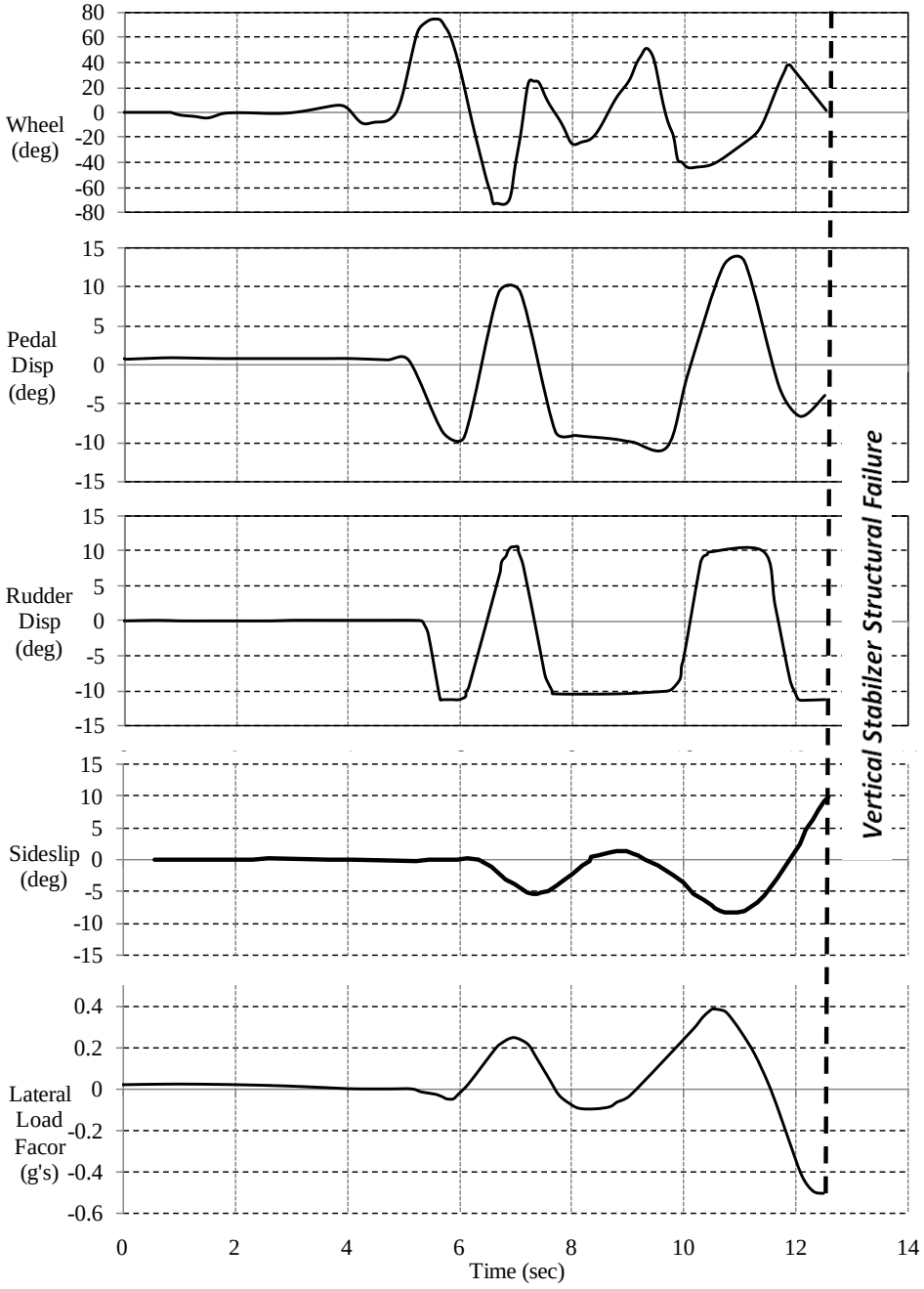

Figure 14 Time Histories Leading to Failure of Vertical Stabilizer

These time histories indicate that the pilot was actively using rudder to augment aileron during the initial portion of the encounter (pilot technique B). This is evidenced by the fact that rudder was used to develop proverse yaw (sideslip has the same sign as rudder and in a direction to augment roll). Approximately 2.5 seconds into the encounter, the rudder is held against the right pedal

stop, while the wheel is reversed to 20 degrees left followed by 50 degrees right and back to 40 degrees left. This lack of correlation between aileron and rudder excited the dutch roll mode resulting in large sideslip angles. This was probably exacerbated by the fact that the yaw damper was only partially functional while the pilot held the pedal on the stop. The pilot then made a full rudder input from one stop to the other resulting in maximum negative rudder in the presence of 10 degrees of positive sideslip (i.e., full rudder input into the shaded overcontrol region in Figure 11) which caused the vertical stabilizer to fail. This scenario is an extreme example of pilot technique B.

The FAA regulatory criteria that relate to vertical stabilizer structural integrity are specified in CFR 14 Part 25.351. The key elements of that requirement are summarized as follows:

(a) With the airplane in unaccelerated flight at zero yaw, it is assumed that the cockpit rudder control is suddenly displaced to the limit of travel.

(b) With the cockpit rudder control deflected so as always to maintain the maximum rudder deflection available, it is assumed that the airplane yaws to the overswing sideslip angle.

(c) With the airplane yawed to the static equilibrium sideslip angle, it is assumed that the cockpit rudder control is held so as to achieve the maximum rudder deflection available.

(d) With the airplane yawed to the static equilibrium sideslip angle of paragraph (c) of this section, it is assumed that the cockpit rudder control is suddenly returned to neutral.

Part 25.351 specifies that the airplane must be design to withstand the loads resulting from the above maneuvers from the minimum control airspeed (V_{MC}) to the maximum dive speed (V_D).

Part 25.351(d) is normally the most critical input because the forces due to sideslip are always higher than the force due to rudder (for example, see equation 4).

The objective of this work is to identify characteristics of the rudder flight control system that make it more likely that rudder usage would result in forces higher than required by CFR 14 Part 25.351(d).

If the force on the vertical stabilizer resulting from the maneuver specified by 25.351(d) is defined as $F_{\beta\max}$, then from equation 3,

$$F_{\beta\max} = \left(C_{Y_\beta}\beta_{ss\max}\right)\frac{S\rho_o V_{CAS}^2}{2} \tag{5}$$

If the rudder structure is designed in accordance with 25.351(d), forces exceeding $F_{\beta\max}$ will result in exceedance of the limit load on the vertical stabilizer. This is expressed as a percentage over the limit load as follows.

$$\Delta F_{EF} = \left(\frac{F_{3\sigma\ peak}}{F_{\beta\max}} - 1\right)100 \tag{6}$$

Where $F_{3\sigma\ peak}$ is defined as the largest expected force on the vertical stabilizer.

Note that if a vertical stabilizer structure is designed so that the design limit load is defined by $F_{\beta\max}$, then the ultimate load (1.5 times the limit load) would be defined when $\Delta F_{EF} = 50\%$. Forces above $F_{\beta\max}$ can only occur if the rudder enters the shaded overcontrol region in Figure 11 in the presence of significant sideslip.

$F_{3\sigma\ peak}$ was calculated from the simulation data as follows:

1. Identify and store the peak (maximum) value of vertical stabilizer force ($\left|F_{peak}\right|$) for a group of runs that is under study, e.g., for all runs where $F_{\lim} = 60\ lbs$ and $\delta_{ped_{\max}} = 1.2$ inches.
2. Calculate the average of $\left|F_{peak}\right|$ for all runs from step 1.
3. Calculate the standard deviation of $\left|F_{peak}\right|$ for all runs.
4. Finally, $F_{3\sigma\ peak} = \left|F_{avg\ peak}\right| + 3 * std\ dev\left(\left|F_{peak}\right|\right)$

It is shown in Appendix E that the $\left|F_{peak}\right|$ data from the simulation is well described by a normal distribution and therefore using the 3σ value is a reasonable estimate of the maximum force on the vertical stabilizer that would ever be encountered while accomplishing a task requiring use of rudder to augment aileron.

The only way that the force on the vertical stabilizer can exceed $F_{\beta\max}$ is for the pilot to make a rudder input into the overcontrol region when sideslip is large. The maximum achievable force that can be obtained from static equilibrium occurs by establishing the conditions specified by 25.351(c) (maximum steady sideslip) and suddenly reversing the rudder to the opposite stop (rather than centering the rudder as required by 25.351(d). An example of that maneuver is shown in Figure 15. Here it is seen that the maximum steady sideslip is 4.4 degrees. From equation 4, this results in $F_{\beta\max}$ = 26,705 lbs. The peak force due to a rudder reversal from maximum sideslip is seen from Figure 15 to be 40,000 lbs. From equation 6, $\Delta F_{EF} = \left[40,000 / 26,705 - 1\right]100 = 49.8\%$

This indicates that a stop-to-stop rudder reversal at maximum steady sideslip can result in reaching the ultimate load factor.

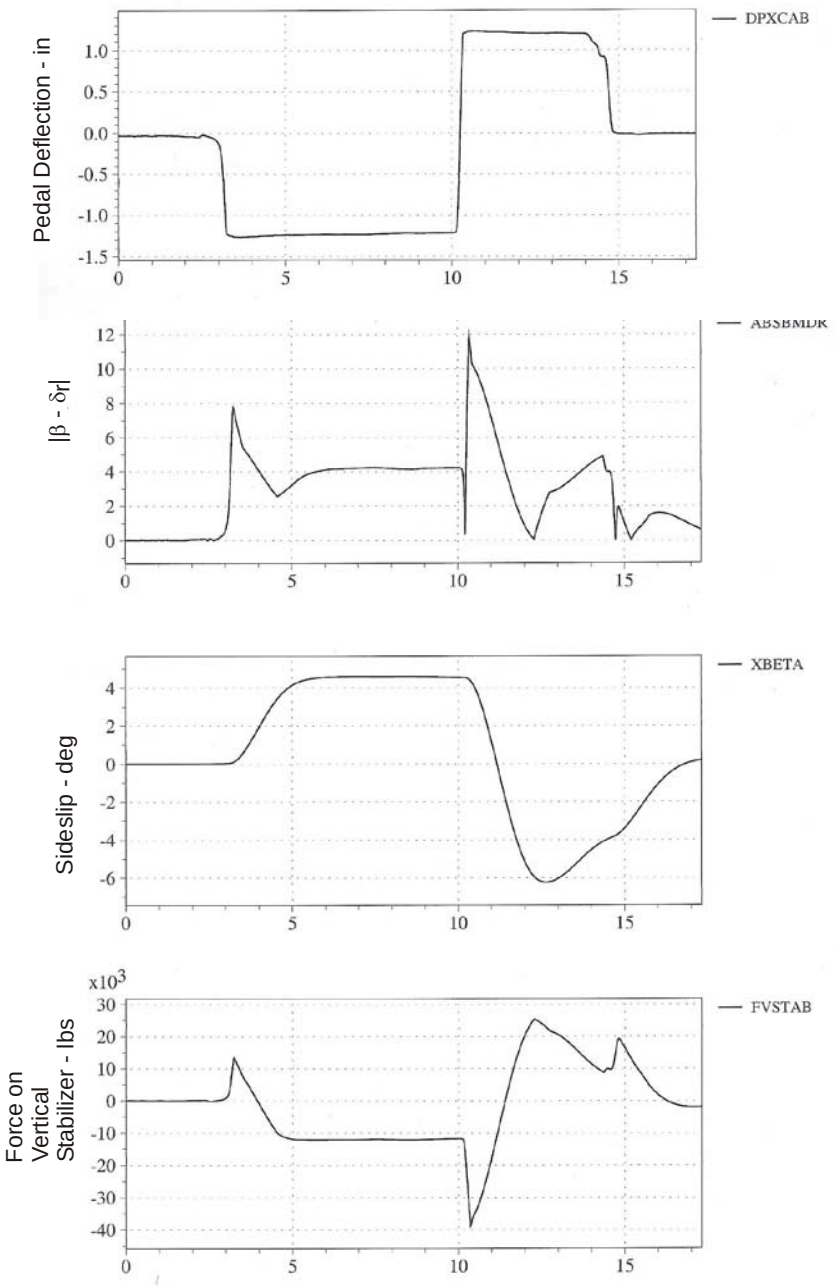

Figure 15 Rudder Reversal at Maximum Sideslip

4.3 RUDDER OVERCONTROL PARAMETER (ROP)

From the discussion in Section 4.2 it can be seen that large vertical stabilizer forces occur when the pilot makes a large rudder input in the presence of sideslip and the sign of rudder deflection is opposite the sign of sideslip. Stated mathematically, this occurs when the parameter $|\beta - \delta_r|$ takes on large values. A generic plot of the effect on increasing $|\beta - \delta_r|$ on the force imposed on the

vertical stabilizer is given in Figure 16.

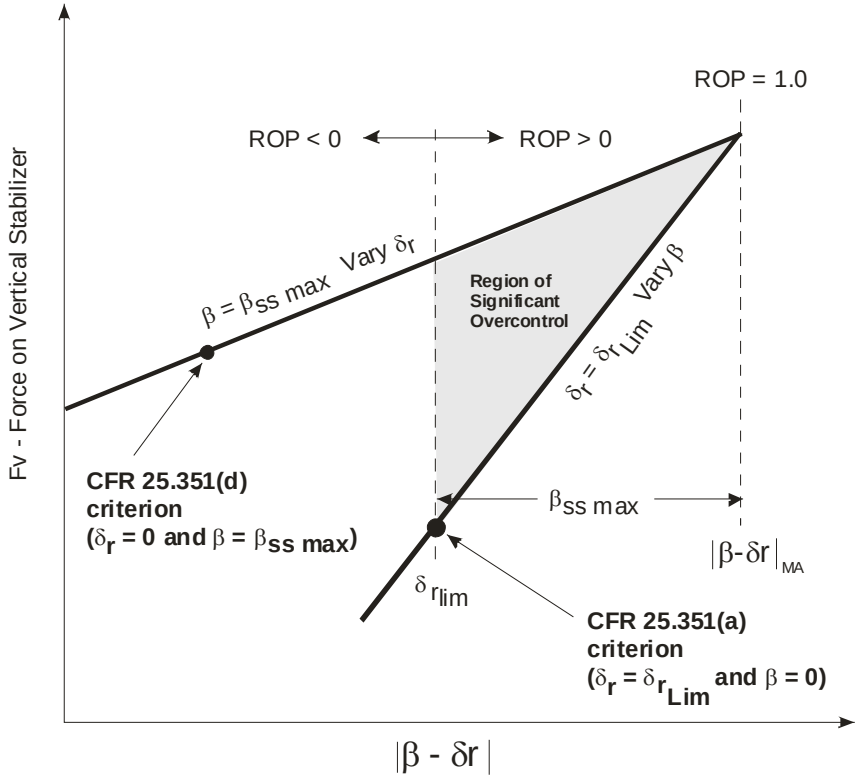

Figure 16 Effect of $|\beta - \delta_r|$ on Vertical Stabilizer Force

The boundaries in Figure 16 are based on steady state conditions. The upper boundary is the vertical stabilizer force that results from a step rudder input in the presence of the maximum achievable steady state sideslip ($\beta = \beta_{ss:\max}$). Higher values of sideslip can be achieved if inputs are made to excite the dutch roll mode. The lower boundary is the force resulting from varying sideslip in the presence of maximum rudder ($\delta_{r\,Lim}$). The curves intersect when $|\beta - \delta_r|$ is at its maximum achievable value $|\beta - \delta_r|_{MA}$ (defined when $\beta = \beta_{ss\max}$ *and* $\delta_r = \delta_{r\,LIM}$ and $sign\beta \neq sign\delta_r$).

The possibility for high vertical stabilizer loads is seen to increase significantly as $|\beta - \delta_r|$ takes on values greater than $\delta_{r\,Lim}$ - shown as the shaded region in Figure 16. This is defined as the region of significant rudder overcontrol. The tendency for rudder reversals that result in excursions into the region of significant rudder overcontrol is quantified by positive values of the rudder overcontrol parameter, ROP.

$$ROP = \frac{|\beta - \delta_r|_{3\sigma\,peak} - \delta_{r\,Lim}}{|\beta - \delta_r|_{MA} - \delta_{r\,Lim}} = \frac{|\beta - \delta_r|_{3\sigma\,peak} - \delta_{r\,Lim}}{\beta_{ss\max}} \qquad (7)$$

ROP is normalized by the condition where sideslip and rudder are at their maximum achievable values without dynamic overshoot. This is done to minimize the effect of rudder control power so that ROP is primarily a measure of the tendency for rudder reversals into the significant overcontrol region in Figure 16.

The following connections may be established between ROP and rudder overcontrol events:

ROP > 0	The force on the vertical stabilizer is greater than can be achieved with rudder alone (i.e. greater than specified by 14 CFR Part 25.351(b)).
ROP = 1	The maximum force that can be achieved at steady sideslip. Accomplished by achieving the maximum steady sideslip with full rudder and rapidly reversing the rudder to the opposite limit.
ROP > 1	Forces exceed what can be achieved at steady sideslip – indicates rudder reversal at sideslip greater than can be achieved in steady state (i.e., $\beta > \beta_{ss\,\max}$).

$\left|\beta - \delta_r\right|_{3\sigma\ peak}$ was calculated from the simulation data as follows:

1. Identify and store the peak (maximum) value of vertical stabilizer force ($\left|\beta - \delta_r\right|_{peak}$) for a group of runs that is under study, e.g., for all runs where $F_{\lim} = 60\ lbs$ and $\delta_{ped_{\max}} = 1.2$ inches.
2. Calculate the average $\left|\beta - \delta_r\right|_{peak}$ for all runs from step 1.
3. Calculate the standard deviation of $\left|\beta - \delta_r\right|_{peak}$ for all runs
4. Finally, $\left|\beta - \delta_r\right|_{3\sigma\ peak} = \left|\beta - \delta_r\right|_{avg\ peak} + 3 * std\ dev\left(\left|\beta - \delta_r\right|_{peak}\right)$

It is shown in Appendix E that the $\left|\beta - \delta_r\right|_{peak}$ data from the simulation is well described by a normal distribution and therefore using the 3σ value is a reasonable estimate of the maximum expected value.

The calculation of the standard deviation of $\left|\beta - \delta_r\right|$ is based on all configurations in the Figure 8 test matrix. The calculation of a separate standard deviation for each configuration did not exhibit a consistent trend, indicating that the variability in the use of rudder was not configuration dependent. It was therefore decided calculate a single standard deviation for all 1014 runs.

The intent of the rudder overcontrol criterion is to provide a metric to distinguish between rudder control systems that are prone to overcontrol from those that are not. Note that it is possible to experience rudder deflections in the region of overcontrol without exerting exceptional forces on vertical stabilizer if sideslip is low when the rudder is over controlled (lower portion of shaded region in Figure 16). Therefore ROP can be quite large without experiencing excessive vertical stabilizer load. The basic concept of ROP is that values greater than zero indicate a tendency to overcontrol, and it is conceptually just a matter of time until such an excursion will occur in the

presence of large sideslip (e.g. Figure 14).

The current CFR 14 Part 25 351(d) criterion plots at a point on the upper boundary in where the steady sideslip is maximum and the rudder deflection is zero, and the Part 25.351(a) criterion plots at a point on the lower boundary where rudder deflection is maximum and sideslip is zero.

The data obtained from the baseline and YD B configurations in Phase 2 is plotted on the Figure 16 boundaries in Figure 17, where the peak force vs. peak value of $|\beta - \delta_r|$ are plotted for each run.

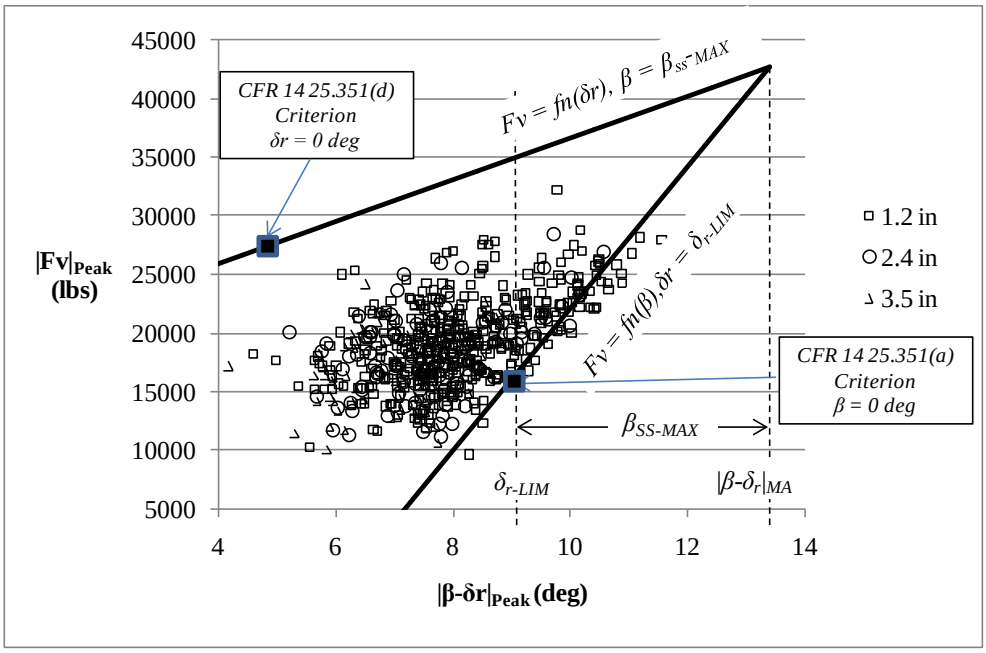

Figure 17 Effect of $|\beta - \delta_r|$ on Vertical Stabilizer Force – Phase 2 Baseline Configurations

($\delta_{r\,Lim} = 9^o$ and $\beta_{ss\max} = 4.4^o$)

These data indicate that most runs did not exhibit significant overcontrol (ROP <0), and that the runs where overcontrol did occur plot near the lower boundary. This indicates that rudder overcontrol occurred mostly at low values of sideslip, which implies that there was little tendency to excite the dutch roll mode during the Phase 2 tests. Time histories for the run corresponding to the highest value of vertical stabilizer force plotted in Figure 17 (approximately 32,000 lbs) are shown in Figure 13.

The data for some runs fall below the lower boundary. This was found to be due to the fact that airspeed was slightly below the target 250 kts when the vertical stabilizer force peaked.

5 CRITERIA DEVELOPMENT

The objective of this work is to develop proposed criteria and supporting data to allow the FAA to make recommendations regarding the design of rudder flight control systems that are resistant to pilot-induced overstressing of the vertical stabilizer in up-and-away flight.

5.1 TECHNICAL APPROACH

The above analysis shows that high vertical stabilizer loads result from a rudder reversal into the region of overcontrol at large values of sideslip. The rudder overcontrol parameter (ROP) has been developed as a tool to analyze the large body of simulation data obtained in this experiment.

As noted in Figure 16, the tendency to overcontrol with rudder increases as ROP takes on values greater than zero. A successful criterion parameter will show good correlation with ROP, and thereby distinguish between configurations that are prone to overcontrol from those that are not. Note that ROP itself cannot be used as a criterion parameter because it requires a large amount of data, which is not practical for evaluation of an actual rudder flight control system design.

As shown in Figure 16 and Figure 17 it is possible to experience a range of forces on the vertical stabilizer for a given value of ROP depending on sideslip. The approach taken here is that a good criterion will ensure that ROP is low so that it will be unlikely to encounter a rudder reversal at any value of sideslip, be it pilot-induced or a result of turbulence or a wake vortex encounter.

The parameter ΔF_{EF} has also been developed to analyze the simulation data. This parameter is a measure of the excess force imposed on the vertical stabilizer relative to the force required to meet the 14 CFR Part 25.351(d). $\Delta F_{EF} = 0$ implies that the peak force on the vertical stabilizer is equal to the force that would occur for maximum steady sideslip with zero rudder as specified by Part 24.351(d). This parameter is intended to put the simulation results in the proper context. Values of 50% or greater are considered to have the potential for structural failure of the vertical stabilizer. This is based on the argument that if the structure is designed so that the limit load just meets the Part 25.351(d) criterion, then the ultimate load would be 50% higher.

5.2 EFFECT OF PEDAL TRAVEL, LIMIT PEDAL FORCE, AND $F_{bo} / F_{\lim}$

The basic hypothesis of the Phase 2 simulation test plan was that rudder overcontrol is strongly dependent on the highly nonlinear nature of the of the rudder pedal force-deflection or "load-feel" curve due to large values of breakout. A simple measure of this nonlinearity is $F_{bo} / F_{\lim}$, the breakout force divided by the limit force (see Figure **7** for definitions of breakout and limit force).

The results of the Phase 2 simulation in terms of $F_{bo} / F_{\lim}$ and the value of ROP taken as an average across all pilots for each baseline configuration are plotted in Figure 18.

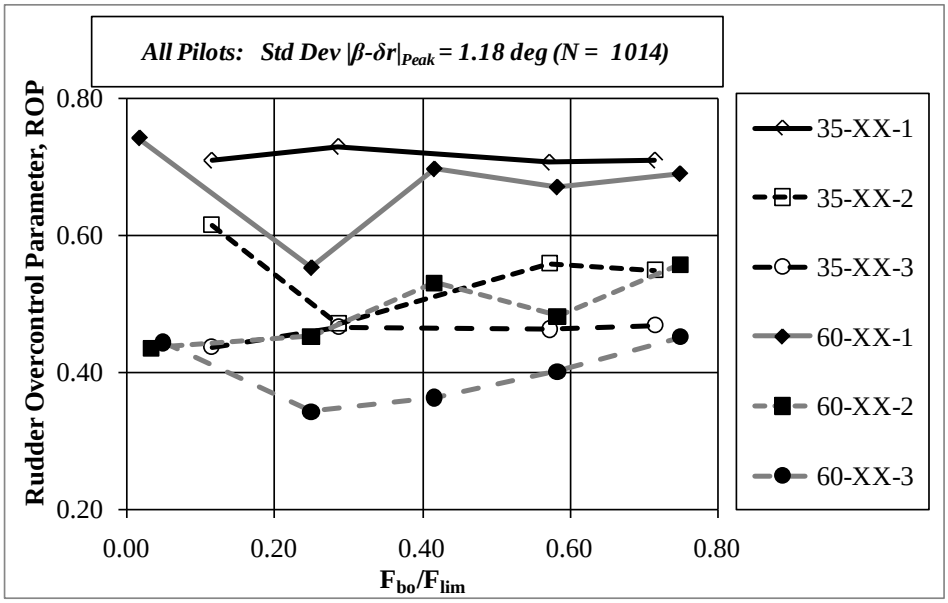

Figure 18 Rudder Overcontrol Parameter as a Function of $F_{bo} / F_{\lim}$ for Baseline Configurations

These results are based on the use of a standard deviation of 1.18 deg to calculate $\left|\beta - \delta_r\right|_{3\sigma\ peak}$ in equation (7) . As noted in Section 4.3, the calculation of the standard deviation of $\left|\beta - \delta_r\right|$ is based on all runs for all configurations in the Figure 8 test matrix.

Each configuration was run an average of 22 times with each pilot nominally evaluating three randomly inserted repeat runs for each configuration. The minimum number of runs for a given configuration was 20 and the maximum was 38. This is judged to be a significantly large sample to provide reliable trends.[1]

The most significant finding from the data in Figure 18 is that the tendency to overcontrol with rudder is primarily dependent on rudder pedal travel. The 3.5 inch "long pedal-throw" configurations (circle symbols) were consistently and significantly less prone to overcontrol than the 1.2 inch "short pedal-throw" configurations (diamond symbols).

Other conclusions from the Figure 17data are:

- The configurations with high limit force, long throw, and $F_{bo} / F_{\lim}$ between 0.25 and 0.42 (60-15-3 and 60-25-3) exhibited the lowest values of ROP indicating a strong resistance to rudder overcontrol.
- Increasing the pedal limit force did not significantly alleviate the tendency for overcontrol for the short throw configurations (compare open and filled diamonds).

[1] Early in the program, the configurations were evaluated three consecutive times before providing a rating. This was changed so that only one run was made before moving to the next configuration. When more than one run was made, only the first run was used in the data analysis.

- The ratio of $F_{bo} / F_{\lim}$ had little effect on the tendency for overcontrol with the following exceptions.
  - A significant decrease in ROP occurred when $F_{bo} / F_{\lim}$ was set equal to 0.25 for the short pedal-throw configuration 60-15-1. This seemingly anomalous trend was noticed during the simulation and extra runs were made to determine if this effect was real. A total of 23 runs with a standard deviation of 1.1^{o} suggests that this was not a random effect. This was the only case where a reduction in $F_{bo} / F_{\lim}$ resulted in a large and beneficial effect on ROP (albeit, not as good as increasing the travel to 3.5 inches).
  - Decreasing the breakout to 5 lbs ($F_{bo} / F_{\lim} \approx 0.10$) resulted in a noticeable increase in ROP for some configurations. The pilot's all complained of a "mushy feel" for this low value of breakout. This result suggests that there is a minimum value of breakout to ensure that ROP is minimized.
  - A slight increase in ROP resulted from increasing $F_{bo} / F_{\lim}$ to values greater than 0.42 for the long throw (3.5 inch) configurations.

An explicit plot of the results in terms of pedal travel is given in Figure 19 by plotting ROP for each pedal displacement/force vs. pedal travel[1]. The symbols represent the averaged value, the thick vertical lines represent the standard deviation of the averaged values, and the end points represent the maximum and minimum values of ROP.

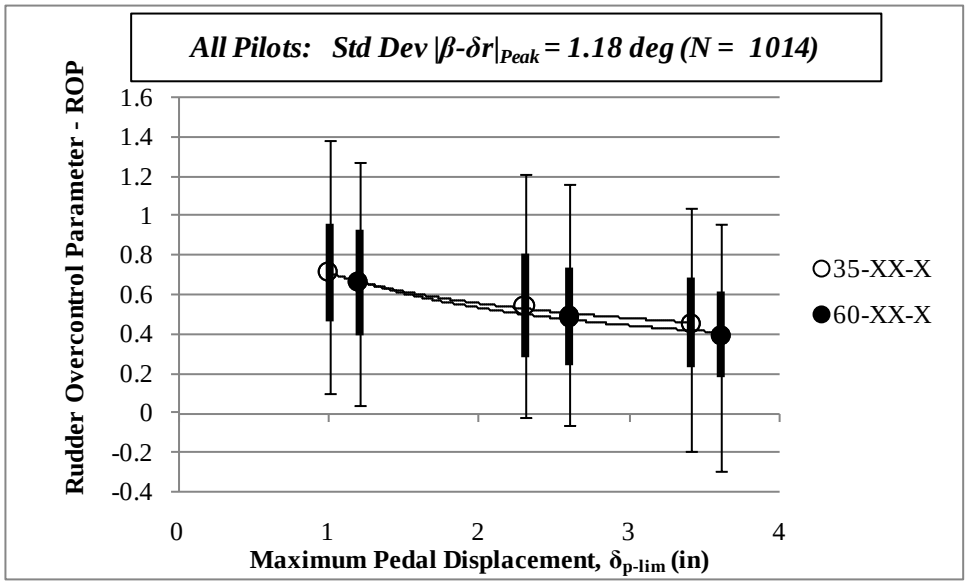

Figure 19 ROP vs. Pedal Travel for Baseline Configurations

This data shows that increasing pedal travel is a considerably more effective way to reduce the

[1] ROP is based on the value of $\left|\beta - \delta_r\right|_{peak}$ averaged across all pilots and $F_{bo} / F_{\lim}$ for each pedal displacement/force configuration.

tendency for rudder overcontrol than increasing pedal force.

The large variation between the maximum and minimum values of ROP for a given pedal displacement/force is a result of different pilot technique. Some pilots were considerably more aggressive than others.

The excess vertical stabilizer force as a function of maximum pedal throw is given in Figure 20 by plotting ΔF_{EF} obtained by averaging $F_{v\ peak}$ across all pilots and configurations at each of the three tested pedal displacements.

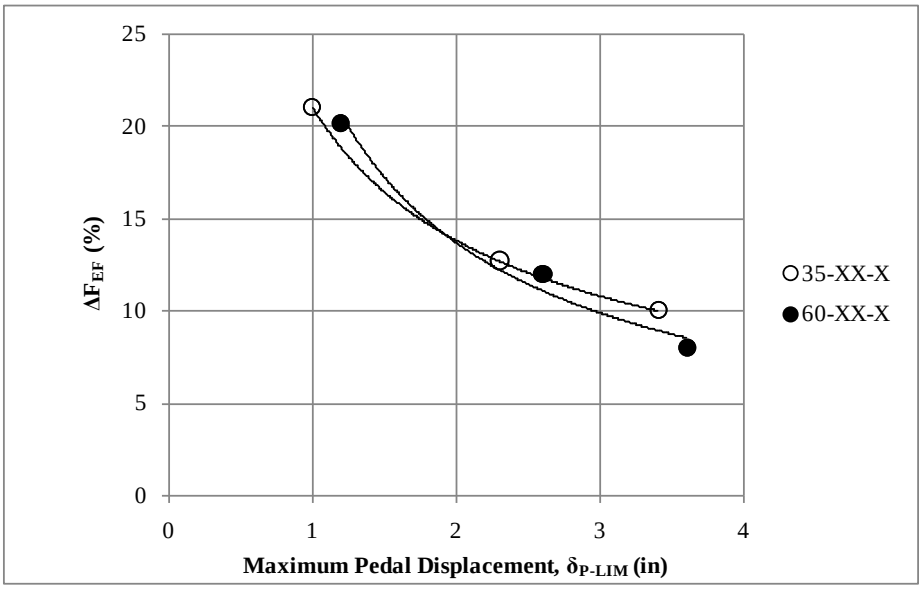

Figure 20 Excess Vertical Stabilizer Force vs. Pedal-Throw

These data indicate that ΔF_{EF} exhibits the same trend as ROP in that the short pedal-throw configurations are more prone to high vertical stabilizer loads, and pedal force plays a less significant role.

This data shows that the worst-case configuration (short pedal-throw and low force) exceeded the 14CFR part 25.351(d) criterion on average by 21% and the best configuration (long pedal-throw and high force) exceeded the criterion by 8%. That is, all the configurations exceeded the criterion limit, but the short pedal-throw configurations were prone to a significantly higher exceedance.

To put these results in context, a full rudder reversal from a maximum steady sideslip conditions would result in ΔF_{EF} = 50%.[1]

The A300-600 vertical stabilizer failed with. $\beta = 10^o, \delta_r = -11^o, and\ Airspeed = 250\ kts$[2]. Substituting these values into the estimated vertical stabilizer force equation (4) results in a force

[1] This result is obtained from the calculation shown in the text above Figure 15.

[2] It is not known why the flight data recorder showed a rudder deflection of -11° when the rudder should have been mechanically limited to 9° based on the data in reference 3.

on the vertical stabilizer of 80,327 lbs. The CFR 14 Part 25.351(d) limit ($F_{\beta \max}$) is calculated from equation (4) by setting $\beta = 4.4^o, \delta_r = 0^o, and\ Airspeed = 250\ kts$, resulting in a value of 26,705 lbs. Therefore the estimated value of ΔF_{EF} at the point of failure was 200%. This is an order of magnitude greater than what was experienced in the Phase 1 or Phase 2 VMS simulations.

As will be discussed in Section 5.5, the less than expected vertical stabilizer loads encountered in the simulation are due to the fact that sideslip excursions were much less than was seen in the accident scenario.

5.3 LINEARITY INDEX PARAMETER

The Linearity Index (LI) was proposed as a measure of tendency to overcontrol with rudder in references 6 and 7. LI was calculated for all the baseline configurations as shown in Appendix F. It is also shown in Appendix F that $LI \approx 1 - F_{bo} / F_{\lim}$ for all the configurations tested in this simulation. ROP was correlated with LI with the result shown in Figure 21.

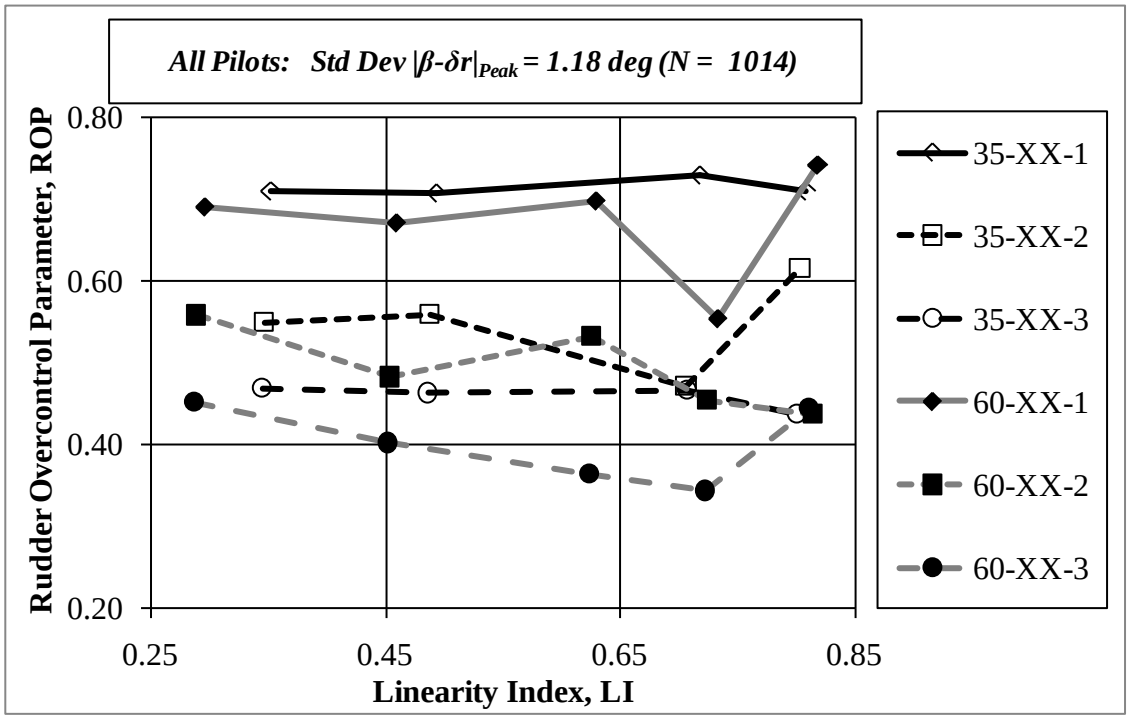

Figure 21 Correlation of Rudder Overcontrol Parameter with the Linearity Index

As expected, the correlation of ROP with LI indicates the same trends as the correlation with $F_{bo} / F_{\lim}$ in Figure 19, albeit flipped horizontally because $LI \approx 1 - F_{bo} / F_{\lim}$.

In conclusion, the linearity index describes the same phenomena as $F_{bo} / F_{\lim}$ and the parameters can be used interchangeably for configurations with similar rudder pedal load-feel characteristics to those tested in this simulation program (i.e., essentially all transport aircraft). It is a moot point because neither parameter successfully predicts a tendency for rudder overcontrol.

5.4 EFFECT OF YAW DAMPER IMPLEMENTATION

As discussed in Section 3.3 a single yaw damper was implemented in different locations relative to the rudder limiter for the Variable Stop configurations. Due to limitations on simulator time, it was not possible to populate all of the YD B configurations with a statistically significant number of runs (taken to be at least 20 runs with at least 6 different pilots). Given that the long pedal-throw cases already represent YD B, efforts were focused on the short pedal-throw cases, and it was possible to get data for three series of configurations (35-XX-1, 60-XX-1, and 35-XX-1). A comparison of ROP vs. $F_{bo} / F_{\lim}$ for YD A vs. YD B for these configurations is given in Figure 22.

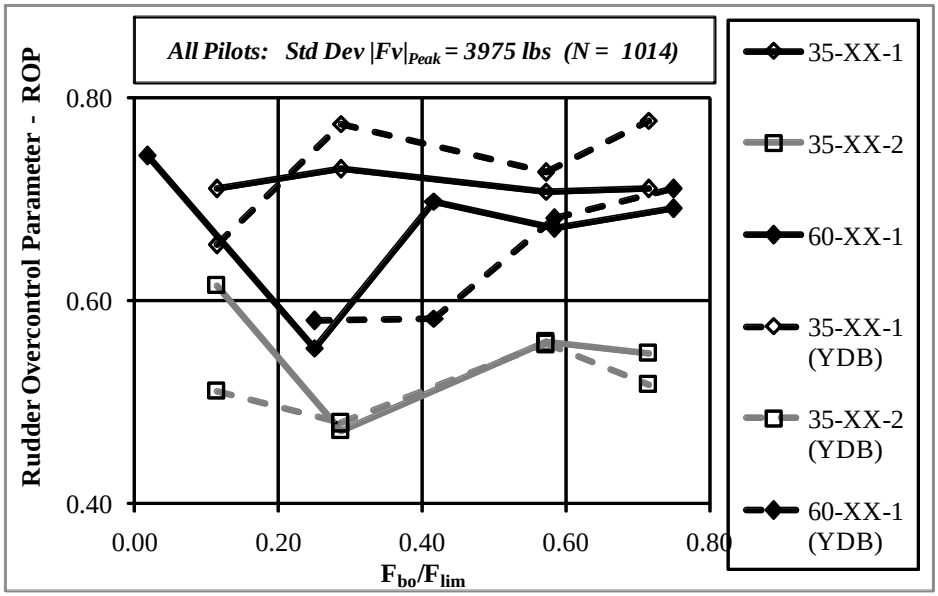

Figure 22 Comparison of Rudder Overcontrol Parameter between YD A and YD B

These data show no significant difference in the tendency for overcontrol of rudder (ROP) between YD A and YD B (compare dashed and solid lines).

The value of maximum steady sideslip used to compute ROP was 4.4^{o} for YD A and YD B. Both yaw dampers reduced the maximum steady rudder deflection by 3^{o}.

A comparison between the excess force induced on the vertical stabilizer for YD A and YD B is given in Figure 23.

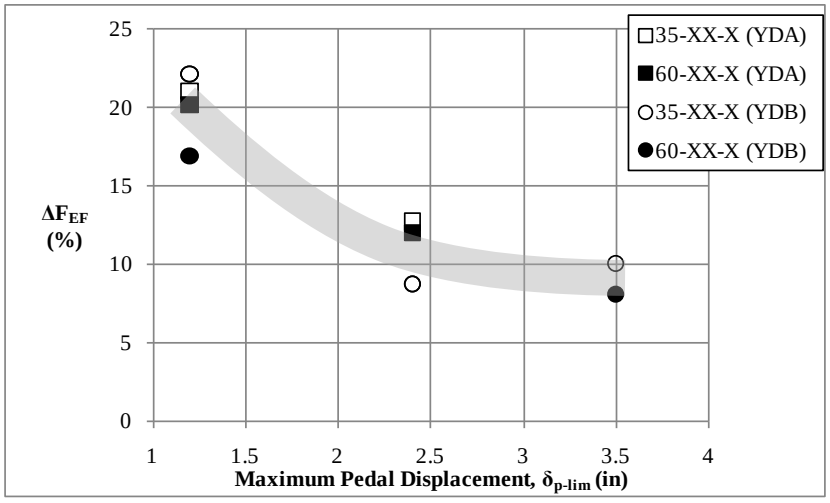

Figure 23 Comparison of Excess force on Vertical Stabilizer between YD A and YD B

These data indicate that there is no significant difference in the force imposed on the vertical stabilizer between YD A and YD B.

5.5 LARGE SIDESLIP AS A CONTRIBUTING FACTOR

From Figure 15 it is seen that the maximum achievable steady sideslip for the baseline configurations was 4.4°, and that a rapid rudder reversal at that sideslip angle resulted in a vertical stabilizer load of approximately 40,000 lbs. This is far below the estimated 80,327 lb load that resulted in the inflight structural failure shown in Figure 14. The large discrepancy between this event and the simulation results can be explained primarily by the fact that sideslip was never increased to the level experienced by the accident aircraft (10°).

The peak sideslip [1] angles that occurred during the simulation for the baseline cases are shown in Figure 24.

[1] The peak sideslip is defined as the maximum sideslip that occurred during a 63 second simulation run.

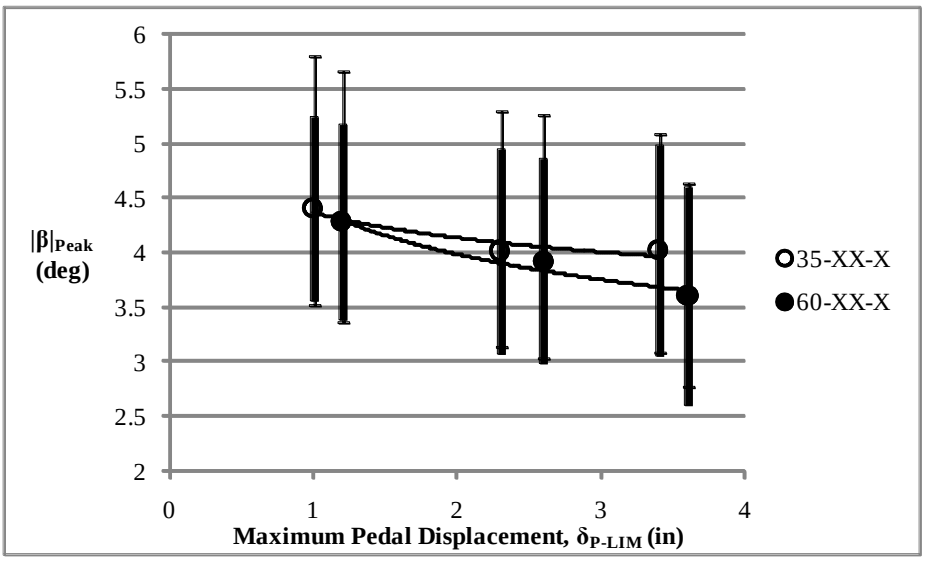

Figure 24 Maximum Sideslip for Baseline Configurations

The symbols in Figure 24 indicate the average peak sideslip, the ends of the thick vertical bars indicate the 1σ variations in peak sideslip, and the T-ends indicate the maximum and minimum values of sideslip achieved for all runs with the baseline configurations.

The short pedal-throw configurations tended to produce larger values of sideslip indicating more dutch roll excitation. The maximum steady-state sideslip that could be achieved with maximum rudder deflection for the baseline configurations was 4.4^{o}. The maximum sideslip achieved in the simulation is seen to be 5.8^{o}, which is 1.4^{o} more than the steady-state value.

The maximum sideslip achieved during the simulation was only slightly more than half that achieved in the accident scenario (10^{o}) shown in Figure 14. From equation 4, the maximum force that could have been exerted on the vertical stabilizer had the pilot reversed the rudder at the worst-case sideslip value of 5.8^{o} would have been 51, 267 lbs (maximum rudder = 9^{o}) as shown by the following calculation.

$$F_v = \left(-0.034\beta + .01\delta_r\right)V_{CAS}^2 = \left[-.034(5.8) + .01(-9)\right](250 * 1.69)^2 = 51,267 lbs$$

This is compared to the force of 40,000 lbs that can be achieved for a maximum rudder reversal at the maximum steady sideslip angle of 4.4^{o} (see Figure 15). Note that the force on the vertical stabilizer increases by approximately 6000 lbs for every degree of sideslip.

These results suggest that a tendency towards large sideslip angles plays a significant role in achieving large aerodynamic loads on the vertical stabilizer. Such a tendency would most likely result from a combination of degraded yaw damper performance and increased rudder control power.

The effect of the yaw damper implementation (YD A and YD B), and of rudder control power on the peak sideslip angle achieved in the simulation is shown in Figure 25.

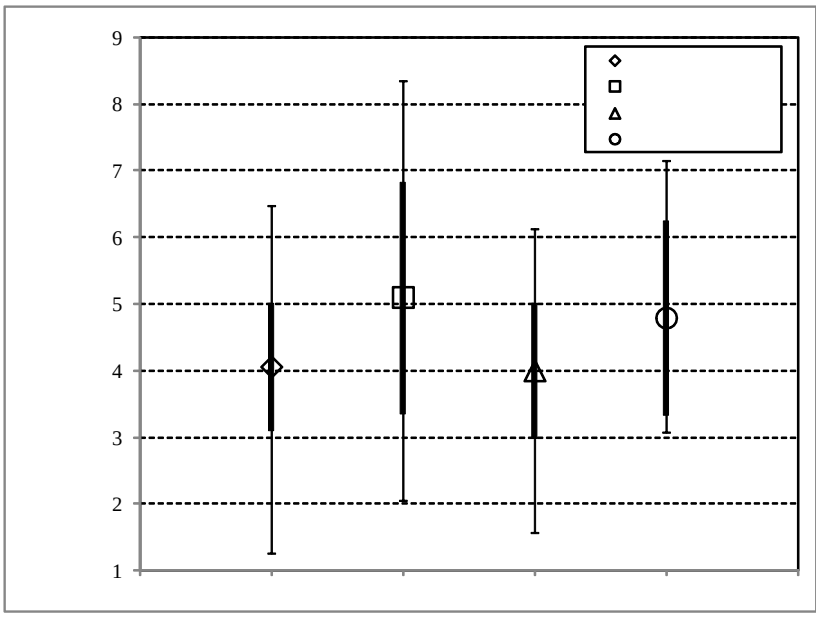

Figure 25 Effect of Yaw Damper A vs. Yaw Damper B on Maximum Sideslip

These data show that the effect of locating the yaw damper before or after the limiter (YD A and YD B respectively) had only a minor effect on the peak sideslip angle. Increasing the rudder authority from 9^o to 12^o resulted in slightly increased sideslip excursions.

These results call into question how the sideslip angle on the A300-600 accident aircraft became so large (10^o at point of failure, see Figure 14). Even with rudder control power increased by 33%, the largest sideslip angle achieved during the simulation was 8.3^o.

A cursory Matlab Simulink™ analysis was accomplished to investigate the effect of degrading the yaw damper and increasing rudder control power on peak sideslip to provide some insight into how very large values of sideslip could be achieved in a transport aircraft. The desktop simulation consisted of a linear model of the Convair 880 as described in Appendix G[1]. Yaw Damper A was implemented into the Convair 880 model. The rudder and aileron inputs from the A300-600 accident were used to drive the model. The time histories of the response with a fully functioning (albeit saturated) yaw damper are shown in Figure 27.

[1] This model was used because linear aerodynamic data was readily available from reference 8.

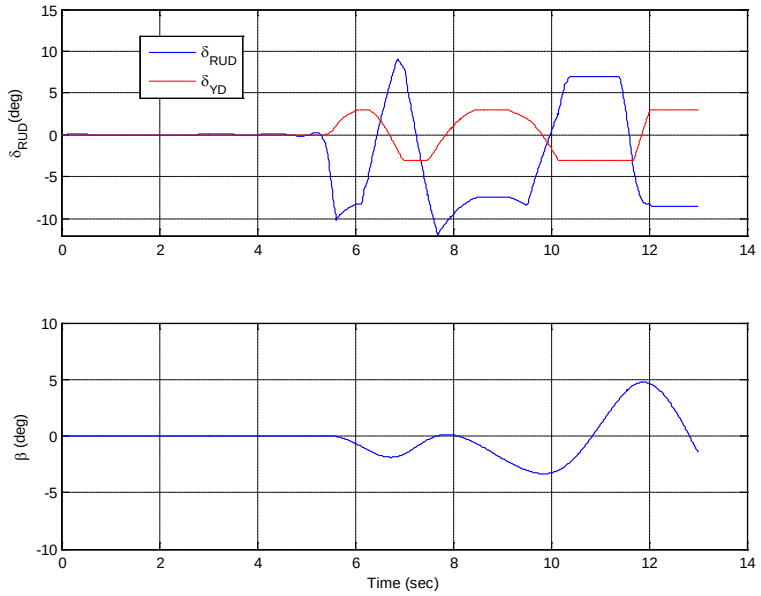

Figure 26 Response of Transport Model to AA 587 Pilot Inputs with Yaw Damper A

These data indicate that the Convair 880 model achieved a peak sideslip angle of 5° - half that exhibited by the A300-600, and similar to what was observed for the baseline cases in the simulation.

One significant difference between the time histories of the rudder response of the Convair 880 in Figure 26 and the A300-600 (Figure 14) is that the maximum rudder deflections are less for the Convair 880 (which used YD A). According to information published in reference 3, the rudder deflection for the A300-600 was mechanically limited to approximately 9° at the 250 kt. airspeed where the vertical stabilizer failed. From Figure 14 it can be seen that the rudder achieved values as high as 11 degrees. It is not known why the rudder reached deflections beyond its mechanical limit.

The yaw dampers mechanized in this simulation (YD A and YD B) respond to a maximum step pedal input by causing the rudder to drive to its limit of travel, and then drop back by the amount of yaw damper authority (3° for this simulation). This drop back results when the yaw damper functions to reduce the yaw rate and sideslip that results from a large pedal input (dashed line in Figure 26). The A300-600 rudder traces in Figure 14 (taken from processed flight data recorder as published in reference 5) do not show any drop back.

The Simulink model was rerun with the yaw damper disabled in the Convair 880 model with the result shown in Figure 27.

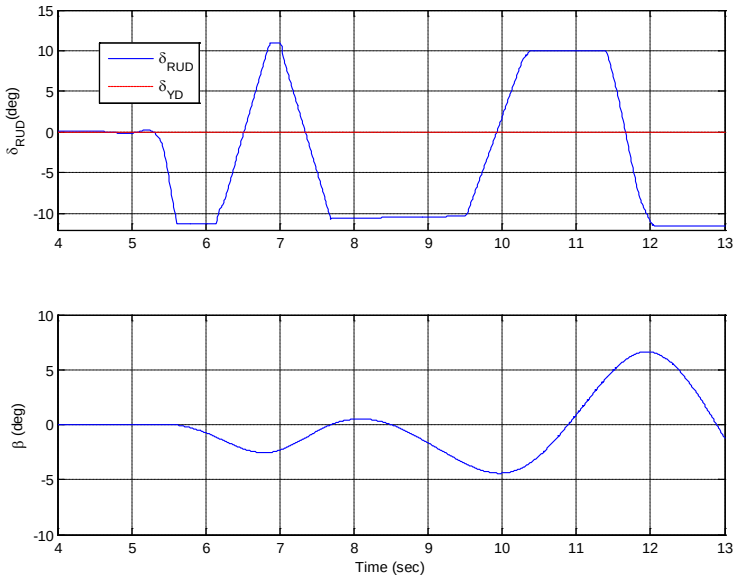

Figure 27 Response of Convair 880 Model to Pilot Inputs from AA 587 accident and Yaw Damper Disabled.

Disabling the yaw damper approximates the effect of increasing the pedal-to-rudder gearing to allow the pilot to command a rudder deflection that is well over the rudder limit as described in Section 3.3.1. This caused the peak sideslip to increase 40% from 5 degrees to approximately 7 degrees.

Finally, the rudder control power of the Convair 880 ($N_{\delta r}$) was increased by 50% to achieve 10^{o} of sideslip with the yaw damper inoperative as shown in Figure 28.

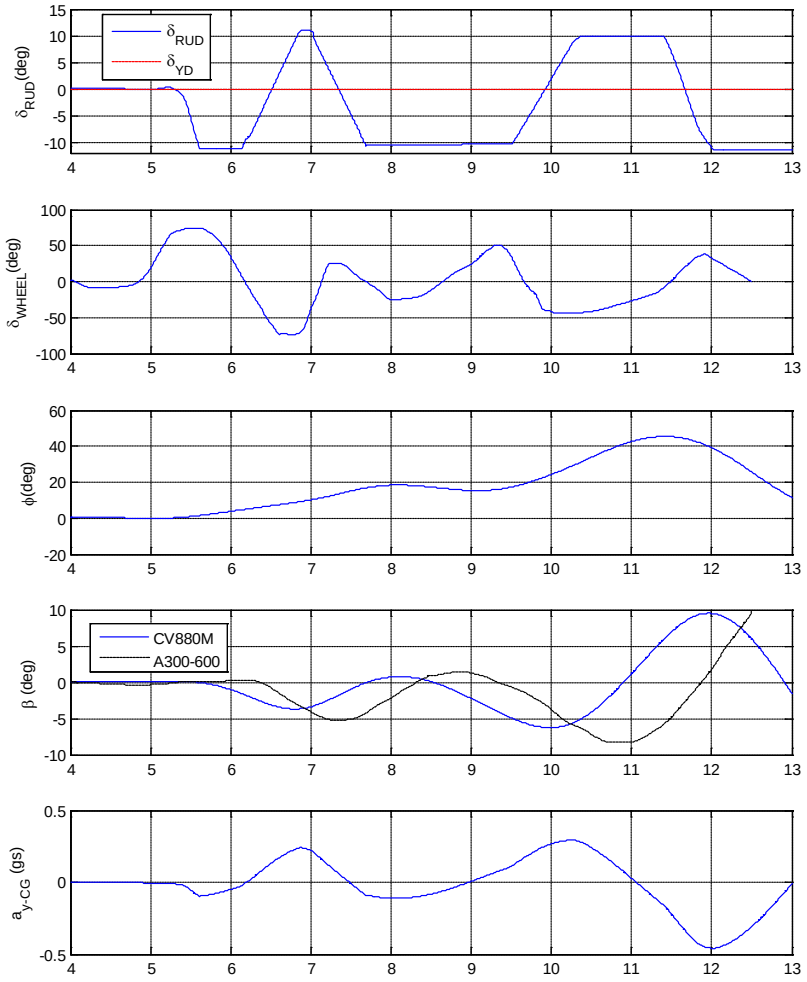

Figure 28 Response of Convair 880 Model and A300-600 to Pilot Inputs from AA 587 accident with the Yaw Damper Disabled, and 50% Increase in Rudder Control Power

The time history of the sideslip angle from the inflight structural failure scenario (from Figure 14) is also shown for comparison. The questions raised by this analysis are:

- What design feature(s) would cause a saturated yaw damper to not deflect the rudder in a direction to reduce yaw rate and sideslip? One example is described in Section 3.3.1.
- What design feature would cause the rudder to deflect to 11 degrees when the mechanical limiter is set at 9 degrees?
- What is a reasonable upper limit of rudder control power for transport aircraft?

Finally, data shown later in Figure 33 indicates that ROP was significantly reduced when rudder

control power was increased in this simulation, which was most likely a result of the fact that less rudder was required to provide the desired augmentation of aileron. This would not be the case if the effective dihedral is reduced (low L_β), thereby requiring the pilot to use more rudder to augment aileron.

In summary, a combination of high ROP, high control power, low effective dihedral, and a yaw damper that does not reduce the maximum rudder deflection when saturated, are all contributing factors that lead to large sideslip angles.

5.6 EFFECT OF HOLDBACK

Holdback is defined in Figure **7**. Physically, the holdback force is the force that exists when returning the pedals to neutral, just prior to the pedals being centered. The value of hold back was set to 2 lbs for most of the test matrix to allow the maximum variation in $F_{bo} / F_{\lim}$ (see discussion in Section 3.2).

The reference 4 rudder study showed that values of holdback between 0 and 8 lbs were acceptable. A brief study of the effect of holdback was conducted with four of the subject pilots. This consisted of conducting runs with holdback of 2 lbs and 8 lbs (configurations 35-25-1 and 36-25-1-HB) presented in the blind, and asking the pilots to describe any differences in rudder pedal characteristics. Excerpts of pilot commentary are given below.

Pilot 1 – Pedals felt the same

Pilot 6 first look – Could not tell the difference

Pilot 6 second look – Can feel better return but it would be easy to miss it. Does not affect the way I fly or the ratings.

Pilot 11 – Like this one best (the configuration with higher holdback) but the difference is minor.

Pilot 12 – Cannot tell one from the other

The values of $\left|\beta - \delta_r\right|_{peak}$ were noted for each of the runs and no consistent difference was observed for the different values of holdback.

These results confirm that holdback is not a factor for rudder overcontrol as long as it is kept within the values recommended in reference 4.

5.7 PILOT TECHNIQUE AND SUBJECTIVE RATINGS

As noted above, two distinct types of pilot technique were observed during the simulation – those that did not use rudder until absolutely necessary (technique A) and those that used rudder continuously (technique B). It was also noted that some pilots used techniques A and B. In those cases, the pilot did not use rudder until necessary (technique A) but once in the loop, the tendency was to employ technique B for the rest of the run.

Some pilots were more aggressive than others, and the more aggressive pilots produced higher values ROP. ROP was calculated for each pilot's evaluations for each configuration with the result shown in Figure 29. The symbols indicate the average value of ROP across all configurations for each of the 12 evaluation pilots, and the thick vertical lines represent one

standard deviation in the average value of ROP. The endpoints of the vertical lines represent the maximum and minim values of ROP experienced by the pilot for all of his evaluations.

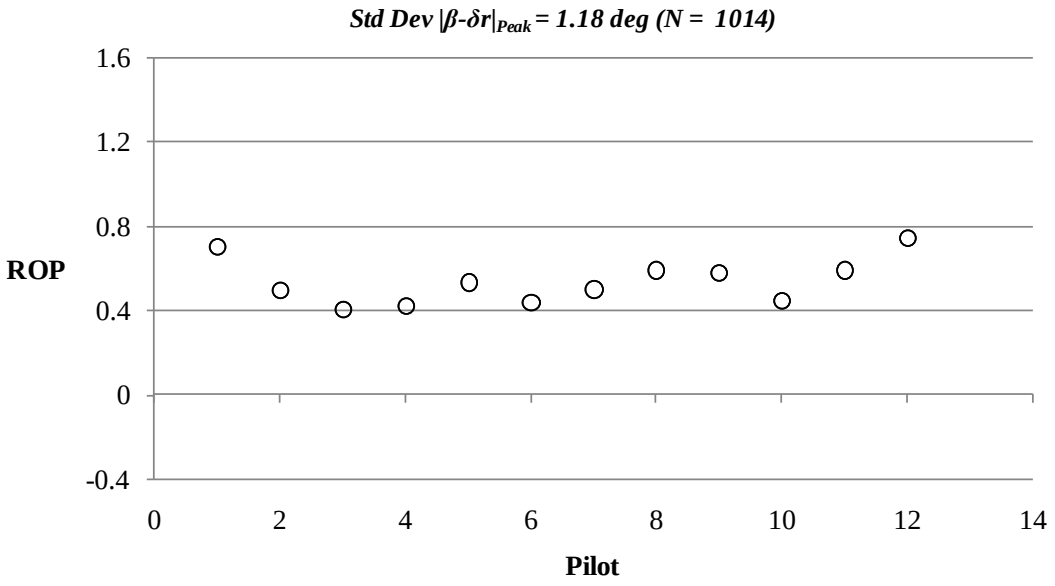

Figure 29 ROP for Each Pilot for All Baseline Configurations

The maximum values of ROP are always associated with the short pedal-throw (1.2 inches) configurations and the minimum values with the long pedal-throw (3.5 inches) configurations.

The variability between pilots is significant, which shows the importance of using a large sample of pilots for this study.

The average subjective overcontrol rating (see rating scale in Figure 5) for each baseline configuration is plotted vs. the value of the rudder overcontrol parameter (ROP) for that configuration in Figure 30 (each point represents a tested configuration).

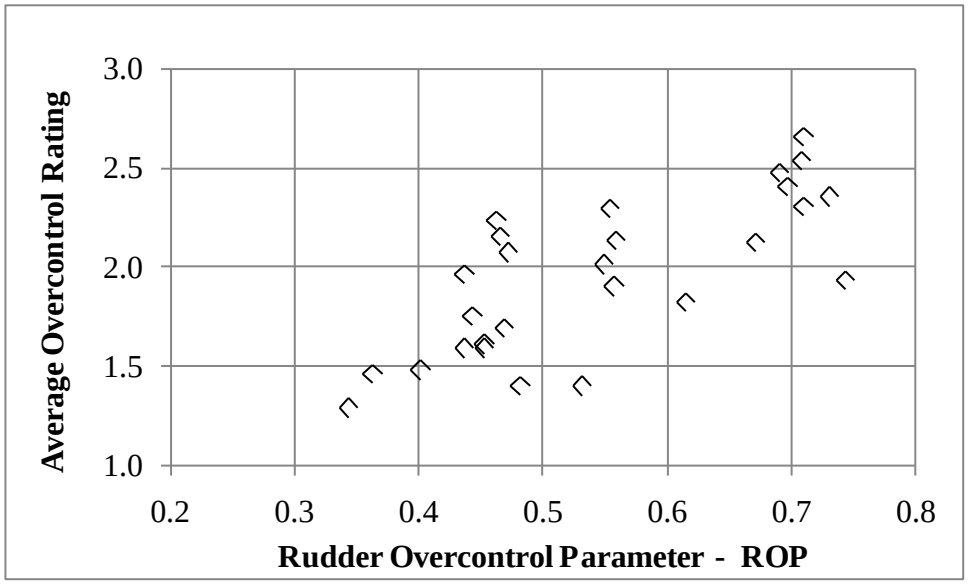

Figure 30 Average Overcontrol Rating vs. Average ROP for Each Baseline Configuration

This data shows a well defined trend toward higher subjective overcontrol ratings with increasing ROP. Ratings less than 3 indicate that, on average, the tendency to overcontrol with rudder was never judged to be worse than "moderate".

The average overcontrol rating is plotted vs. the average value of $F_{3\sigma\ peak}$ for each of the baseline configurations in Figure 31. (recall that $F_{3\sigma\ peak}$ is the largest expected force on the vertical stabilizer and is defined in Section 4.2.)

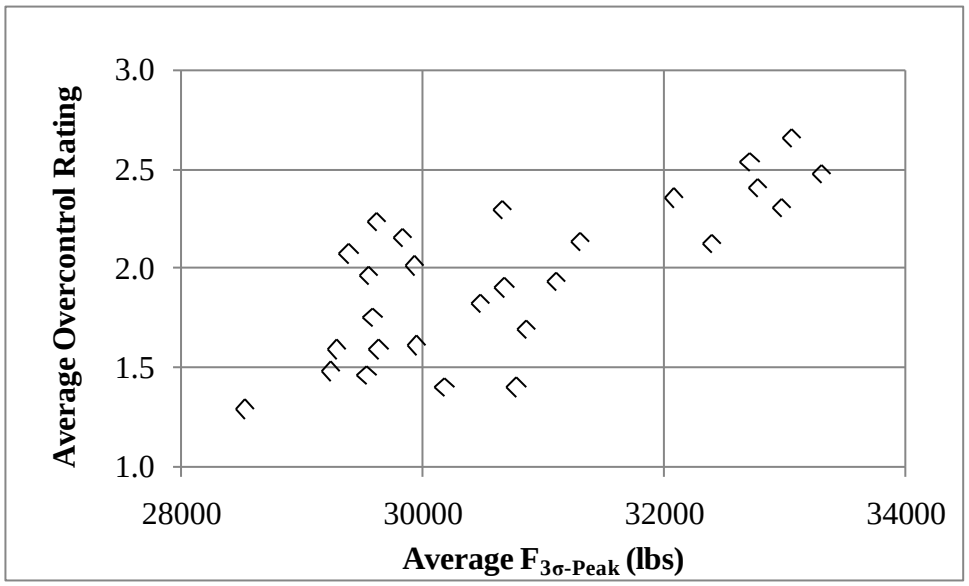

Figure 31 Averaged Overcontrol Rating vs. Averaged $F_{3\sigma\ peak}$.

As expected, the forces imposed on the vertical stabilizer tend to increase in proportion to the

increase in overcontrol rating.

The average Cooper-Harper handling qualities rating (HQR) for each configuration is plotted vs. the rudder overcontrol parameter (ROP) for that configuration in Figure 32.

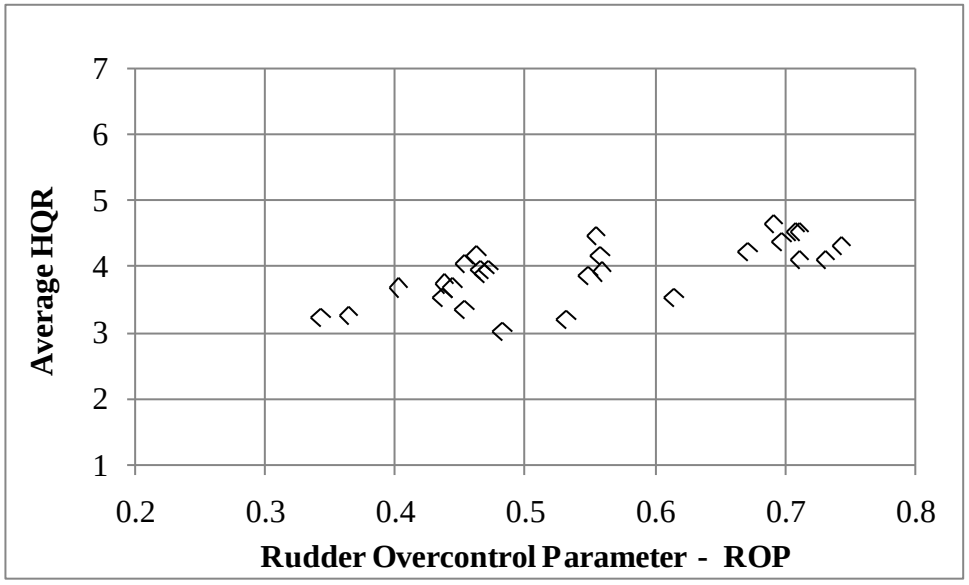

Figure 32 Average HQR vs. Average ROP for Each Tested Configuration

These data indicate a weak trend showing increasing HQR with increasing values of ROP.

There was considerable pilot commentary and discussion during the simulation regarding the assignment of subjective ratings. Most pilots agreed that because the task involved a semi out-of-control situation, it was difficult to separate out the effect of rudder usage when assigning a Cooper-Harper handling qualities rating. Likewise, the overcontrol rating was found to be difficult to assign because most pilots could not decide exactly what constituted overcontrol.

Attempts to define rudder overcontrol in terms of something that a pilot can identify were not successful. The rudder overcontrol parameters defined in Section 4.2 are couched in terms of variables that are not obvious to the pilot (e.g., $|\beta - \delta_r|$). This suggests that there are few cues in the directional axis to warn the pilot of a potentially catastrophic failure, which is a significant consideration in the development of an overcontrol criterion. That is, the criterion cannot depend on pilot cueing in a similar manner to the stick force per g criterion in the longitudinal axis.

5.8 CONTROL POWER

The effect of increased control power was investigated by increasing the rudder authority from 9^o to 12^o degrees for some runs (Configurations 40 through 51 in Figure 8).

The effect of increased control power on excess force on the vertical stabilizer (equation (6), Section 4.2) and the rudder overcontrol parameter is shown in Figure 33.

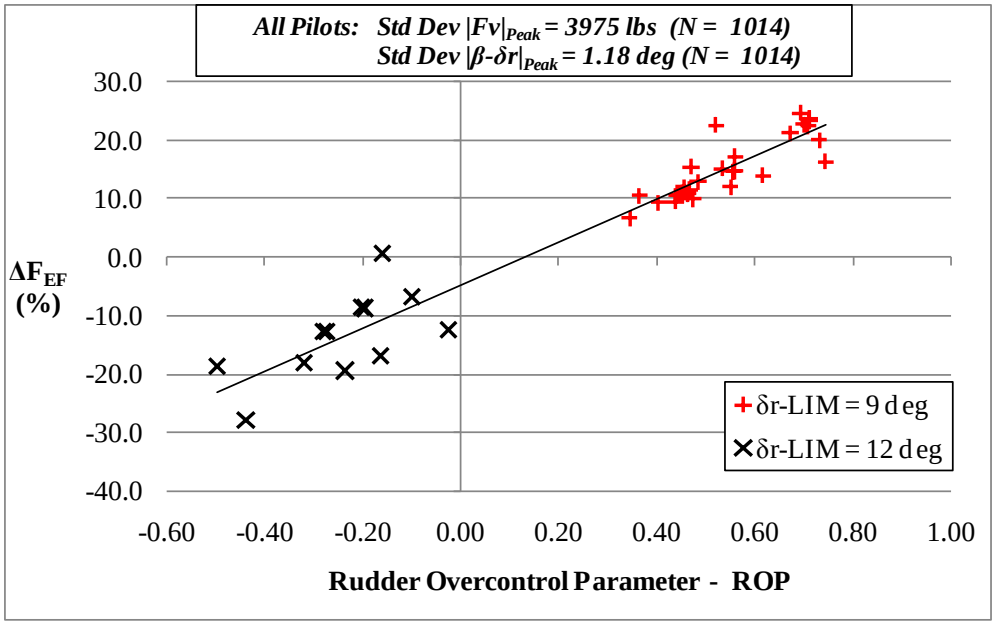

Figure 33 Effect of Rudder Control Power

These results indicate that there is less tendency for overcontrol and therefore lower excess force on the vertical stabilizer for larger values of rudder control power. This is due to two factors:

1. The 14 CFR Part 25.351(d) criterion force ($F_{\beta\max}$) is higher (see Section 4.2) by virtue of the fact that larger steady sideslip angles can be achieved.
2. The pilots were able to achieve the desired effect of augmenting aileron with less rudder input.

These results should not be interpreted to mean that increased rudder control power is desirable because the increase in $F_{\beta\max}$ that goes with increased authority translates into a requirement for increased structural strength and therefore increased weight. Also, there is a tendency to incur larger values of sideslip with higher rudder control power as shown in Figure 25.

6 SIMULATOR MOTION EFFECTS

As noted in Section 2.2, a short exercise was accomplished towards the end of the simulation trials to investigate the use of a higher lateral motion gain (G_{yf} was increased from the nominal value of 0.4 to 0.6). This was accomplished with four of the evaluation pilots and both short pedal-throw and long pedal-throw configurations were evaluated (35-25-1 and 60-15-3 respectively). The excerpted pilot comments were as follows.

Pilot 2 Can definitely feel more lateral acceleration cues with increased motion gain, especially at high frequency. I doubt that it has an effect on my rudder technique. If anything I may tend to be less aggressive with rudder with the higher motion gain because the effect of a rudder input is felt immediately in the seat of the pants.

Pilot 6 Concerned with hitting the wall with the higher motion gain – what we are using is good enough. A little more kick in the seat of the pants. I m putting in the same pedal inputs as I

use with the lower motion gain and see no effect on rating. I forgot the change 2/3 of the way through the run.

Pilot 11 I am more cautious with rudder with the higher motion gains with the short throw configuration. The motion gain has less effect on my rudder behavior for the long pedal-throw configurations.

Pilot 12 I can definitely feel the increased lateral motion. It provides better situational awareness and feels more realistic.

The values of $\left|\beta - \delta_r\right|_{peak}$ were noted for each run with the higher motion gain and the results were unremarkable (i.e., consistent with values obtained with the lower motion gain).

Pilot 11 was especially concerned with lateral motion and made numerous comments during his evaluations regarding the lack of lateral acceleration cues. He felt that the higher motion gain afforded with G_{yf} = 0.6 would provide better results if the motion stop problem could be solved.

One possible approach would be to test the higher motion gain by tailoring the disturbance input so that most of the disturbances in a given run come from one direction. This would make it possible to set the initial condition of the simulator cab near one end of the lateral travel. Several such disturbance inputs would have to be provided so that the cab initial condition could be randomly biased to a point near the right and left ends of the 40 ft VMS travel.

This approach should be investigated for Phase 3 testing. It would be desirable to verify the primary results of Phase 2 with increased motion before proceeding with the Phase 3 objectives. This could be done by testing 3 values of $F_{bo} / F_{\lim}$ for the short pedal-throw configuration and two values of pedal travel (1.2 and 3.5 inches) at a nominal value of $F_{bo} / F_{\lim}$.

7 SUMMARY OF RESULTS

The results of this Phase 2 simulation and data analysis are summarized as follows.

- Very high vertical stabilizer forces result from rudder overcontrol in the presence of a large sideslip angle.
    - Rudder overcontrol is most likely with short pedal-throw designs (on the order of 1.2 inches of travel) than with the 3.5 inch long pedal-throw configurations.
    - Large sideslip angles depend on the details of the yaw damper functionality when the yaw damper is saturated, rudder control power, and effective dihedral.
    - Slightly larger sideslip excursions are more likely with short pedal-throw configurations than with long pedal-throw designs.
- Increasing the maximum pedal force did not noticeably reduce the tendency for rudder overcontrol for short pedal-throw designs.
- Long pedal-throw in combination with higher maximum pedal force was shown to

be an effective way to minimize the probability of rudder overcontrol and to minimize sideslip excursions.

- The forces imposed on the vertical stabilizer were not large enough to cause structural failure based on the 14 CFR Part 25.351(d) criterion, which stated mathematically, is $\Delta F_{EF} \geq 50\%$. That is most likely because of the yaw damper, rudder control power, and effective dihedral used for the aircraft model in this simulation.
- The location of the yaw damper relative to the rudder limiter was not found to significantly affect:
    - The tendency for overcontrol of rudder.
    - The peak values of sideslip.
    - The forces imposed on the vertical stabilizer
- Criteria to limit the possibility of overstressing the vertical stabilizer must include:
    - Lower limits on the maximum pedal travel
    - Specifications on the functionality of the yaw damper in the presence of maximum pedal displacements.
    - Consideration of rudder control power and effective dihedral.

Other conclusions from the simulation are:

- The rudder overcontrol parameter (ROP) was a good predictor of high forces on the vertical stabilizer for a given yaw damper, rudder control power, and effective dihedral.
- Parameters that attempt to quantify the pedal load feel curve nonlinearity such as $F_{bo} / F_{\lim}$, or the Linearity Index are not effective in predicting the tendency for rudder overcontrol with a few minor exceptions:
    - For the 1.2 inch pedal-throw configurations, using $F_{bo} / F_{\lim}$ = 0.25 minimized the tendency for overcontrol. However, this was not nearly as effective as increasing the pedal throw to 3.5 inches.
    - For the 3.5 inch pedal-throw configurations, the optimal range of $F_{bo} / F_{\lim}$ was found to be between 0.25 and 0.42.
- Pilot technique varied significantly between pilots. Some pilots were more prone to overcontrol than others.
- Very low values of breakout, on the order of 5 lbs, in the rudder feel system resulted in degraded pilot opinion due to a “mushy feel”. Low breakout also increased the tendency for rudder overcontrol, especially for short pedal-throw configurations.

8 CONCLUSIONS

Factors that lead to a tendency to overstress the vertical stabilizer have been identified as short pedal-throw limits (less than approximately 3 inches), in combination with a yaw damper that becomes dysfunctional when saturated, and high rudder control power and low effective dihedral. Further work is needed to quantify the effects of the yaw damper, rudder control power, and effective dihedral.

The use of high pedal force gradients is only effective for long pedal-throw designs where the pedal throw is approximately 3.5 inches or greater.

Nonlinearities in the load-feel curve are not a significant factor for rudder overcontrol

9 RECOMMENDATIONS

Short pedal-throw has been identified as a primary contributor to rudder overcontrol. However, the tendency to overstress the vertical stabilizer also requires large sideslip angles. It is recommended that the Phase 3 study focus on factors that lead to large sideslip angles when augmenting aileron with rudder. These are:

- A yaw damper that becomes dysfunctional in terms of reducing rudder travel in the presence of maximum or near maximum pedal deflection.
- High rudder control power in combination with low effective dihedral

Include a subset of runs in Phase 3 to check the effect of increased motion. Bias the initial condition of the simulator cab and disturbance inputs so that the simulator does not hit lateral stops with increased motion.

APPENDIX A RUDDER FLIGHT CONTROL SYSTEMS

Generic versions of the three types of rudder flight control systems included in this study are given in this section. These are the same models that were used in the Phase 1 simulation, except that cable stretch was assumed to be zero in Phase 2. This was done so that rudder control power was the same for the low and high values of rudder pedal force. Another deviation from Phase 1 was that the maximum rudder and pedal deflections were not allowed to vary with airspeed. This was done to ensure that rudder control power did not vary if the pilot deviated from the target airspeed of 250 kts.

As in the Phase 1 tests, the effects of structural compliance were not simulated. If the pilot applies a force of approximately 50 lbs to the pedal on a typical transport rudder flight control system, structural compliance accounts for approximately 2% of the total pedal travel, which is judged to be insignificant for the purposes of this experiment.

A.1 VARIABLE GEARING

The variable gearing design was used to simulate the long pedal-throw designs. It is the only practical implementation for systems with long pedal-throw.

The block diagram to simulate a generic variable-gearing system is shown in Figure **34** below.

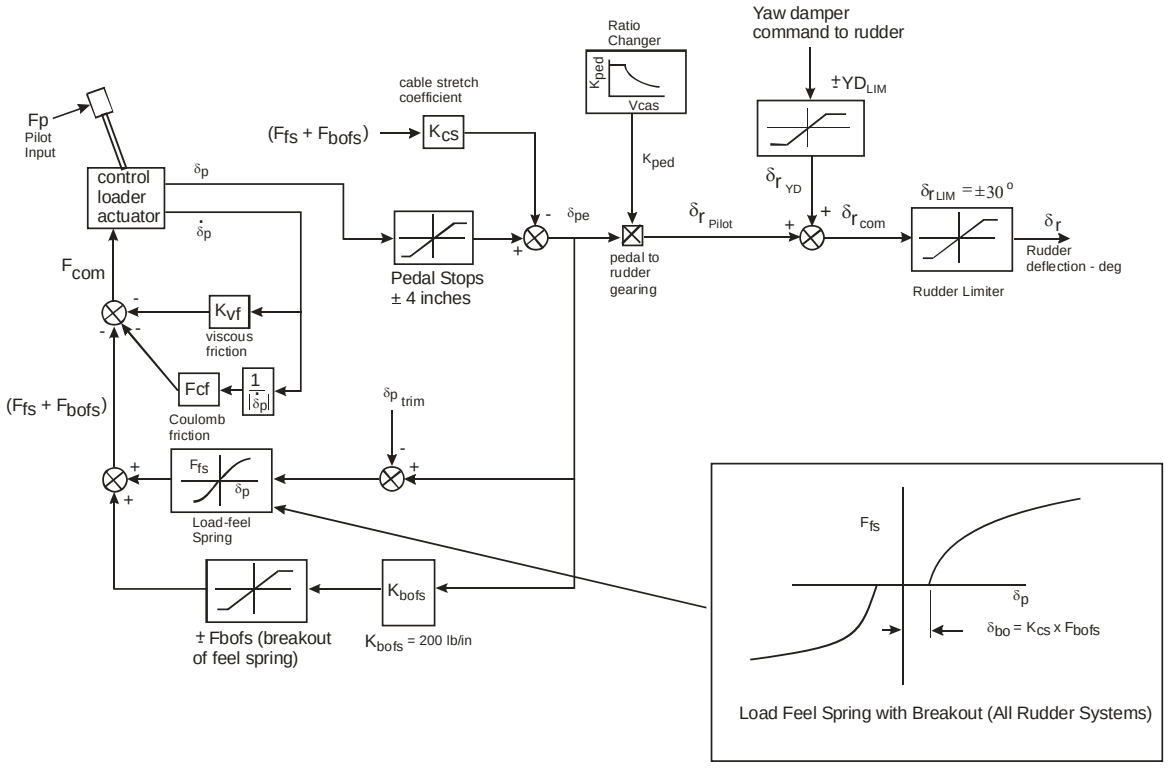

Figure **34** Generic Variable-Gearing Rudder System

The force command to the control loader actuator (F_{com}) is the sum of the viscous friction,

Coulomb friction, load-feel spring, and breakout of the load-feel spring. Pedal motion occurs when the pilot force is not equal to F_{com}.

The pedal stops are achieved within the control loaders by increasing the spring force to a very large value. This is constant for the Variable Gearing system, but is a calculated variable in the Variable Stop (Figure **37**) and Force Limit systems (Figure **39**).

Note that because K_{bofs} is a large number (100 lb/in), the feel spring breakout is a constant (F_{bofs}) for pedal deflections above approximately 0.10 to 0.20 inches (F_{bofs} / K_{bofs}), and has the sign of the pedal deflection.

Cable stretch is accounted for as a result of the sum of the feel spring and feel spring breakout forces. This assumes that the rudder feel spring is located at the aft end of the aircraft near the rudder. δ_{ped} is the "effective pedal travel", which is defined as the pedal travel that contributes to moving the rudder. It is always slightly less than the actual pedal travel due to cable stretch.

A provision for rudder trim is included in the model, to show where it will be included in later testing. For the pilot tasks used in this experiment (Figures 1 and 2), there is no need for rudder trim, so it may be excluded.

Variable-gearing systems reduce the rudder control gearing (K_{ped} = ratio of rudder travel to pedal travel) as a function of airspeed or dynamic pressure. As a result, the total pedal travel does not change, but the gradient of rudder surface deflection-to-pedal travel decreases as airspeed increases.

Note that the rudder is not mechanically limited, its maximum travel being "limited" solely by the reduced gearing between pedal and rudder. The Variable Gearing is usually accomplished by means of a mechanical ratio changer (e.g., a variable lever arm). Since the yaw damper is always in series with the pedals (i.e., yaw damper does not cause pedals to move), the yaw damper servo effectively sums with the output of the ratio changer. As a consequence of this, the sum of the yaw damper input and pilot pedal motion can cause the rudder to momentarily exceed its theoretical limit. The advantage of this is that the yaw damper continues to perform its function regardless of the magnitude of the pilot input. The disadvantage of such a system is that a hardover failure could cause the rudder to move full travel (30 degrees) at any airspeed. As noted in Reference 8 (section 1.6.2.2), the motivation for Airbus to change from a Variable Gearing system in the A300B2/B4 to a Variable Stop system in the A300-600 was that "it was less complex and had less severe failure modes".

The rudder pedal limits for the Variable Gearing system are fixed at ± 4 inches. Rudder limiting is achieved by reducing K_{ped} as a function of airspeed as shown. The schedule of K_{ped} vs. calibrated airspeed is made such that the rudder deflection at full pedal is identical to the Variable Stop system at full pedal, at the same calibrated airspeed. The difference between the systems for this experiment is that full pedal will be 4.0 inches for the variable-gearing system, and 1.2 inches for the Variable Stop and Force Limit systems.

The variation of maximum rudder deflection as a function of airspeed is typically inversely proportional to the square of calibrated airspeed. i.e., dynamic pressure. The generic curve in Figure **35** reflects this relationship with minor adjustments based on a review of available data for

(Douglas/Boeing and Airbus).

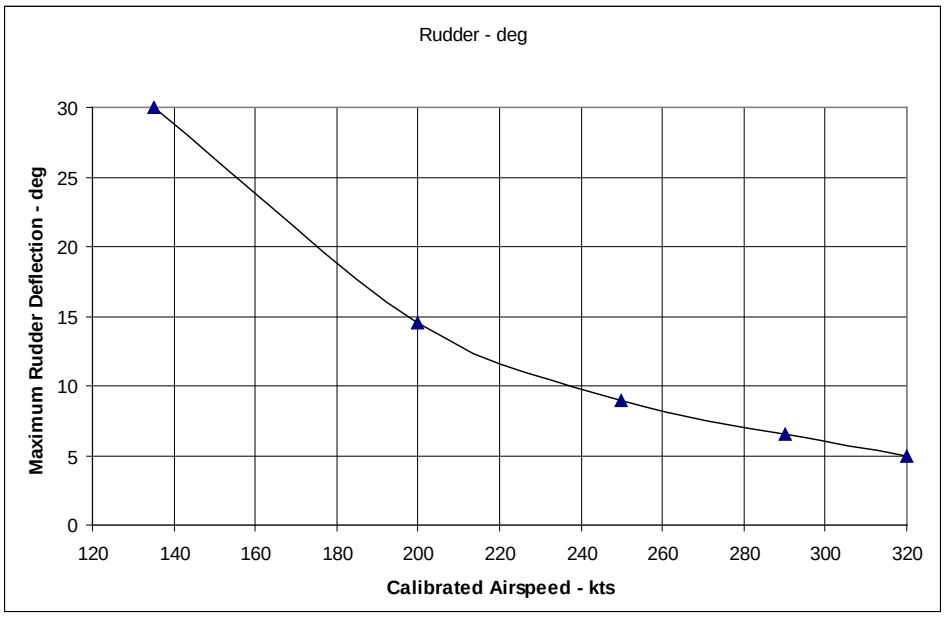

Figure **35** Limit on Rudder Travel as a Function of Calibrated Airspeed - Variable Gearing

The pedal deflection at airspeeds below 135 kts is based on a pedal-to-rudder gearing of K_{ped} = 7.5 deg/in. This gearing is calculated to produce 30 deg of rudder deflection when the pedal is deflected 4.0 inches (i.e., $Kped = \delta_{rMAX} / 4$). At calibrated airspeeds above 135 kts, $\delta_{r_{MAX}}$ is reduced (Figure **35**), and the resulting variation in K_{ped} with airspeed is shown in Figure **36**.

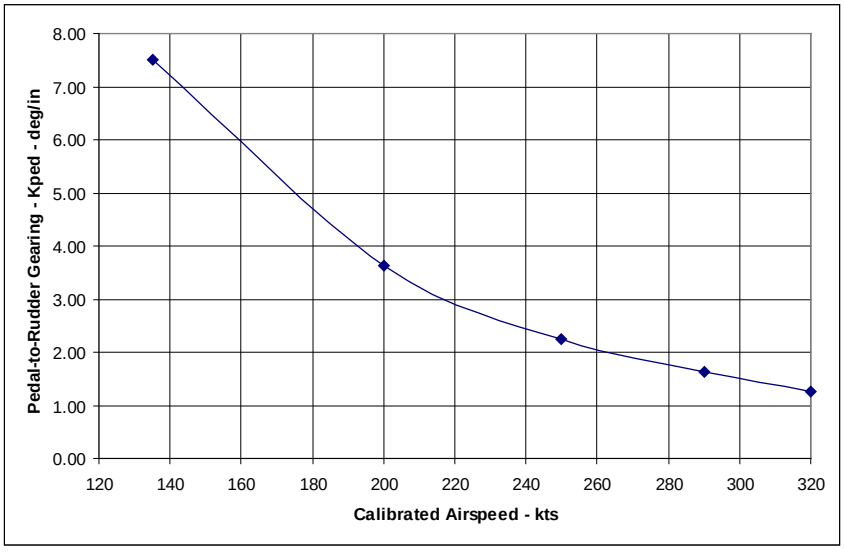

Figure **36** Variation of Kped with Airspeed - Variable Gearing

In this experiment airspeed was nominally constant at 250 kts. Nonetheless, the nonlinear ratio

changer is necessary to account for the effect of changes in the pedal-to-rudder gearing with airspeed changes during the run.

The variation in rudder gearing with airspeed was not used in the Phase 2 simulation and the rudder gearing was set so that 3.5 inches of pedal travel resulted in a rudder deflection of 9° for the baseline configurations and 12° for the high control power configurations.

A.2 VARIABLE STOP

The Variable Stop design results in short pedal-throw. It was therefore used to simulate the configurations with 1.2 and 2.4 inch pedal-throw.

In this design, the rudder pedals and rudder surface are mechanically limited as a function of airspeed. The control gearing between rudder surface and rudder pedal (K_{ped}) remains constant.

The block diagram to simulate a generic Variable Stop system is shown in Figure **37** below.

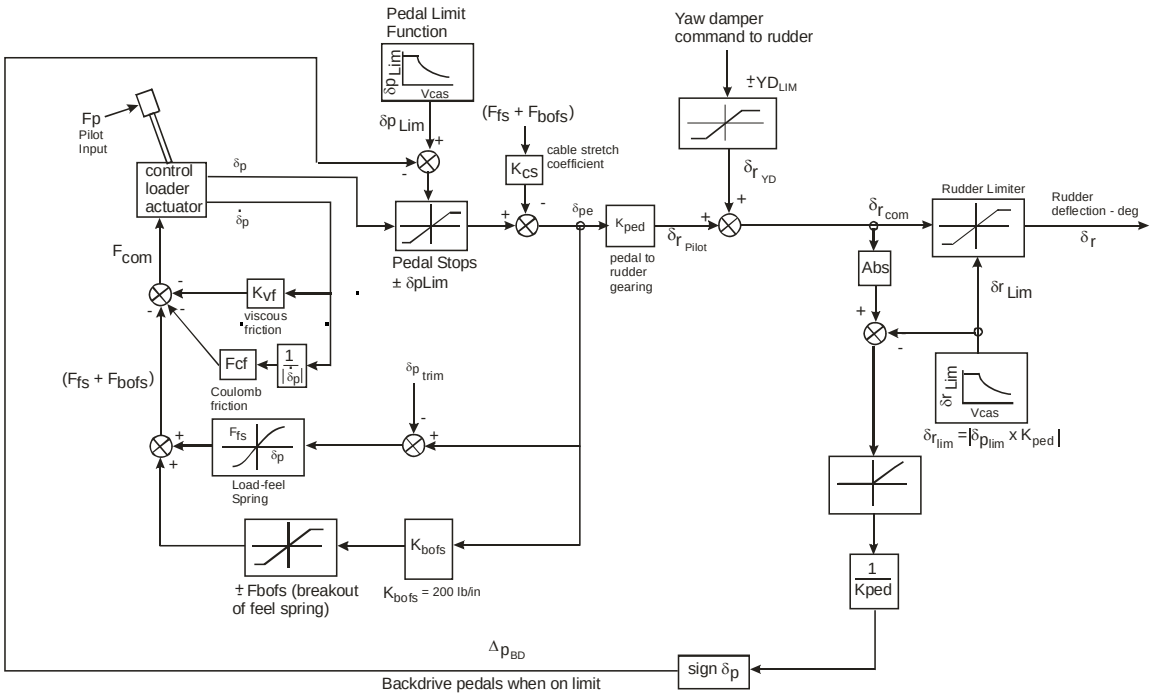

Figure **37** Generic Variable Stop Rudder Control System

The pedal stop is a calculated variable in this mechanization. The A-300-600 Variable Stop function is achieved by means of a mechanical limit on rudder travel that is varied as a function of airspeed. The commanded rudder position ($\delta_{r_{com}}$) is determined by the sum of the pilot's rudder pedal input ($\delta_{p_{pilot}}$) and yaw damper command ($\delta_{r_{YD}}$). Since $\delta_{r_{\lim}} = \delta_{p_{\lim}} \times K_{ped}$, the only way for $\delta_{r_{com}}$ to exceed the rudder limit is via yaw damper inputs that occur simultaneously with a large pedal input. According to Reference 8, yaw damper inputs that cause the rudder limit to be exceeded result in the pedal being pushed aft while the rudder position remains constant on the

limit. This is simulated by the Δp_{BD} input to the control loader in Figure **37**. This is not shown as a force input to denote that it cannot be resisted by the pilot because the hydraulic system forces are very high.

The variation of maximum rudder deflection with airspeed is identical to that used for the Variable Gearing system. The variation of pedal deflection limit with calibrated airspeed was achieved by dividing the rudder deflection by the constant K_{ped} = 7.5 deg/in to achieve the result shown in Figure **38**.

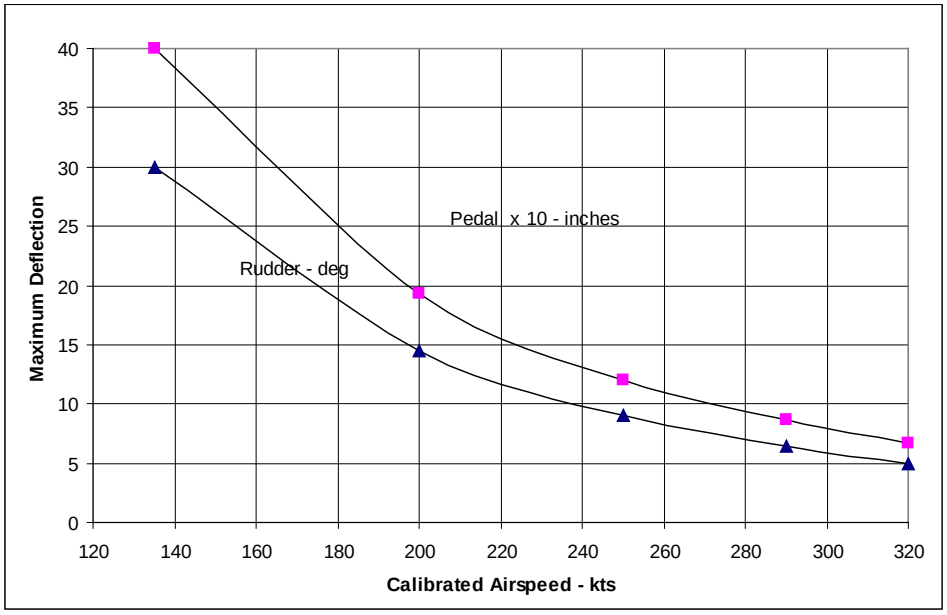

Figure **38** Reduction in Pedal and Rudder Deflection with Airspeed - Variable Stop

The maximum rudder deflection plot shown in Figure **35** and Figure **38** was adjusted slightly to achieve a maximum pedal of 1.2 inches at 250 kts for the Variable Stop system (value common to A300-600, A300B2/B4, A310, A330-300). The maximum pedal deflection of the MD-80 and MD-90 at 250 kts is 1.1 inches.

The variation in maximum rudder deflection with airspeed was not used in the Phase 2 simulation and the maximum rudder deflection was set to 9^o for the baseline configurations and 12^o for the high control power configurations.

A.3 FORCE LIMIT

This system was not tested in Phase 2 due to a lack of sufficient simulator time to get through the entire test matrix. It was tested in Phase 1, and showed good resistance to overcontrol. This resistance to overcontrol is not well understood, and additional testing in Phase 3 is recommended.

The Force Limit rudder system is intended to prevent excessive loads on the vertical stabilizer and rudder. This is typically done by limiting the rudder hinge moment, which is assumed to be proportional to the loads on the vertical stabilizer and rudder. The rudder hinge moment is given

as:[1]

$$H_{M_r} = S\bar{c}\frac{\rho_0}{2}V_{CAS}^2 C_{Hr}(\delta r, \beta) \qquad \text{A-1}$$

Where S = rudder area, $\bar{c}$ = m.a.c. of rudder, ρ_0 = sea level air density = .00238 slug-ft^2, V_{CAS} is the calibrated airspeed, and C_{Hr} is the rudder hinge moment coefficient which is a function of rudder deflection and sideslip angle. It is important to note that β is the aerodynamic sideslip angle, i.e.,

$$\beta = \beta_{inertial} - \beta_{gust}$$

$$where\ \beta_{inertial} = track\ angle - heading\ angle$$

The Force Limit system usually operates by providing a method to bypass hydraulic fluid around or through the actuator piston, such as by drilling an orifice in the piston. This bypass is set so that the actuator will stall at some level of reactive force (i.e., rudder hinge moment divided by lever arm). Once the actuator stalls, the pilot can move the control valve by increasing pedal deflection until the control valve bottoms. However, when the actuator is stalled, the inflow of hydraulic fluid is equal to the flow through the orifice, and therefore the actuator piston does not move, and hence the rudder does not move. Inherent in this design is the fact that the rudder pedal must move through some stroke, $\Delta\delta_p$, (typically about 0.7 inches) before the control valve bottoms. The rudder surface does not move during that interval. Once the control valve bottoms, additional force on the pedals is transmitted directly to the rudder surface. The aerodynamic loads are sufficiently high, that this is equivalent to a hard stop.

Simulation of a generic Force Limit rudder flight control system is accomplished with the block diagram shown below in Figure **39**.

[1] The total force on the vertical stabilizer is a result of rudder deflection and sideslip. Limiting the rudder hinge moment to a value that limits rudder deflections that would exceed the allowable loads on the rudder mitigates the chances of exceeding the limit loads. However, the rudder hinge moment is an indirect measure of load on the vertical stabilizer, and it may be possible to exceed the allowable load due to certain combinations of sideslip and rudder deflection, with an operational Force Limit system.

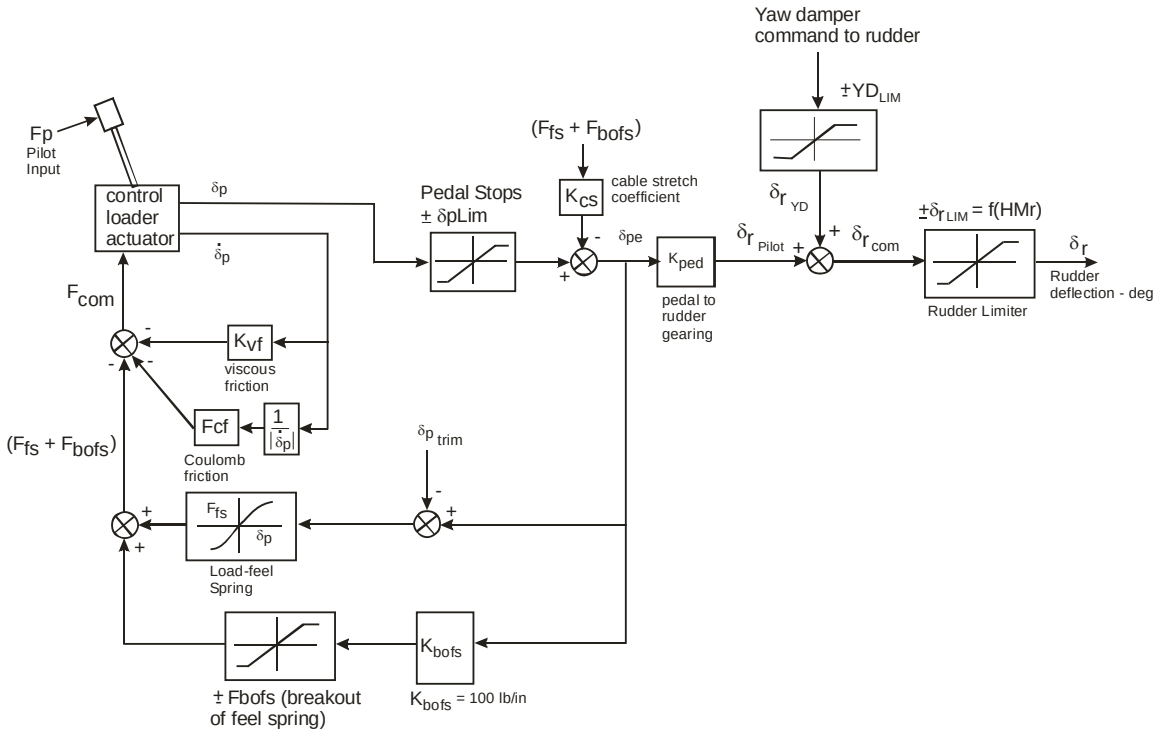

Figure **39** Generic Force Limit Rudder Control System

The pedal stops are variable in this mechanization, and are a function of rudder hinge moment as described below. Note that if the aircraft is accelerated with a large rudder deflection, the effect should be to backdrive the pedals (as the value of the pedal limiter is reduced).

The commanded rudder is the sum of the pilot pedal input and yaw damper. A combination of large pedal input and yaw damper activity could cause hinge moment limiting, and render the yaw damper ineffective. For mechanical implementations of this system, it would not be practical to sum the yaw damper input downstream of the rudder limiter. However, for a fly-by-wire implementation it would be possible to set limits only on the portion of the input due to pedal, leaving the yaw damper to operate independent of pedal input.

As long as the rudder hinge moment (HMr) is equal to or less than the maximum specified hinge moment (HMr_{max}), the rudder deflection is proportional to the pedal input according to the control gearing, K_{ped}. When the rudder hinge moment increases above HM_{max}, the rudder actuator stalls resulting in a effective rudder deflection limit, $\pm\delta_{rLIM}$. The calculation of the rudder limit is derived below. The pedal stop limiter is set to allow the pedal travel required to reach the rudder limit, and then to bottom the servo valve, $\Delta\delta_p$. Therefore, the pedal limiter is set as follows.

$$\delta_{pLIM} = \frac{1}{K_{ped}}\delta_{rLIM} + \Delta\delta_p \, sign(\delta p) \qquad \text{A-2}$$

For this series of experiments the rudder travel to bottom the control valve ($\Delta\delta_p$) shall be set to 0.7 inches.

The rudder limit (δ_{rLIM}) is set by calculating the rudder deflection that results in HMr_{max} as follows. The rudder hinge moment coefficient corresponding to HMr_{max} is:

$$CH_{r\max}(\beta,\delta_r) = \frac{HMr_{\max}}{KrV_{CAS}^2} \qquad \text{A-3}$$

$$where: \quad Kr = \frac{1}{2}S\bar{c}\rho_o$$

S = area of rudder and $\bar{c}$ = mean aerodynamic chord of rudder

The rudder hinge moment characteristics to be used in this simulation are a generic representation of large transport aircraft rudders. The variation of hinge moment with sideslip tends to be highly nonlinear as shown in Figure **40**.

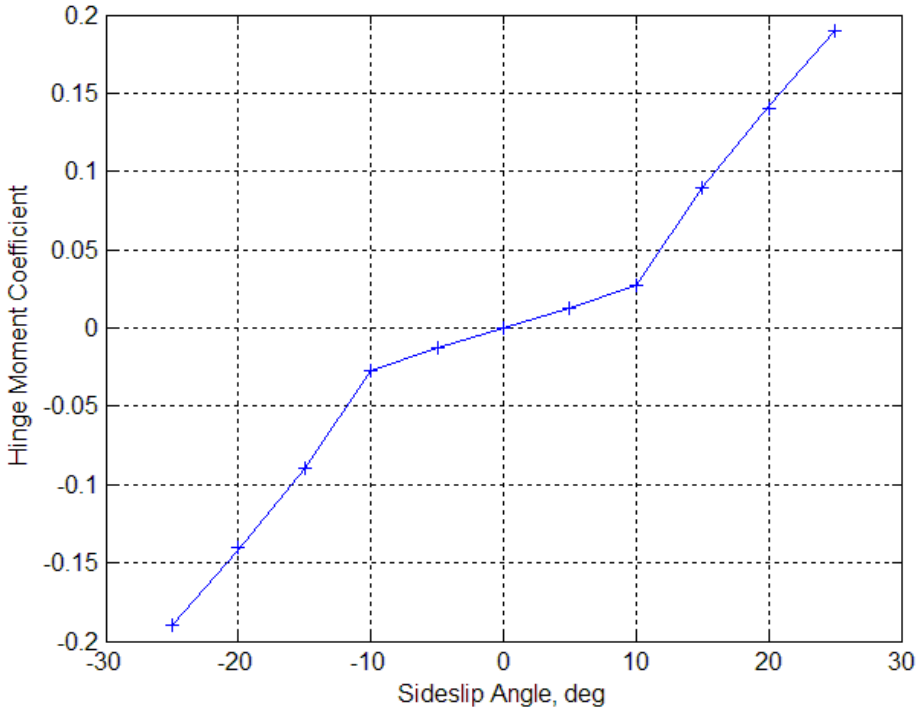

Figure **40** Generic Variation of Rudder Hinge Moment With Sideslip

The plus signs in Figure A-7 indicate the results of a 5th order polynomial fit to the solid line as follows.

$$CH(\beta) = [4.9\times10^{-7}\,|\beta^5| - 3.21^{-5}\beta^4 + 7.16\times10^{-4}\,|\beta^3| - 6.04\times10^{-4}\beta^2 + .0186\,|\beta|]sign\beta \qquad \text{A-4}$$

Where β is in degrees. The variation of the hinge moment with rudder deflection is well represented as a linear function for rudder deflection angles less than 20 degrees as follows.

$$CH(\delta_r) = C_{H_{\delta r}}\delta_r$$

$$where: C_{H_{\delta r}} = -.009\,1/\deg \qquad \text{A-5}$$

The total hinge moment is:

$$CH(\beta,\delta_r) = CH(\beta) + CH(\delta_r) = CH(\beta) + C_{H_{\delta r}}\delta_r \qquad \text{A-6}$$

The maximum hinge moment occurs when the rudder is on its limit:

$$CH_{r\max}(\beta,\delta_r) = CH(\beta) + C_{H_{\delta r}}\delta_{r_{LIM}} = \frac{HMr_{\max}}{KrV_{CAS}^2} \qquad \text{A-7}$$

Finally, solving for the rudder limit:

$$\delta_{r_{LIM}} = \left[\frac{HM_{\max} sign(\delta_{ped})}{KrV_{CAS}^2} - CH(\beta)\right]\frac{1}{C_{H_{\delta r}}} \quad (V_{CAS} \text{ in ft/sec and } \delta_{r_{LIM}} \text{ in deg.}) \qquad \text{A-8}$$

Where $CH(\beta)$ is calculated from the fifth order polynomial in Equation A-4. Recall that the pedal deflection when the rudder is at the limit is calculated from Equation A-2.

The value of the rudder hinge-moment limit (HM_{max}) is set to 3508 ft-lbs[1] so that the rudder limit is nominally 8 deg (at zero sideslip), to be consistent with the Variable Gearing and Variable Stop configurations at 250 KCAS. Kr = .27 lb sec^2/ft for the generic rudder configuration used in this experiment.

Recall from Equation A-2 that the rudder reaches its limit at 0.7 inches of pedal ($\Delta\delta_p$) before the pedal reaches its limit. At the 250 KIAS used in this experiment, the rudder limits at 1.2 inches of pedal travel, and the pedal continues to move an additional 0.7 inches. As a result, the final 35% of pedal travel occurs with no response from the rudder ("unproductive pedal travel" = 0.7 inches). Comparison with the Variable Stop configuration with the same pedal travel (compare Configurations 7 and 2) will determine if this is good, bad, or not important.

Equation A-8 shows that for the Force Limit system, the rudder limit depends on the hinge moment limit and aerodynamic sideslip angle. So for example, if the pilot applies and holds a positive (left) rudder-pedal input, a positive sideslip results. From Figure A-7 this results in a positive hinge-moment coefficient, which from equation A-8 causes a higher value of rudder limit ($C_{H_{\delta r}}$ is negative) than would occur with a Variable Stop system, i.e., more control authority. However, if there is a positive sideslip (tending to cause a left roll rate), and the pilot uses negative (right) rudder to decrease the sideslip and thereby reduce the left roll response, the sideslip term in Equation A-8 subtracts from the HM_{max} term, resulting in a decreased rudder limit compared to the Variable Stop system. This scenario was what existed at the time of structural failure of the vertical stabilizer in the AA 587 accident, so it is possible that a Force Limit system would have prevented the failure. This is especially true because the combination of positive sideslip and negative rudder deflection is additive in terms of aerodynamic load on the vertical stabilizer and rudder.

[1] A value of 3947 ft-lbs was used for all runs prior to run 528. This was reduced when pilots noted that Configuration had more control power (rudder was limiting at 9 deg).

A.4 GENERIC YAW DAMPER

A generic yaw damper that is representative of large aircraft was implemented into the simulation math model. Since the primary purpose of a yaw damper is to damp the dutch roll mode, and to enhance turn coordination, all transport yaw dampers have similar dynamic response characteristics. Therefore a single generic yaw-damper that accomplishes that function is judged as adequate for this study. Such a yaw damper is given in the block diagram in Figure **41**.

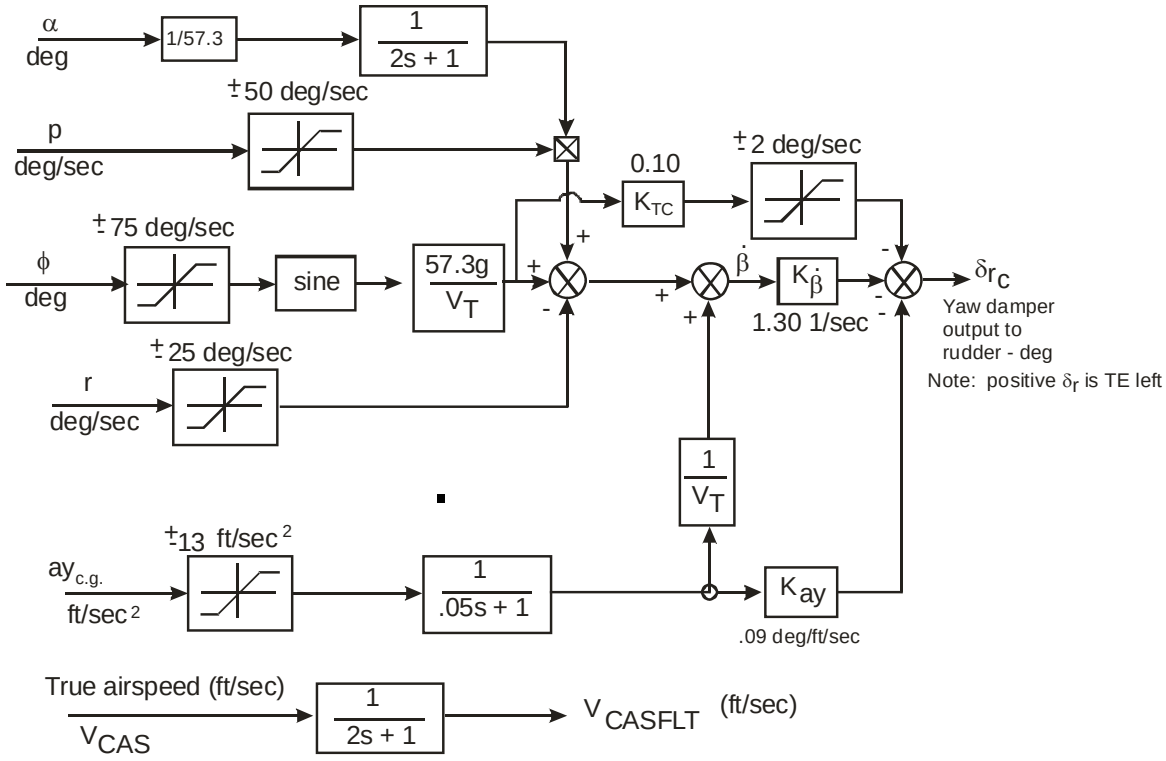

Figure **41** Generic Yaw Damper

This commonly used yaw damper design is essentially a feedback of sideslip rate to rudder, where sideslip rate is calculated as:

$$\dot{\beta} = \frac{ay_{c.g.}}{V_T} + \frac{g}{V_T}\sin\phi - r_{stab}$$

where V_T = true airspeed and $r_{stab} = r\cos\alpha - p\sin\alpha \approx r - p\alpha$.

As shown in the rudder control system block diagrams, the yaw damper authority is limited for each of the rudder system designs. This limit is usually inversely proportional to airspeed above some reference airspeed. For example, Reference 8 notes that the A300-600 is limited to ± 10 deg at and below 165 kts, and to $10(1-165/V_{CAS})$ at airspeeds above 165 kts. This works out to 3.4 deg at 250 kts. By comparison, the Boeing 737NG limits the yaw damper travel to ± 3 deg at 250 kts. The yaw damper limit was fixed at ± 3 deg for this simulation study.

The Version A and B yaw damper implementations (discussed in Section 3.3) are incorporated into the Variable Stop and Force Limit rudder flight control system designs as shown in Figure **42**

and Figure **43**.

Variable Stop

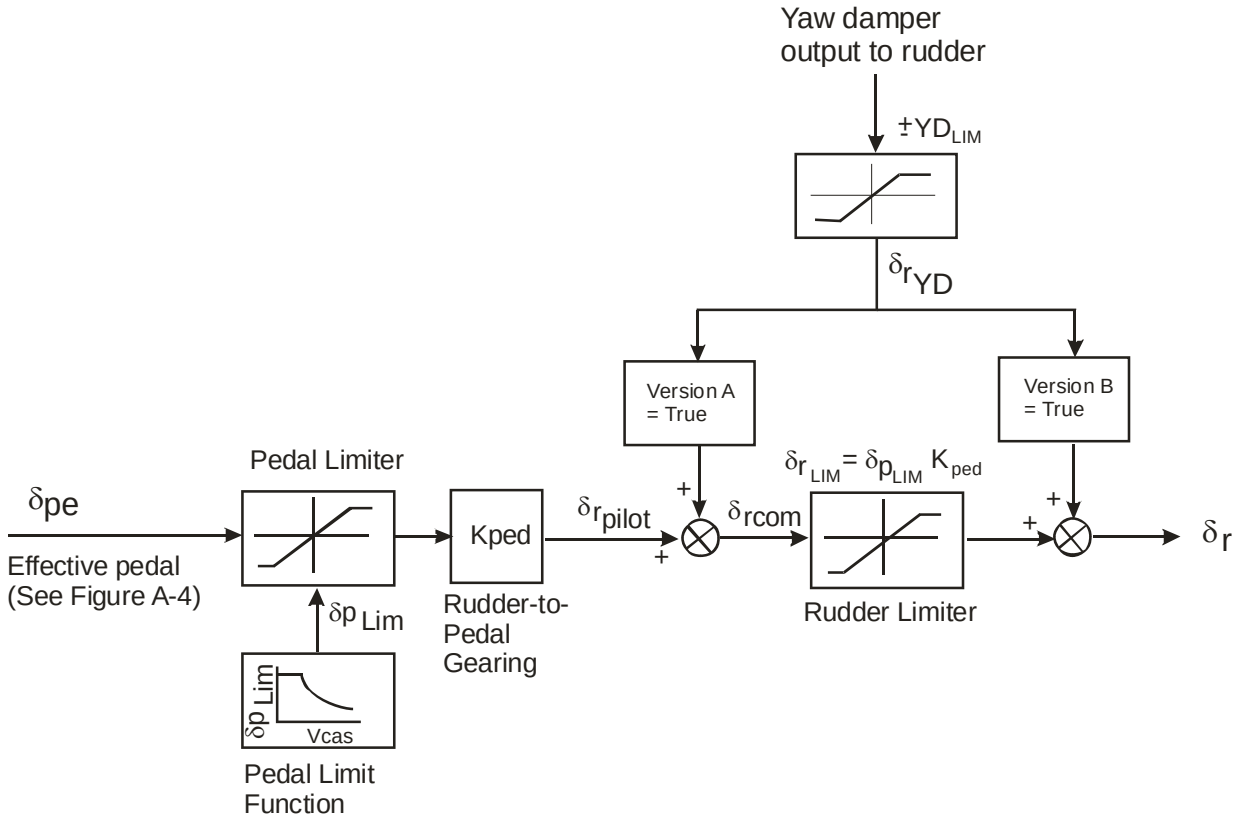

Figure **42** Variable Stop System with Version A and B Yaw Dampers

With this mechanization, there is the possibility that the pilot's rudder command could saturate the rudder limiter so that the Version A yaw damper becomes ineffective.

Force Limit

The block diagram in Figure **43** illustrates how Yaw Damper B would be integrated with a Force Limit system.

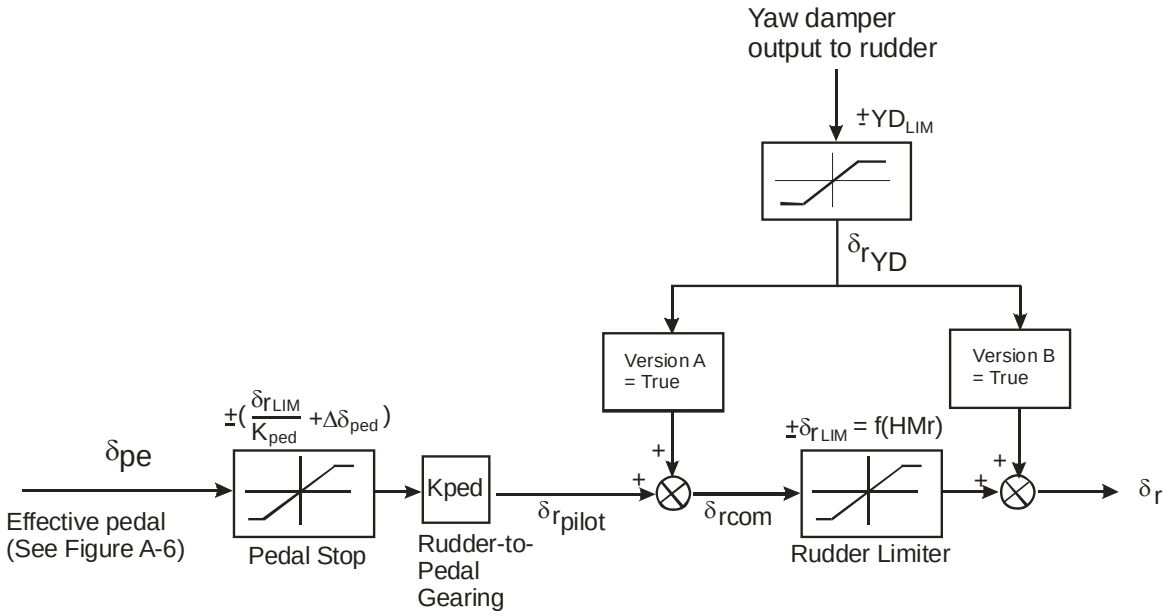

Figure **43** Force Limit System with Version A and B Yaw Dampers

APPENDIX B SIMULATOR MOTION SYSTEM

Pilot generated rudder pedal frequency sweeps of the transport model were obtained with the motion system engaged to characterize the quality of the motion system. An example of one such sweep can be found in Figure 44. An accelerometer was mounted in the center console of the cab to determine the lateral acceleration at the pilot station (AYPILOT) without the possibility of errors in coordinate transformations from accelerometers in the motion base.

The frequency response of the lateral motion system was obtained by applying an DFT to the ratio of (AYPILOT) /(AYPG), where AYPILOT is the output of the lateral accelerometer mounted in the simulator cab next to the pilot, and AYPG is the math model output for lateral acceleration at the pilots station. All transfer function estimates were reduced with STIs FREDA (FREquency Domain Analysis) software. FREDA software executes a traditional DFT over the entire unit circle employing log-binning to average the power of adjacent frequencies to improve overall coherence. The input time histories were conditioned with a cosine taper. The DFT log-binned scale factor was 1.2 with a minimum of 3 points per bin.

The motion system frequency responses for the two motion gain settings employed during the Phase 2 study ($G_{yf} = 0.4 \; and \; 0.6$, where the 0.4 value was used for most of the simulation) are shown in Figure 45 and Figure 46.

Although the high gain response was judged to be more ideal in terms of realistic motion, this gain setting caused the cab to reach software and hardware motion limits and was only used for a few trials as discussed in Section 6. As can be seen in both responses, the magnitude curve is reasonably flat throughout with the phase beginning to roll off near 4 rad/sec.

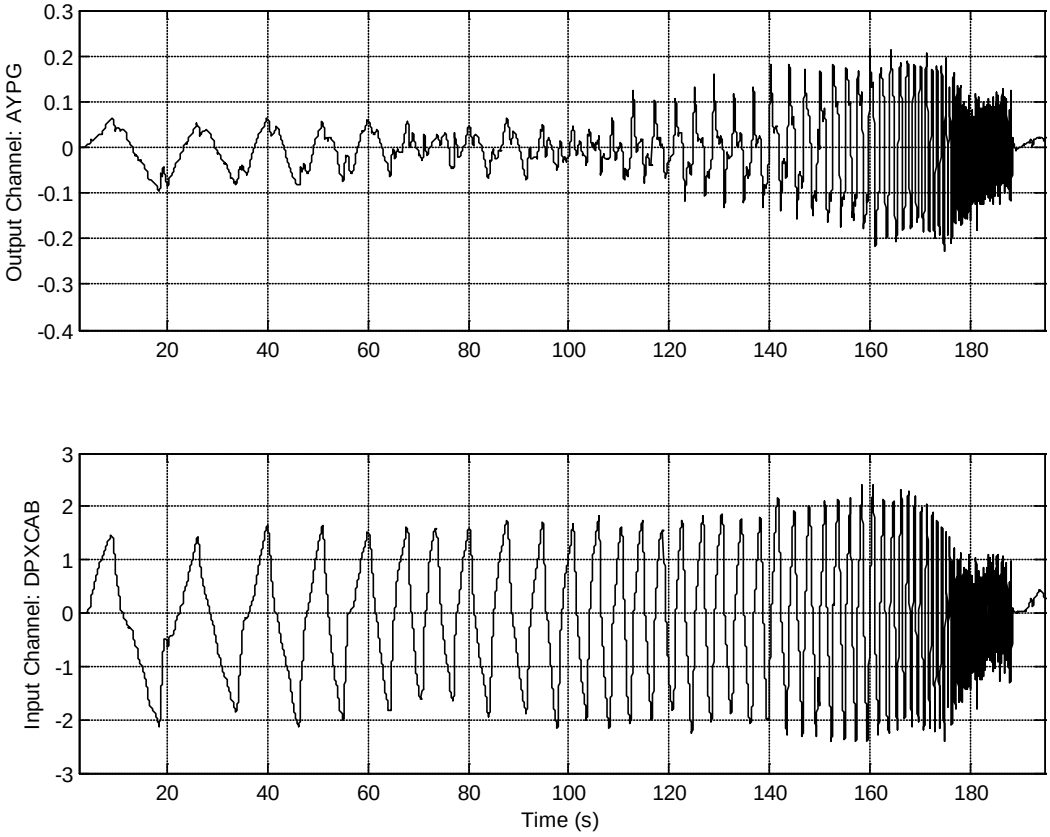

Figure 44. Typical Frequency Sweep

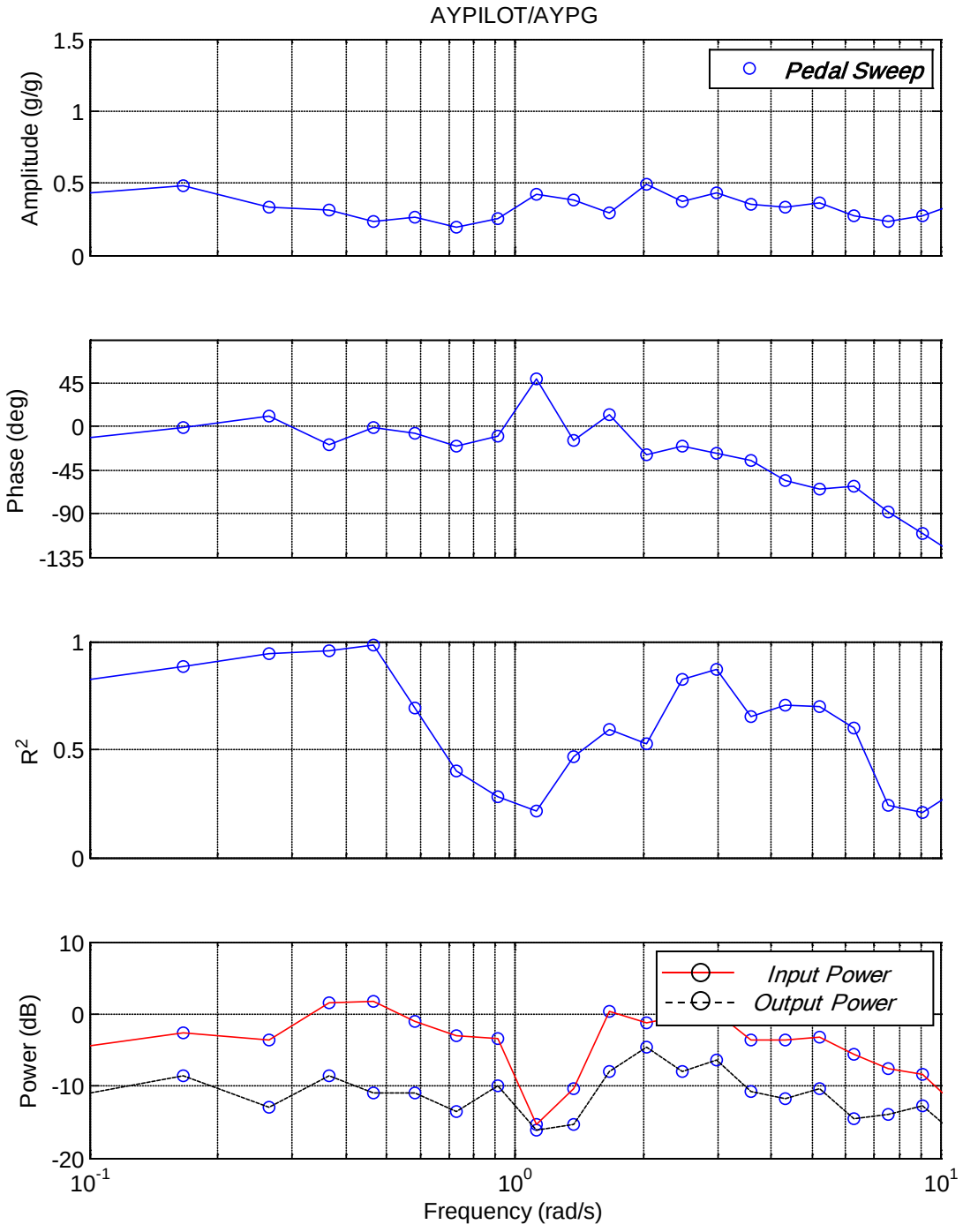

Figure 45. Transfer Function Estimate of VMS Lateral Acceleration Response; Nominal Lateral Motion Gain (G_{yf} = 0.4).

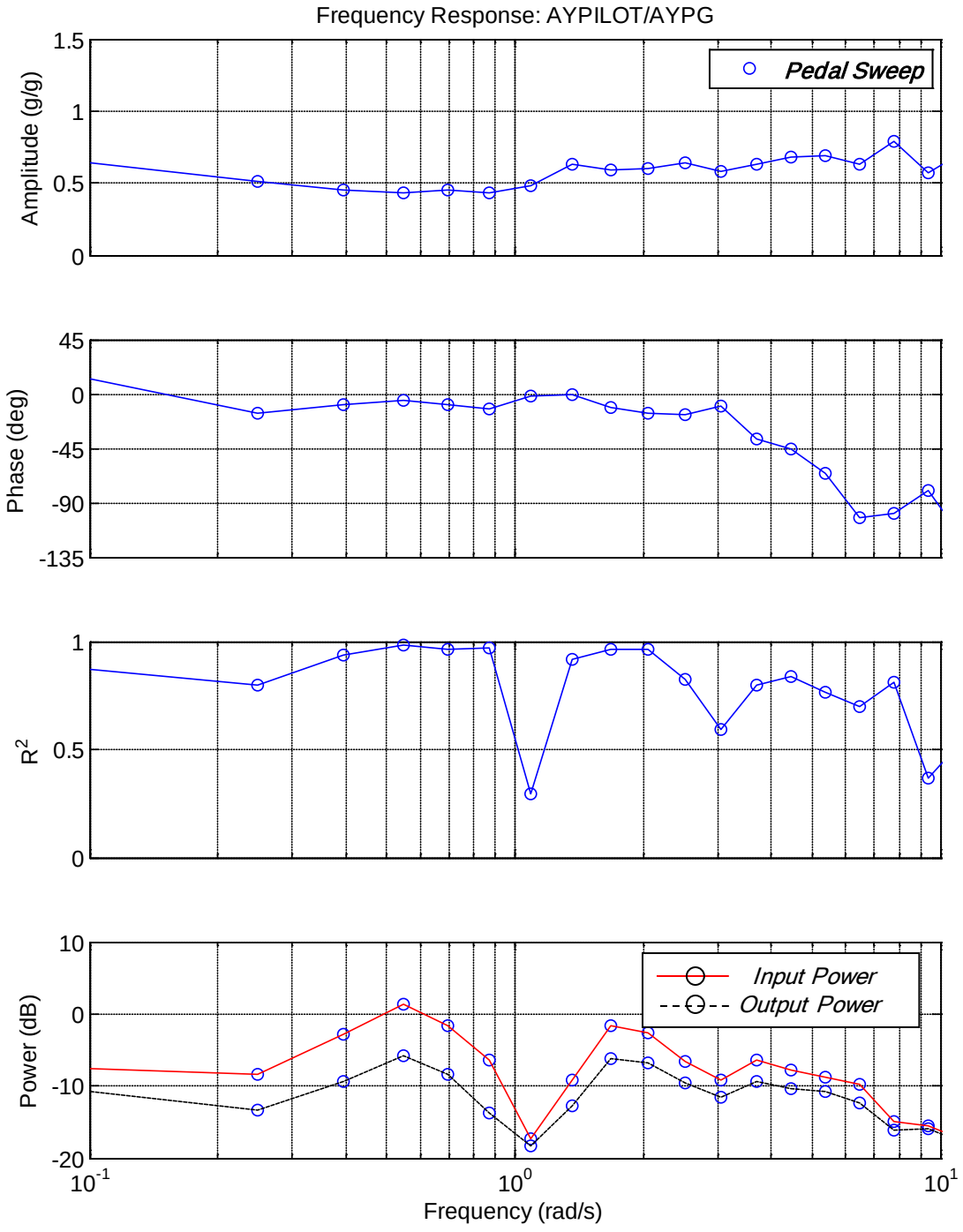

Figure 46. Transfer Function Estimate of VMS Lateral Acceleration Response; High Lateral Motion Gain (G_{yf} = 0.6).

A distinct dip in input power is observed in the vicinity of 1 rad/sec. This leads to decreased

coherence in the vicinity of this frequency. An investigation into the dip in output power was accomplished to make sure that this was not a motion system abnormality. The Power Spectral Density (PSD) plot of the model output *AYPG* in Figure 47 shows that the drop in power near 1 rad/sec is a characteristic of the math model, which is probably related to pilot location ahead of the center-of-gravity.

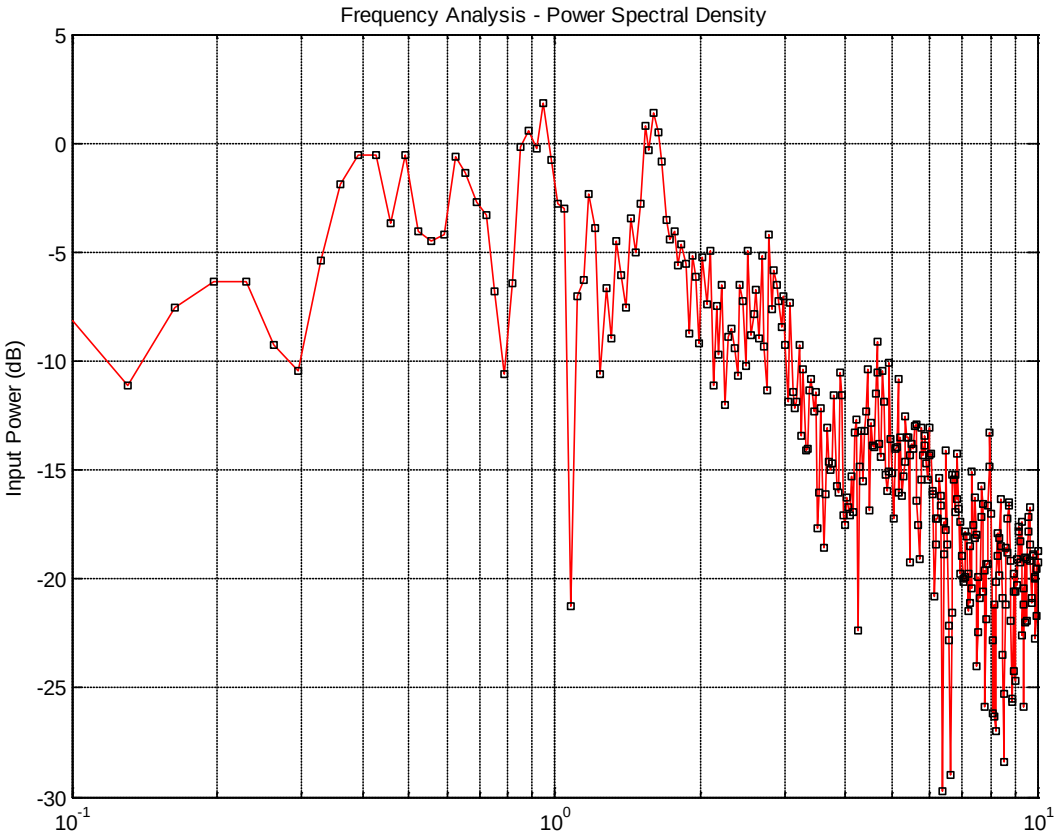

Figure 47. Power Spectral Density of $a_{y\text{-}p}$

The dip in power is also illustrated by observing the frequency response of $a_{y\text{-}p}$ to pedal inputs (Figure 48).

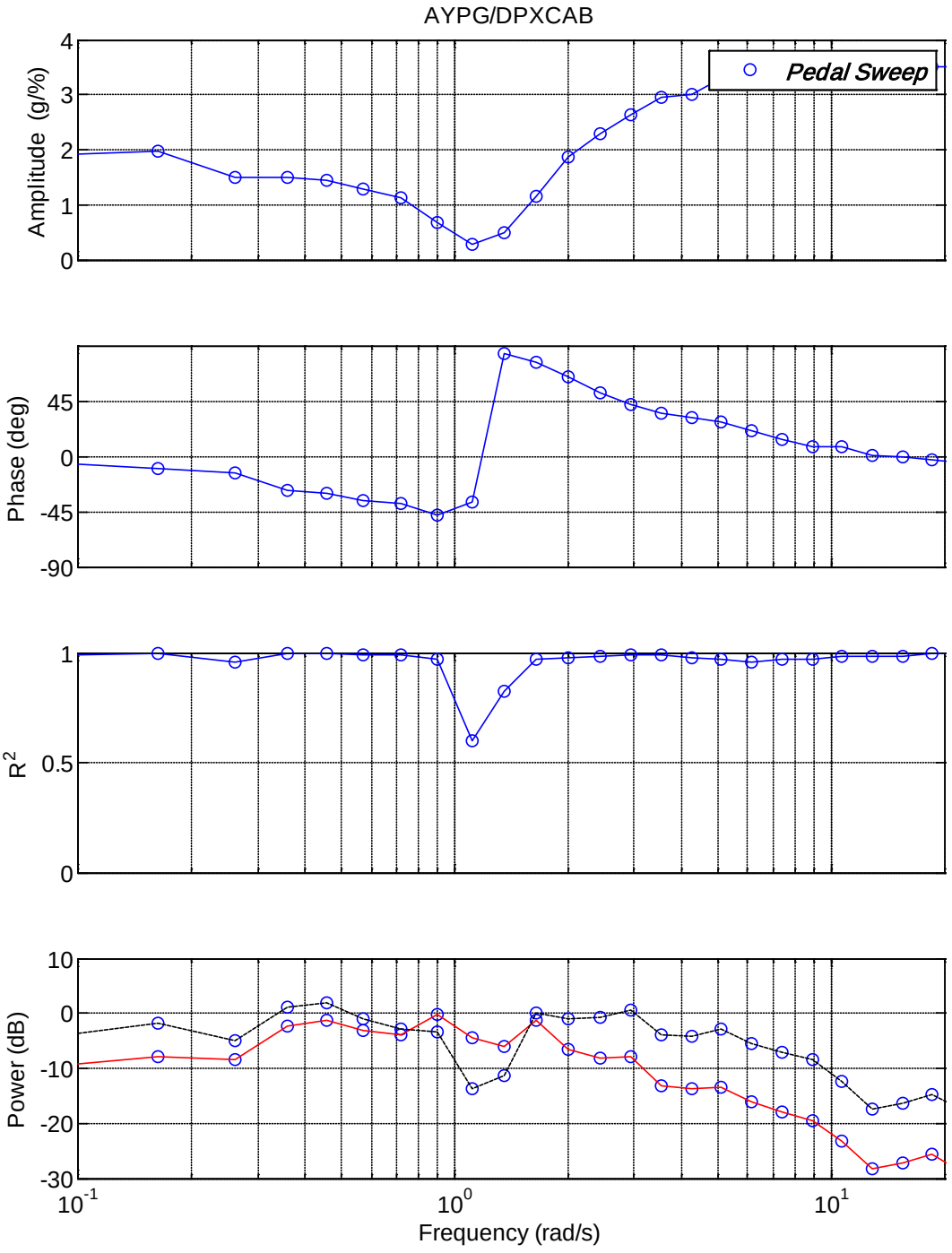

Figure 48. Frequency Response of Pilot Station Lateral Acceleration to Pedal Inputs; Math Model Only

APPENDIX C PILOT BRIEFING

Pertinent excerpts of the briefing that was sent to all pilots who participated in the program.

TESTING

Pilots will fly the task using a matrix of the different directional control system architectures, breakout, feel system curves, etc. Pilot performance data will be automatically recorded, as well as pilot opinions for each configuration via qualitative rating scales and a short questionnaire. Data analysis from Phase I determined that a large amplitude in-flight and/or ground-based simulator is required to complete the study.

The objectives of Phase 2 are to develop the following:

- A methodology for determining the maximum force that the pilot can exert on the vertical stabilizer in the event of an overcontrol event.
- A criterion that can be applied to any rudder flight control system to determine the tendency for overcontrol.
    - Passing this criterion will allow a lighter vertical stabilizer structure
    - Failing this criterion will require a vertical stabilizer structure that can withstand the maximum possible force on the vertical stabilizer (see first bullet).

VMS Protocol

A safety briefing for the operation of the VMS will be conducted prior to the first session of each test pilot by qualified personnel. An Authorization card must be completed and signed by the guest pilot. Pilots will be in constant communication with the simulator operators at all times via intercom. Rest breaks will be taken on an "as-needed" basis and in no case will a single session exceed 45 minutes. In most cases, two subject test pilots will be scheduled simultaneously and will trade out testing on a daily schedule suited to their individual needs and time constraints. A pre-flight briefing and de-brief will be conducted by testing staff. It was found beneficial in Phase I for new subject pilots to initially observe several data runs being performed by "experienced" pilots in the middle of their matrix.

Flight Test General

The simulated aircraft is a generic transport-category swept-wing twin-engined jet aircraft with a conventional planform. Weight is approximately 175,000 lbs. with a nominal c.g. All other physical dimensions are not relevant to the study. The "cockpit" has a conventional yoke and rudder pedals, and the displays are a generic PFD with an EFIS version of "steam-era" engine gauges. There is no autopilot, flight director nor autothrottles. The initial flight condition is steady level flight at 250 KIAS, 2000' MSL on a heading of 300 degrees. Each task will take approximately 75 seconds. The pilot shall fly an investigative run on each new configuration to

perform any desired exploratory techniques seen fit. Following that, at least 3 consecutive tasks in the same configuration will be flown prior to assigning an opinion using the subjective rating scales and questionnaire in the appendix. The Scales will be available to the pilot in the VMS cab.

A large matrix of different directional control systems will be presented to the pilot at random. It is not necessary and perhaps undesirable for the pilot to know in advance the configuration that is being tested. Performance data for each run will also be recorded automatically by the simulation for analysis, and will not be revealed to the pilot after each run. This is to avoid interjecting any preconceived notions into the data.

Piloting Tasks

This semi-realistic piloting task is designed to require aggressive use of rudder and is not necessarily indicative of real-world flying. The testing premise is in recognition that pilots of transport aircraft are almost exclusively trained to only use rudder for crosswind take-offs and landings, engine-out procedures and some flight control malfunctions. However, if in a critical situation and the pilot does have to use rudder aggressively, the aircraft response must be predictable, and there should be no tendency for overcontrol, PIO, or control surface reversals that could overstress the vertical stabilizer. The task is designed to force use of the rudder in order to expose deficiencies in aircraft handling qualities in the directional axis.

The task will require a return to trim condition, and some pilot action will be required to set trim e.g. throttles. Cockpit displays are provided to assist in trimming and in maintaining desired flight parameters.

Piloting Task : Rolling Gusts

The task is to maintain heading in the presence of random rolling gusts, some of which are of sufficiently large amplitude so as to exceed the aileron control power of the test aircraft. In some gusts, rudder will be required to assist in roll control so that the bank angles do not become sufficiently large and/or sustained so as to exceed the heading tolerance of +/- 10 deg. Gusts will be generated continuously throughout the data run after an initial 5 seconds quiescent period.

Performance targets are:

Task	Desired	Adequate
Primary	Heading +/- 10 deg	Heading +/- 20 deg
Secondary	Altitude +/- 100’ Airspeed +/- 10 KIAS	Altitude +/- 200’ Airspeed +/- 20 KIAS

When assigning ratings, please consider only the primary task. If you deviate significantly from desired performance on the secondary tasks, make additional runs as necessary to remain in desired performance most of the time. Occasional excursions out of desired are not considered to be a problem.

DATA REDUCTION AND ANALYSIS

The data will consist of pilot ratings and commentary as well as quantitative data such as time histories and discrete parameters (e.g., RMS pedal deflection and maximum force on the vertical stabilizer). For this Phase 2 effort, the primary objective of the data analysis will be to develop criteria to evaluate the tendency for overcontrol for any rudder flight control system.

Pilots will be asked to use the rating scales and the questionnaire that is given in the appendix after completion of each run. Since the task has been designed to require aggressive use of rudder, it is expected that any deficiencies in the directional axis will be reflected in the ratings.

APPENDIX D LOAD-FEEL CURVES

Design of the rudder pedal load-feel curves to be employed for the study were constrained by the following parameters:

- Curves are non-linear consistent with standard industry practice to achieve a desirable pedal force gradient around center without excess force at large deflections. For configurations with high values of breakout, it was not possible to use a nonlinear gradient.
- F_{bo} ; each curve has a pre-defined breakout force
- F_{lim}; each curve has a pre-defined limit force
- F_{cf}; each curve has a predefined Coulomb friction force
- F_{hb}; each curve has a pre-defined hold back force
- $\delta_{P\text{-}lim}$; each curve has a set maximum pedal travel

It is generally accepted that a non-linear force-feel curve provides the pilot a greater amount of proprioceptive feedback when compared to a linear force-feel curve allowing for steep gradients near the detent and lower control forces near maximum controller deflection as shown in Figure 49.

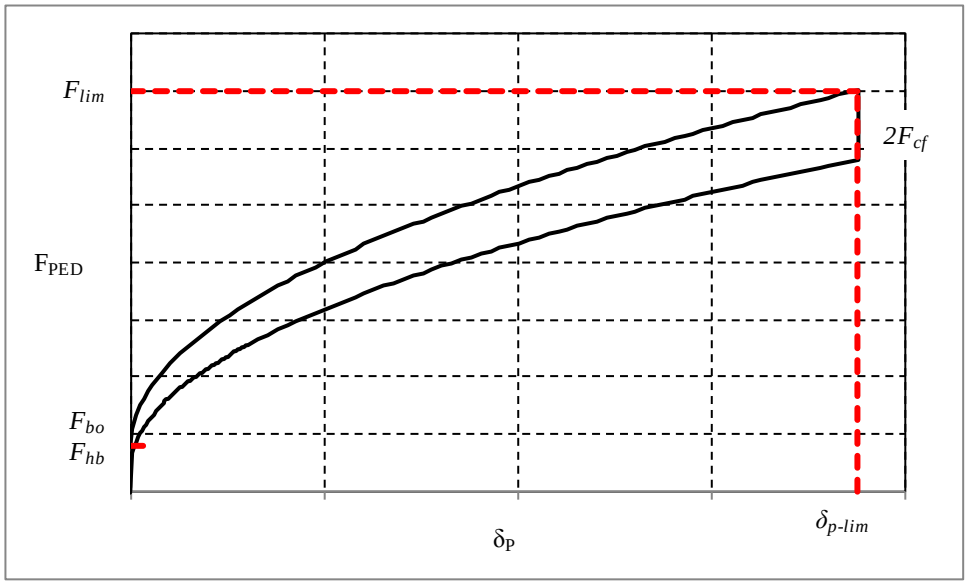

Figure 49. Generic Non-Linear Force-Feel Curve

For simplicity, the majority of the load-feel curves used in this study were second order. A generic expression for a second order curve in terms of the constraining variables for the up stroke is as follows:

$$F_{ped} = c\sqrt{\delta_p} + F_{bo} \qquad \text{Equation (A-1)}$$

Solving for c in terms of the constraints at known values of F_{ped} yields:

$$c = \frac{F_{lim} - F_{bo}}{\sqrt{\delta_{P-lim}}} \qquad \text{Equation (A-2)}$$

For the down stroke, similar logic can be utilized, knowing that $F_{bo} = 2F_{cf} + F_{hb}$:

$$\left(F_{ped}\right)_{DOWN} = c\sqrt{\delta_p} + F_{hb} \qquad \text{Equation (A-3)}$$

$$c = \frac{F_{\lim} - 2F_{cf} - F_{hb}}{\sqrt{\delta_{p\lim}}} \qquad \text{Equation (A-4)}$$

Configurations with high values of $F_{bo} / F_{\lim}$ were treated with linear force-feel curves (35-20, 25-X and 60-25, 35, 45-X):

$$F_{ped} = \frac{F_{lim} - F_{bo}}{\delta_{P-LIM}}\delta p + F_{bo} \qquad \text{Equation (A-5)}$$

$$\left(F_{ped}\right)_{down} = \frac{F_{\lim} - 2F_{cf} - F_{hb}}{\delta_{p\lim}}\delta_p + F_{hb} \qquad \text{Equation (A-6)}$$

The theoretical force feel curves for the phase 2 simulation are shown in Figure 50 through Figure 55,

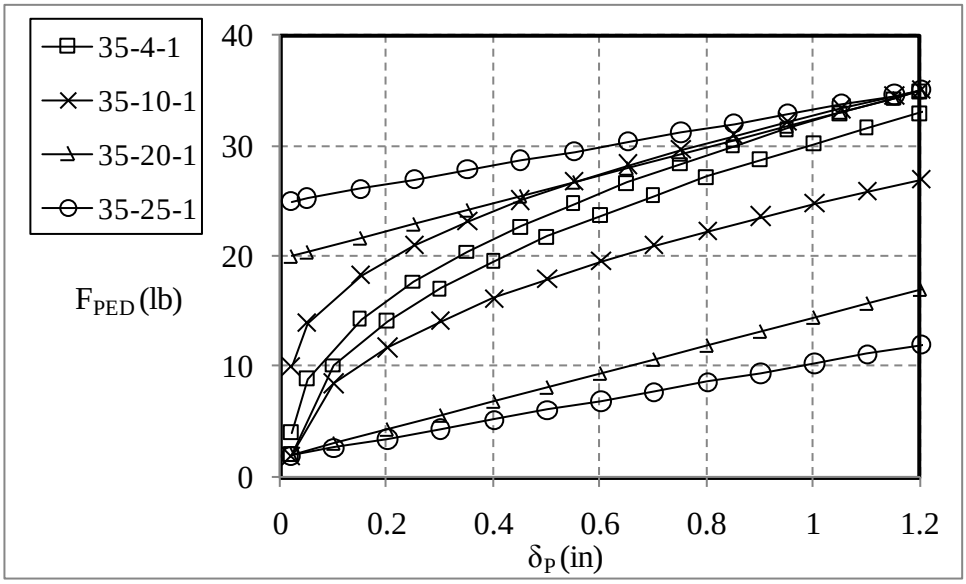

Figure 50. Theoretical Force-Feel Curves for $F_{\lim} = 35\ lbs\ and\ \delta_{p\lim} = 1.2\ in$ (35-XX-1)

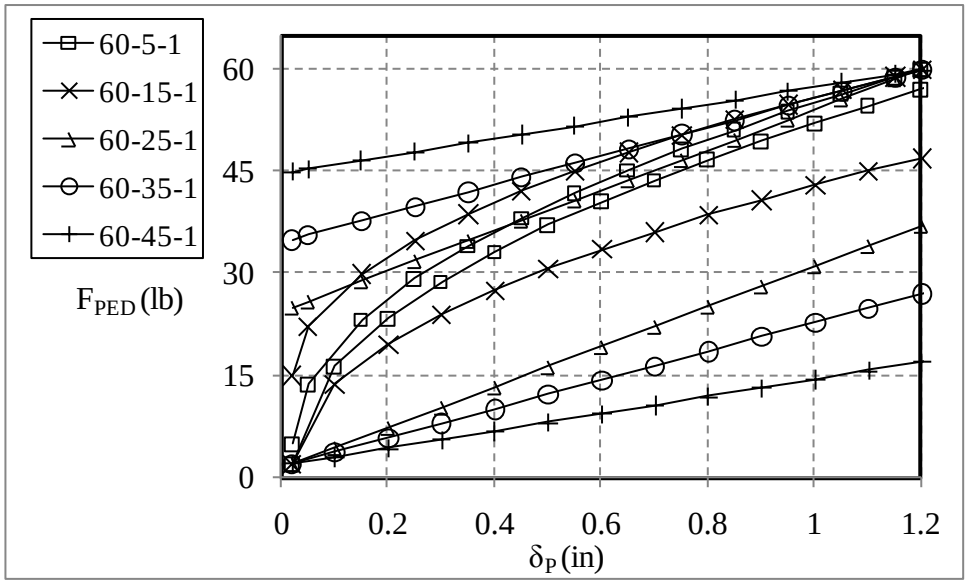

Figure 51. Theoretical Force-Feel Curves for $F_{\lim} = 60\ lbs\ and\ \delta_{p\lim} = 1.2\ in$ (60-XX-1)

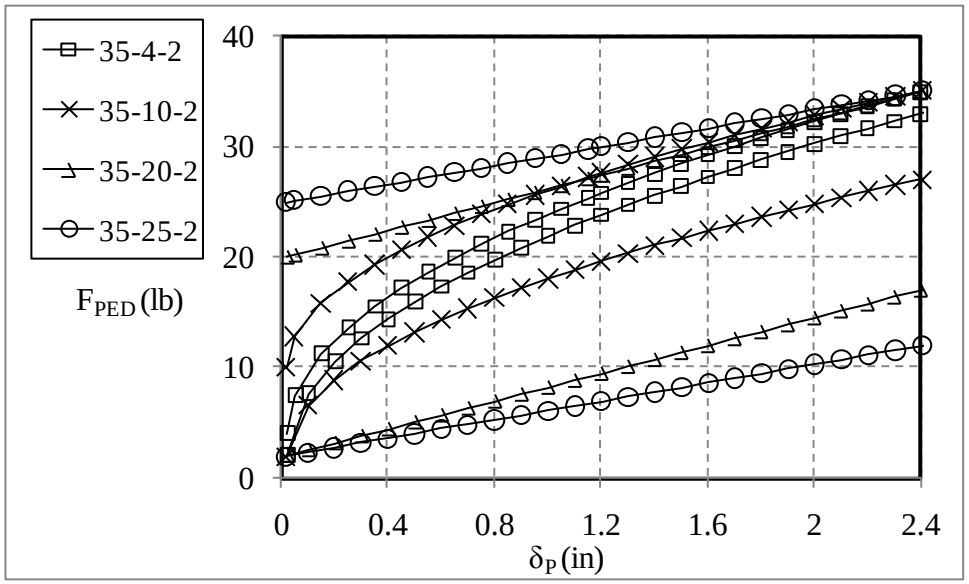

Figure 52. Theoretical Force-Feel Curves for $F_{\lim} = 35\ lbs\ and\ \delta_{p\lim} = 2.4\ in$ (35-XX-2)

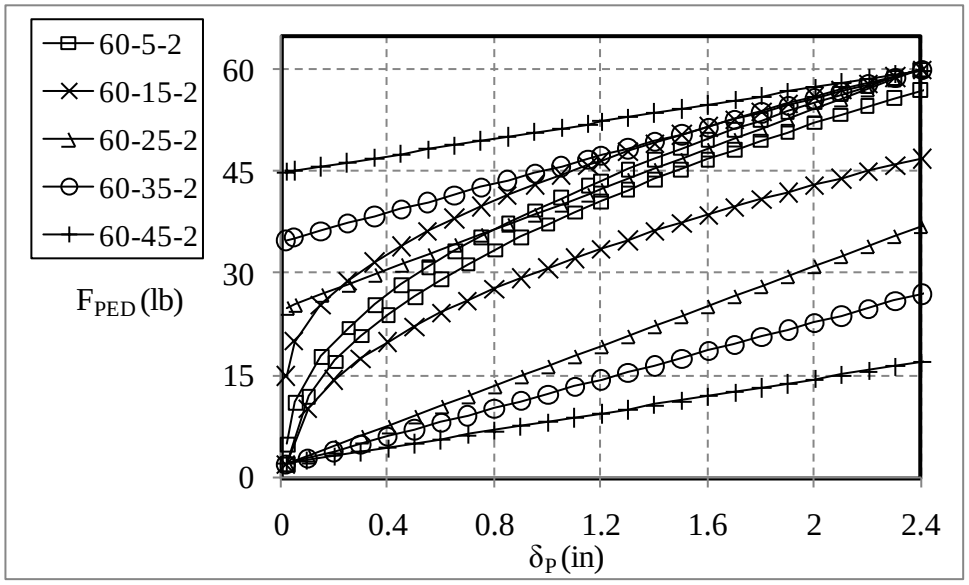

Figure 53. Theoretical Force-Feel Curves for $F_{\lim} = 60\ lbs\ and\ \delta_{p\lim} = 2.4\ in$ (60-XX-2)

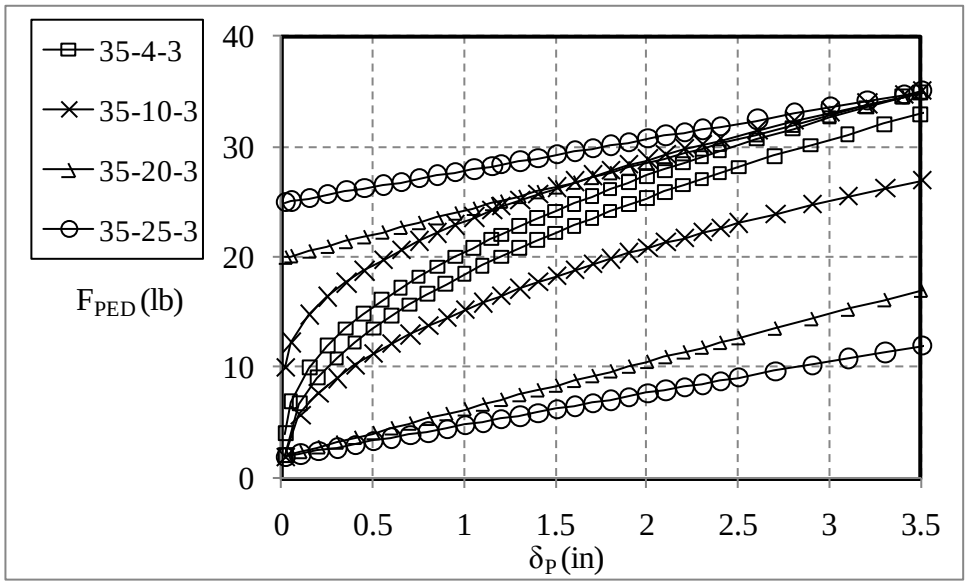

Figure 54. Theoretical Force-Feel Curves for $F_{\lim} = 35\ lbs\ and\ \delta_{p\lim} = 3.5\ in$ (35-XX-3)

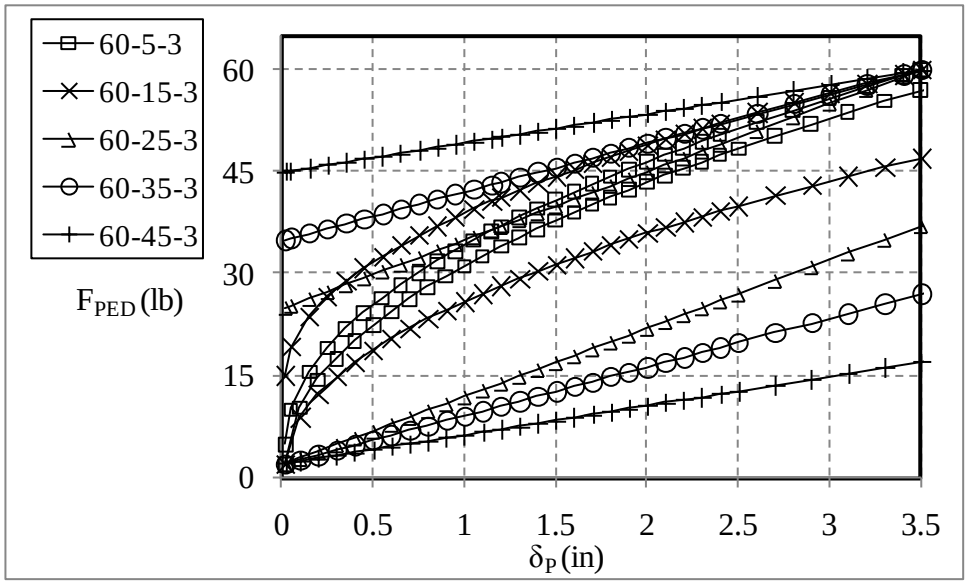

Figure 55. Theoretical Force-Feel Curves for $F_{\lim} = 60\ lbs\ and\ \delta_{p\lim} = 3.5\ in$ (60-XX-3)

Pedal Control Loader Input Points

The VMS's pedal control loaders, accept only the force gradient at a given pedal displacement as inputs and only a maximum of 10 total points can be used. The derivative of Equation (1) was taken to compute the gradient. When applied to the generic case depicted in Figure 49, the resulting gradient curve can be found in Figure 56:

$$\frac{\partial F_{PED}}{\partial \delta_P} = \frac{F_{LIM} - F_{BO}}{2\sqrt{\delta_{P-LIM}}\sqrt{\delta_P}}$$ Equation (A-7)

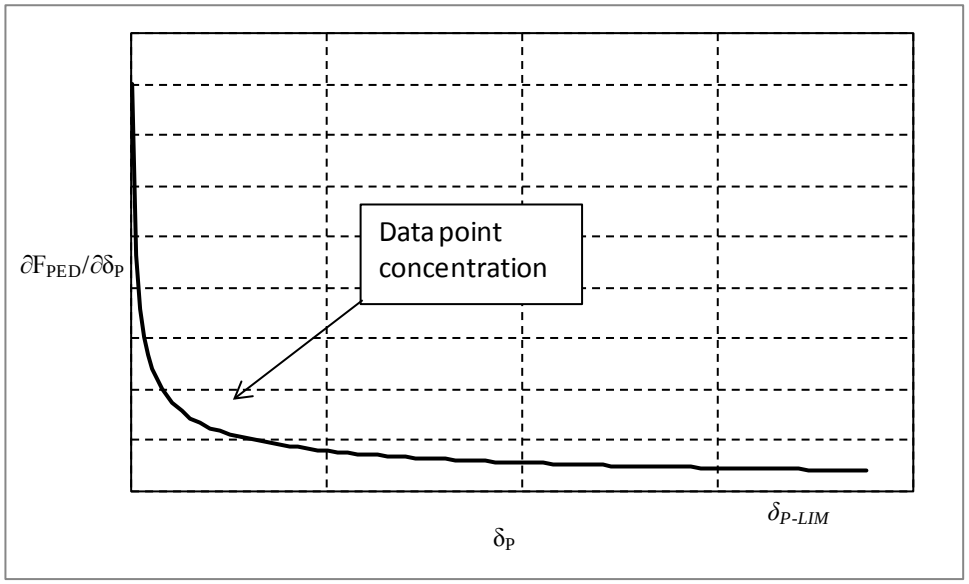

Figure 56. Generic Non-Linear Force Gradient Curve

As the gradient when $\delta_P = 0$ is undefined, a supplementary gradient was 200 lb/in. The resulting data points were adjusted to provide a maximum resolution where the force gradient rapidly changes. The following tables document the force gradient for each configuration (Table 2 through Table 7):

Table 2. Pedal Control Loader Points for 35-XX-1

F_{LIM}	35	lbs		
$\delta_{P\text{-}LIM}$	1.2	in		
	Configuration (F_{lim}-F_{bo}-$\delta_{p\text{-}lim}$)			
δ_P	35-4-1	35-10-1	35-20-1	35-25-1
0	0.00	0.00	0.00	0.00
0.1	0.00	0.00	0.00	0.00
0.1	125.95	46.88	12.71	8.47
0.2	46.62	33.68	12.71	8.47
0.3	34.16	27.65	12.71	8.47
0.5	24.61	21.51	12.71	8.47
0.9	17.57	16.08	12.71	8.47
1.3	14.39	13.39	12.71	8.47
1.9	11.78	11.09	12.71	8.47
2.5	10.21	9.67	12.71	8.47
3.1	9.14	8.69	12.71	8.47
3.6	8.46	8.06	12.71	8.47

Table 3. Pedal Control Loader Points for 60-XX-1

F_{lim}	60	lbs			
$\delta_{p\,lim}$	1.2	in			
	Configuration (F_{lim}-F_{bo}-$\delta_{p\text{-}lim}$)				
δ_{PED}	60-5-1	60-15-1	60-25-1	60-35-1	60-45-1
0	0.00	0.00	0.00	0.00	0.00
0.1	0.00	0.00	0.00	0.00	0.00
0.1	297.94	93.76	29.66	21.19	12.71
0.2	82.90	62.50	29.66	21.19	12.71
0.3	59.78	50.11	29.66	21.19	12.71
0.5	42.71	38.27	29.66	21.19	12.71
0.9	30.35	28.27	29.66	21.19	12.71
1.3	24.83	23.44	29.66	21.19	12.71
1.9	20.29	19.34	29.66	21.19	12.71
2.5	17.59	16.84	29.66	21.19	12.71
3.1	15.73	15.11	29.66	21.19	12.71

3.6	14.57	14.01	29.66	21.19	12.71

Table 4. Pedal Control Loader Points for 35-XX-2

F_{lim}	40	lbs		
$\delta_{p\,lim}$	2.4	in		
	Configuration (F_{lim}-F_{bo}-$\delta_{p\text{-}lim}$)			
δ_{PED}	35-4-2	35-10-2	35-20-2	35-25-2
0	0.00	0.00	0.00	0.00
0.1	0.00	0.00	0.00	0.00
0.1	62.97	23.44	6.30	4.20
0.2	30.92	19.34	6.30	4.20
0.3	23.31	16.84	6.30	4.20
0.5	17.08	13.82	6.30	4.20
0.9	12.30	10.75	6.30	4.20
1.3	10.11	9.11	6.30	4.20
1.9	8.29	7.63	6.30	4.20
2.5	7.20	6.70	6.30	4.20
3.1	6.45	6.04	6.30	4.20
3.6	5.97	5.62	6.30	4.20

Table 5. Pedal Control Loader Points for 60-XX-2

F_{lim}	60	lbs			
$\delta_{p\,lim}$	2.4	in			
		Configuration (F_{lim}-F_{bo}-δ_{plim})			
δ_{PED}	60-5-2	60-15-2	60-25-2	60-35-2	60-45-2
0	0	0.00	0.00	0.00	0.00
0.1	0	0.00	0.00	0.00	0.00
0.1	148.96	46.88	14.71	10.50	6.30
0.2	56.47	36.77	14.71	10.50	6.30
0.3	41.45	31.25	14.71	10.50	6.30
0.5	29.89	25.06	14.71	10.50	6.30
0.9	21.35	19.14	14.71	10.50	6.30
1.3	17.49	16.08	14.71	10.50	6.30
1.9	14.32	13.39	14.71	10.50	6.30
2.5	12.41	11.72	14.71	10.50	6.30
3.1	11.11	10.55	14.71	10.50	6.30

3.6	10.29	9.80	14.71	10.50	6.30

Table 6. Pedal Control Loader Points for 35-XX-3

F_{lim}	35	lbs		
$\delta_{p\,lim}$	3.5	in		
	Configuration (F_{lim}-F_{bo}-$\delta_{p\text{-}lim}$)			
δ_{PED}	35-4-3	35-10-3	35-20-3	30-25-3
0	0.00	0.00	0.00	0.00
0.1	0.00	0.00	0.00	0.00
0.1	43.17	16.07	4.31	2.87
0.2	24.29	13.98	4.31	2.87
0.3	18.72	12.54	4.31	2.87
0.5	13.91	10.63	4.31	2.87
0.9	10.10	8.50	4.31	2.87
1.3	8.32	7.29	4.31	2.87
1.9	6.84	6.17	4.31	2.87
2.5	5.94	5.44	4.31	2.87
3.1	5.32	4.93	4.31	2.87
3.6	4.93	4.59	4.31	2.87

Table 7. Pedal Control Loader Points for 60-XX-3

F_{lim}	60	lbs			
$\delta_{p\,lim}$	3.5	in			
	Configuration (F_{lim}-F_{bo}-$\delta_{p\text{-}lim}$)				
δ_{PED}	60-5-3	60-15-3	60-25-3	60-35-3	60-45-3
0	0.00	0.00	0.00	0.00	0.00
0.1	0.00	0.00	0.00	0.00	0.00
0.1	102.13	32.14	10.06	7.18	4.31
0.2	45.29	26.89	10.06	7.18	4.31
0.3	33.73	23.58	10.06	7.18	4.31
0.5	24.53	19.51	10.06	7.18	4.31
0.9	17.60	15.27	10.06	7.18	4.31
1.3	14.44	12.97	10.06	7.18	4.31
1.9	11.83	10.89	10.06	7.18	4.31
2.5	10.26	9.57	10.06	7.18	4.31
3.1	9.19	8.63	10.06	7.18	4.31
3.6	8.51	8.04	10.06	7.18	4.31

Control Loader Plots

In order to verify that the pedal control loaders were operating as intended, time histories were recorded while a VMS technician, seated in the cab, moved the pedals through the full range of motion (+/-$\delta_{p\text{-}lim}$). Each run was started at full deflection. The resulting time histories depicted below show the measured force on the pedal (RUNDUM channel "FORCEPED") versus pedal displacement as measured from the motion cab (RUNDUM channel "DPXCAB"). A slight error in force at maximum pedal displacement was found. Reason being that the pedal dead band was changed without recalculation of the gradient points. However, this error was consistent throughout all trials and placed no limitations on data analysis.

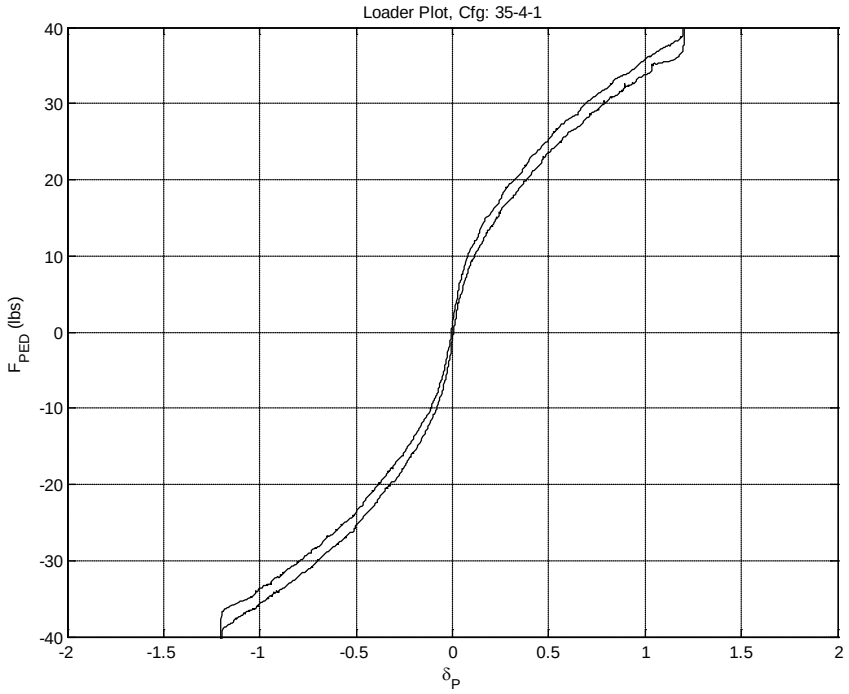

Figure 57. Pedal Control Loader F_{PED} Versus δ_P (35-4-1)

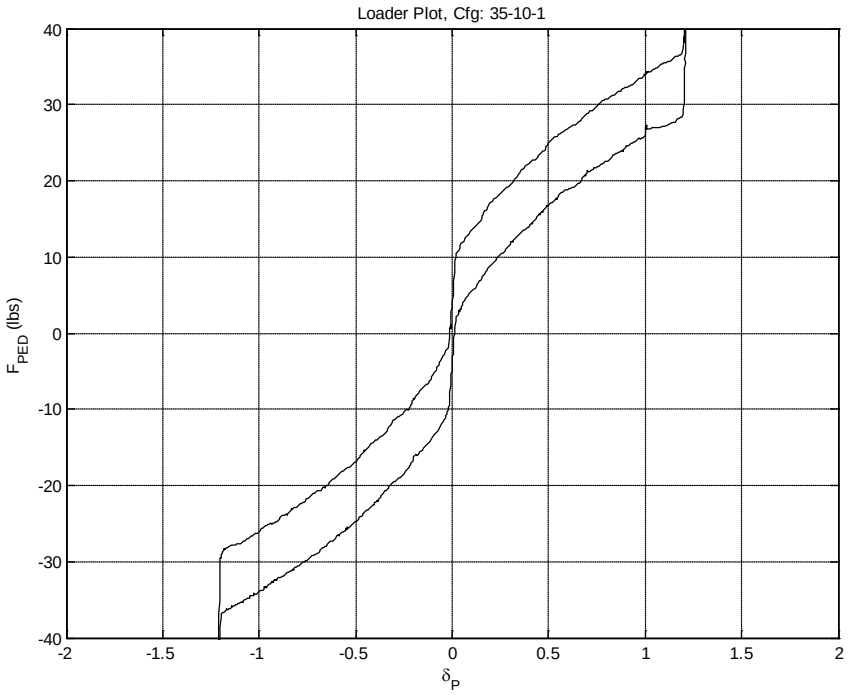

Figure 58. Pedal Control Loader F_{PED} Versus δ_P (35-10-1)

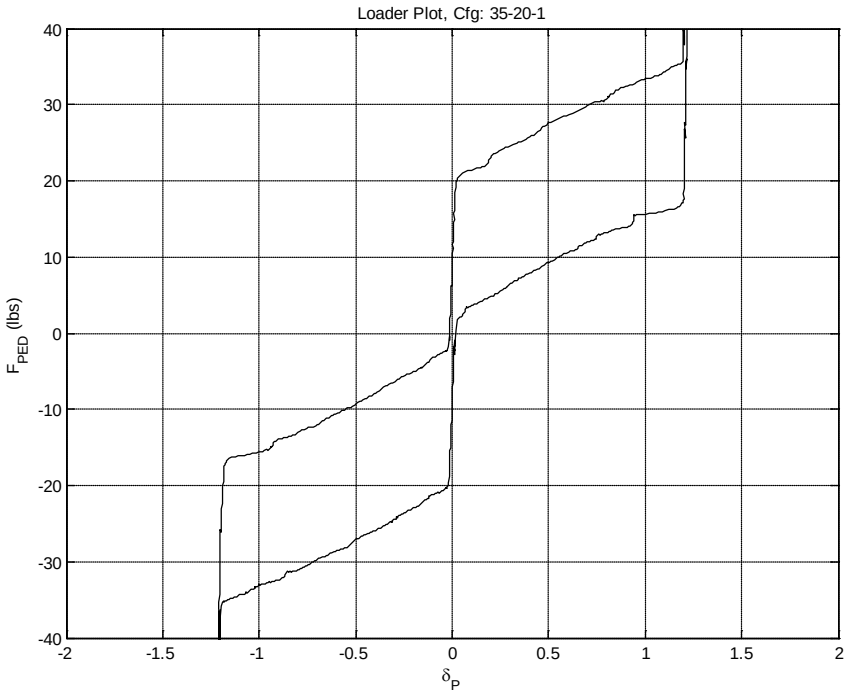

Figure 59. Pedal Control Loader F_{PED} Versus δ_P (35-20-1)

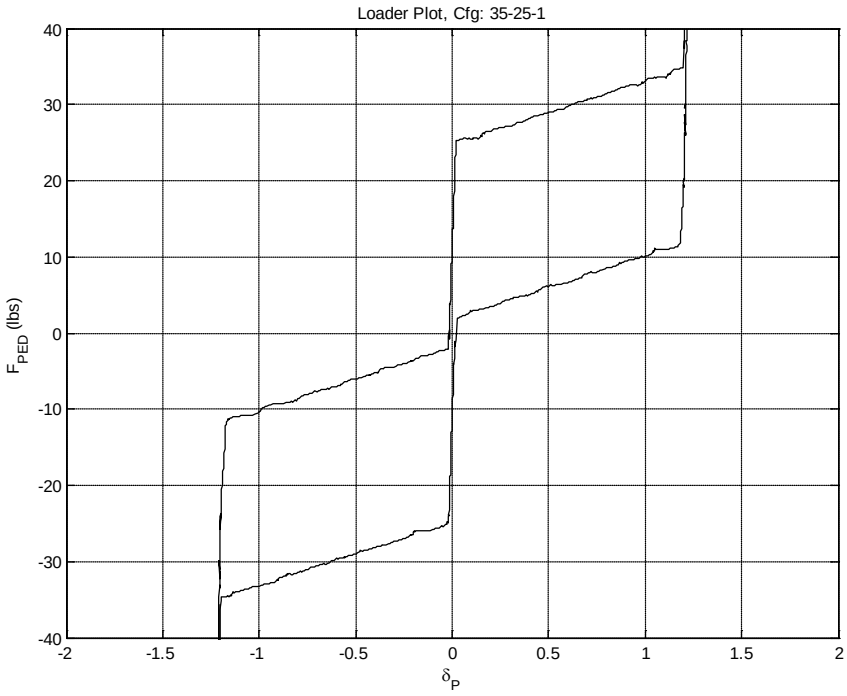

Figure 60. Pedal Control Loader F_{PED} Versus δ_P (35-25-1)

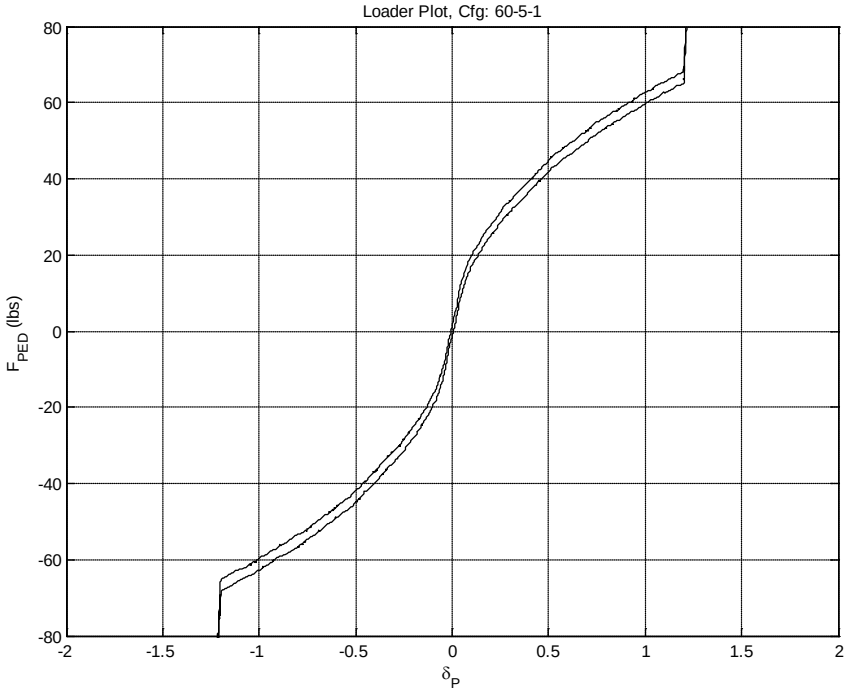

Figure 61. Pedal Control Loader F_{PED} Versus δ_P (60-5-1)

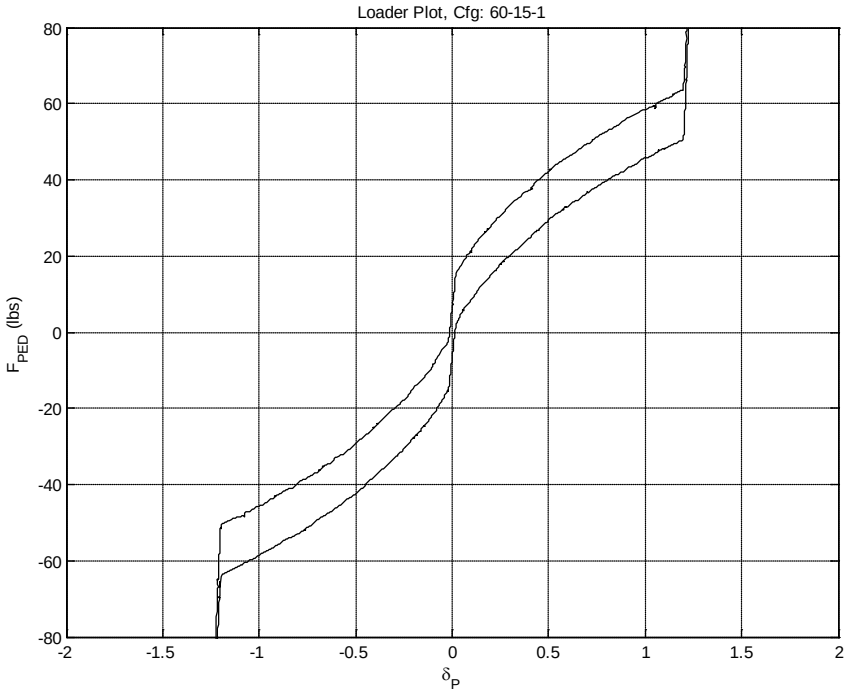

Figure 62. Pedal Control Loader F_{PED} Versus δ_P (60-15-1)

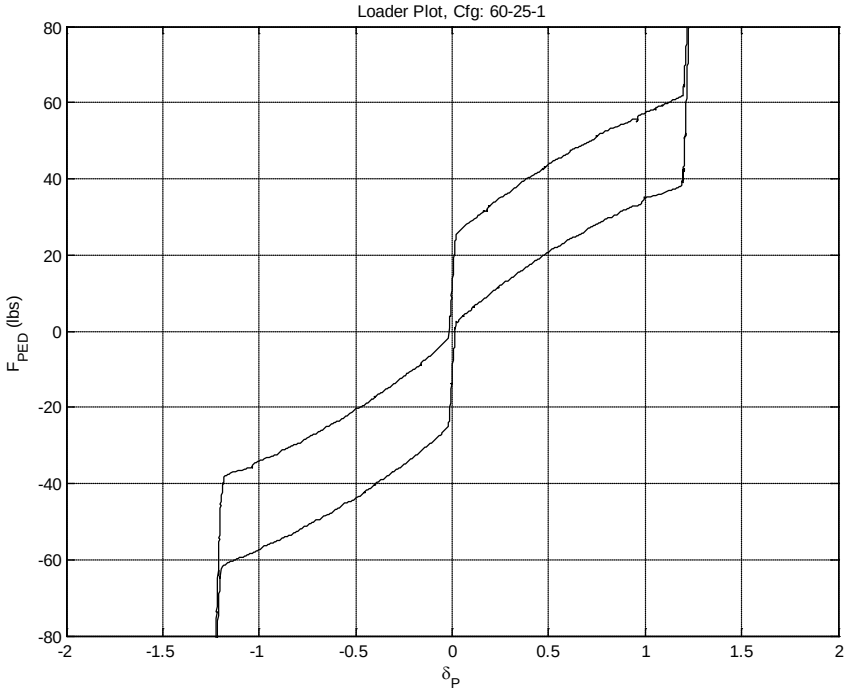

Figure 63. Pedal Control Loader F_{PED} Versus δ_P (60-25-1)

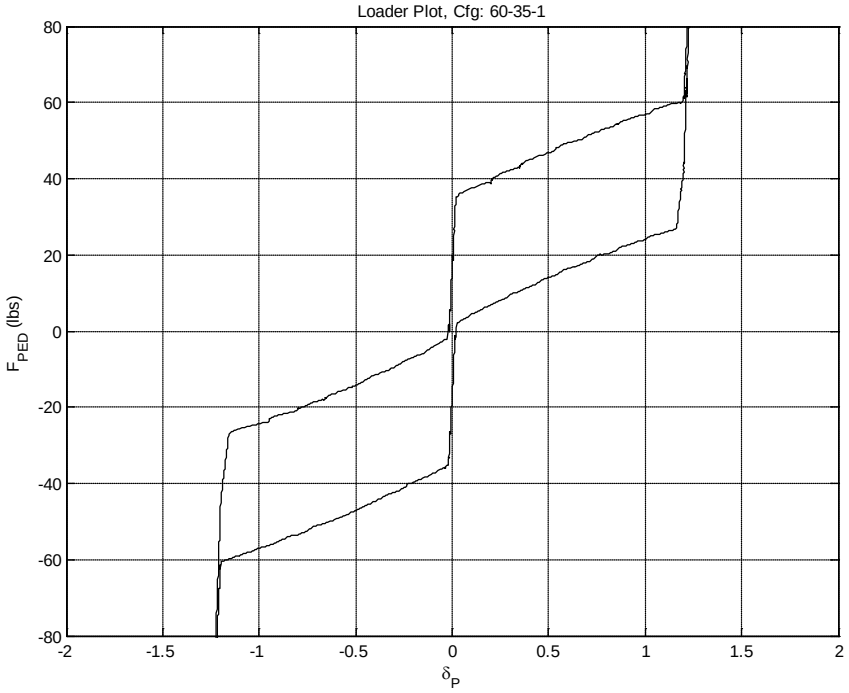

Figure 64. Pedal Control Loader F_{PED} Versus δ_P (60-35-1)

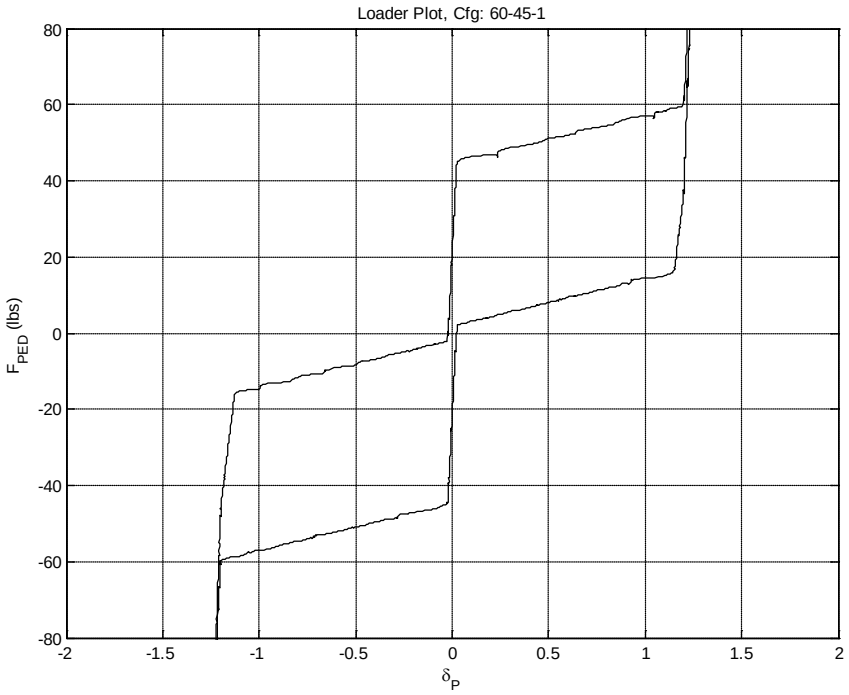

Figure 65. Pedal Control Loader F_{PED} Versus δ_P (60-45-1)

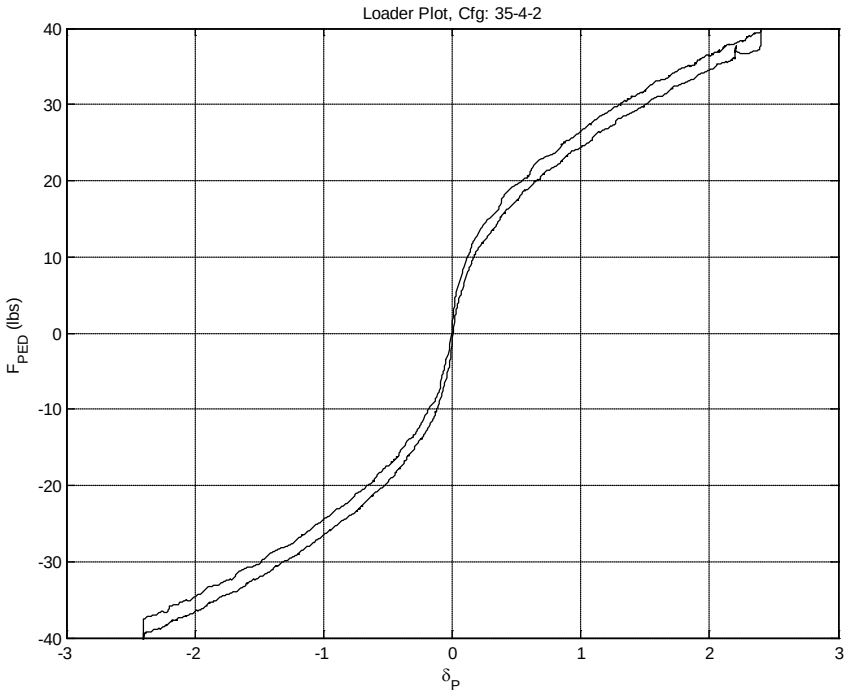

Figure 66. Pedal Control Loader F_{PED} Versus δ_P (35-4-2)

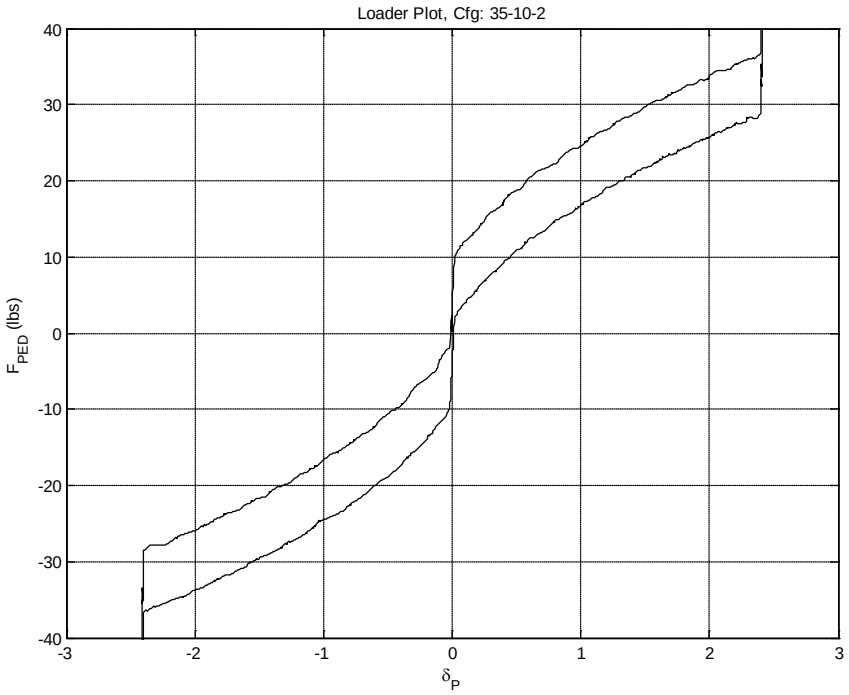

Figure 67. Pedal Control Loader F_{PED} Versus δ_P (35-10-2)

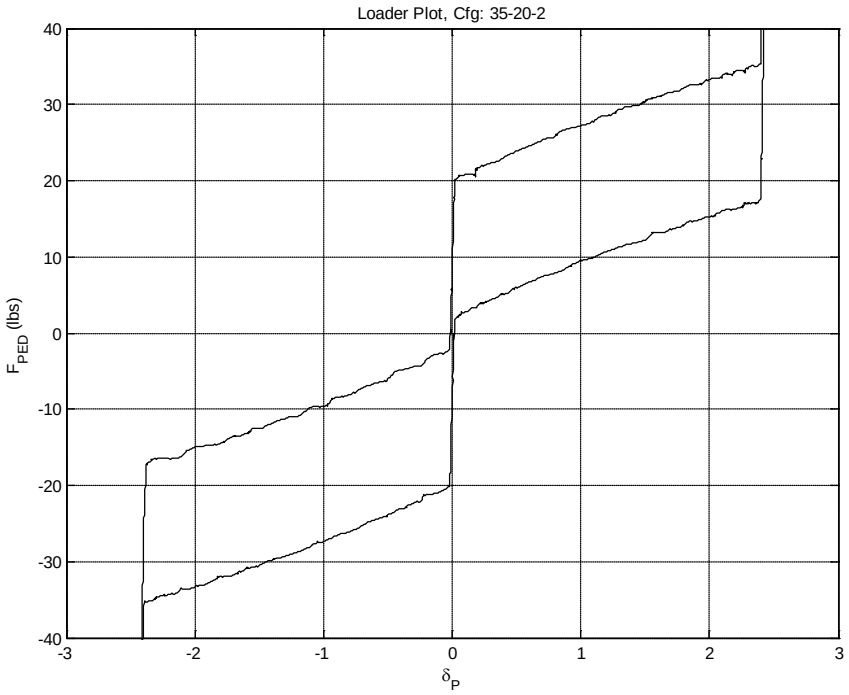

Figure 68. Pedal Control Loader F_{PED} Versus δ_P (35-25-2)

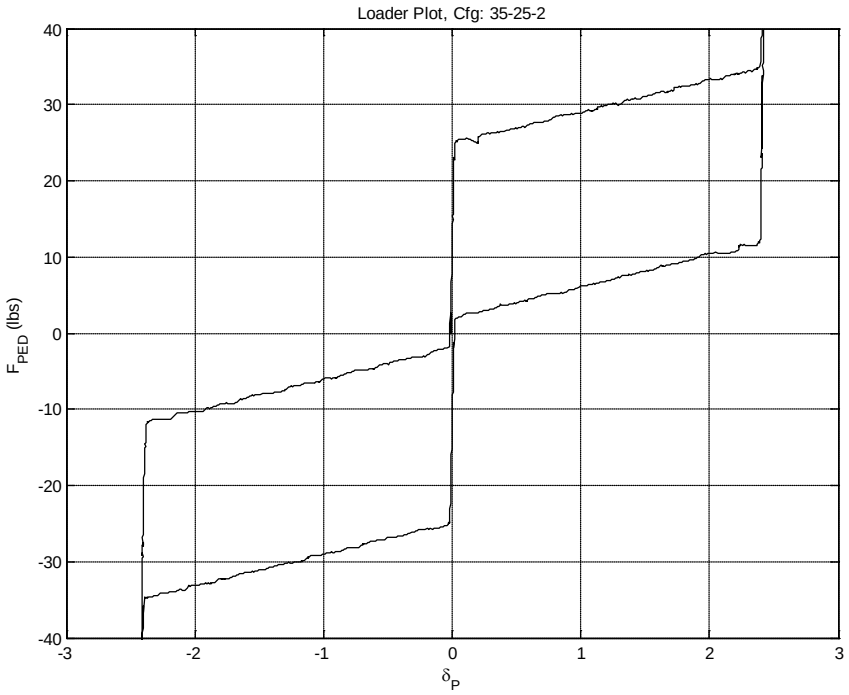

Figure 69. Pedal Control Loader F_{PED} Versus δ_P (35-25-2)

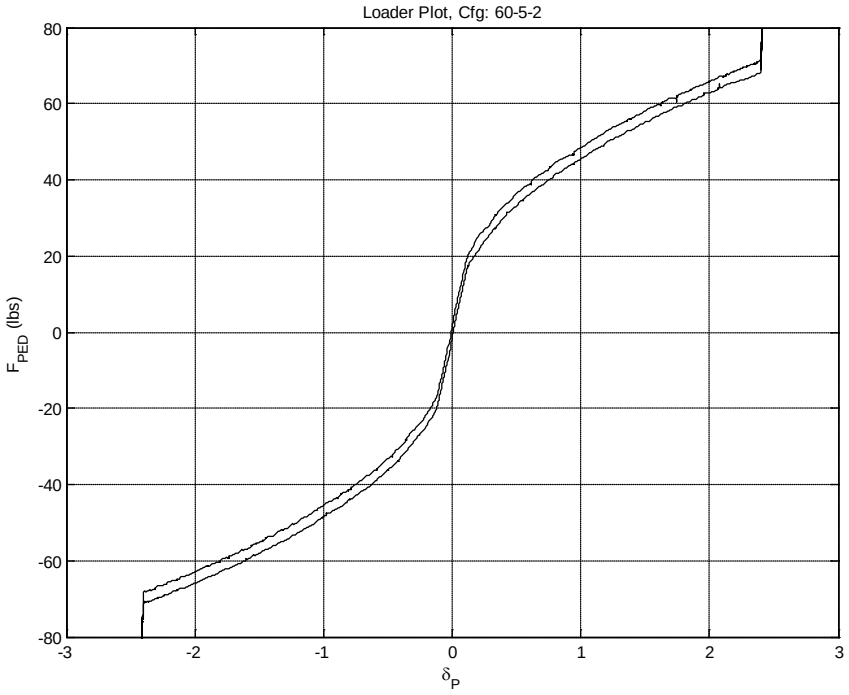

Figure 70. Pedal Control Loader F_{PED} Versus δ_P (60-5-2)

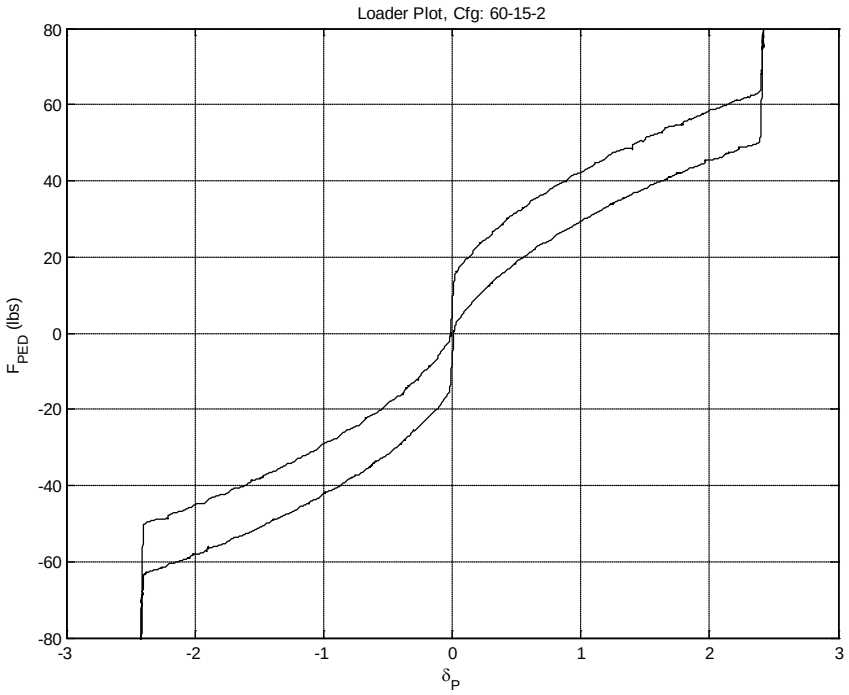

Figure 71. Pedal Control Loader F_{PED} Versus δ_P (60-125-2)

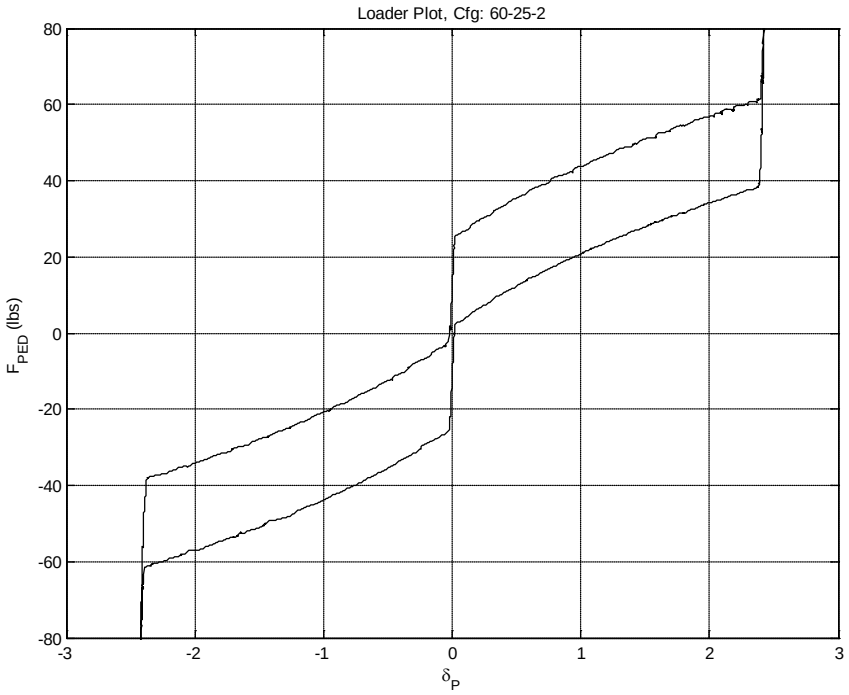

Figure 72. Pedal Control Loader F_{PED} Versus δ_P (60-25-2)

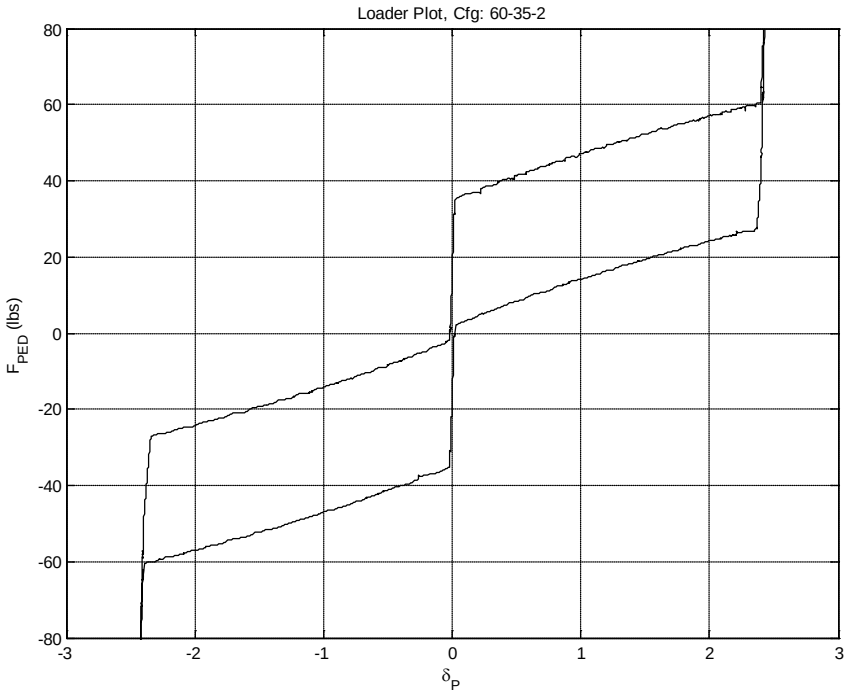

Figure 73. Pedal Control Loader F_{PED} Versus δ_P (60-35-2)

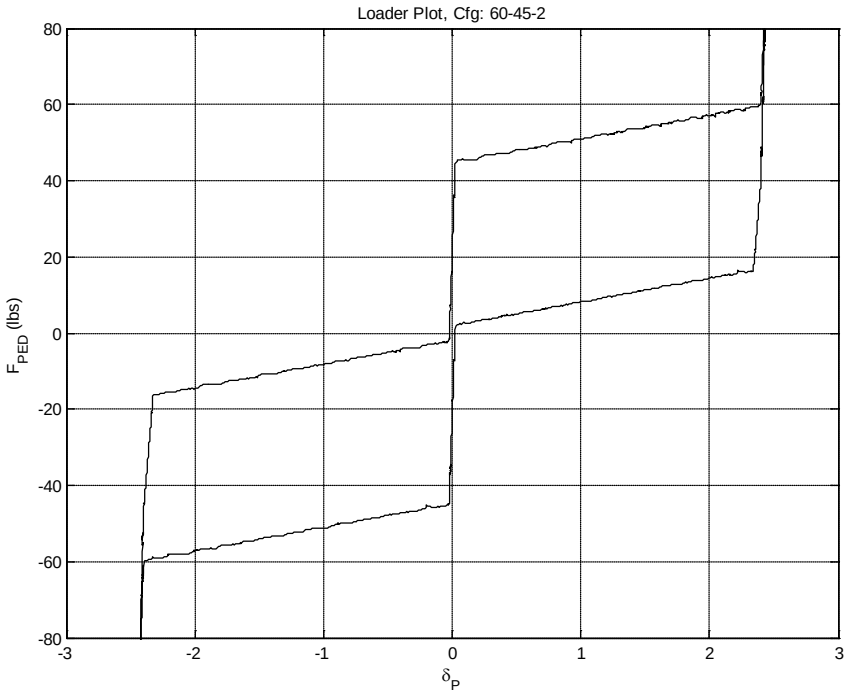

Figure 74. Pedal Control Loader F_{PED} Versus δ_P (60-45-2)

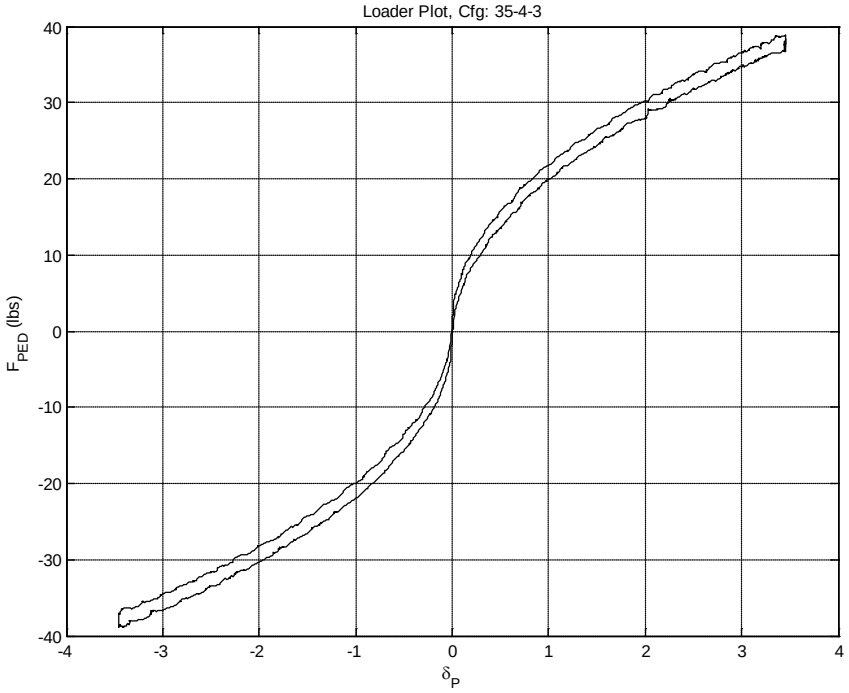

Figure 75. Pedal Control Loader F_{PED} Versus δ_P (35-4-3)

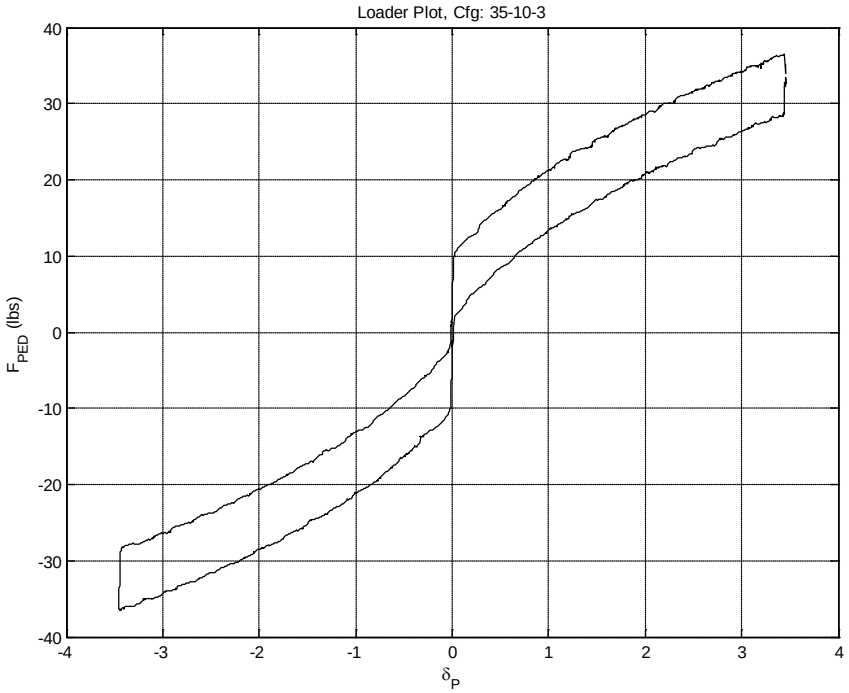

Figure 76. Pedal Control Loader F_{PED} Versus δ_P (35-10-3)

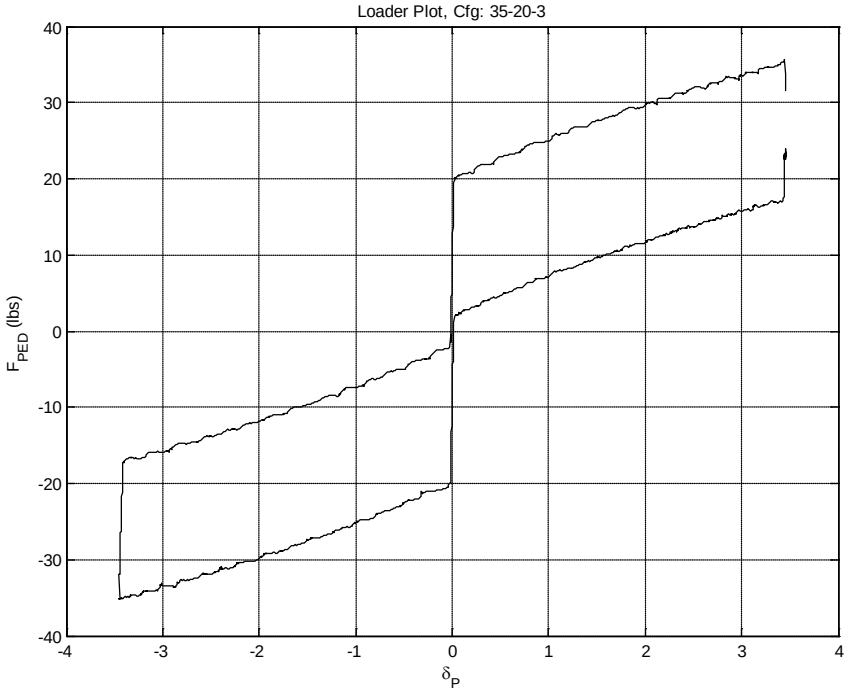

Figure 77. Pedal Control Loader F_{PED} Versus δ_P (35-20-3)

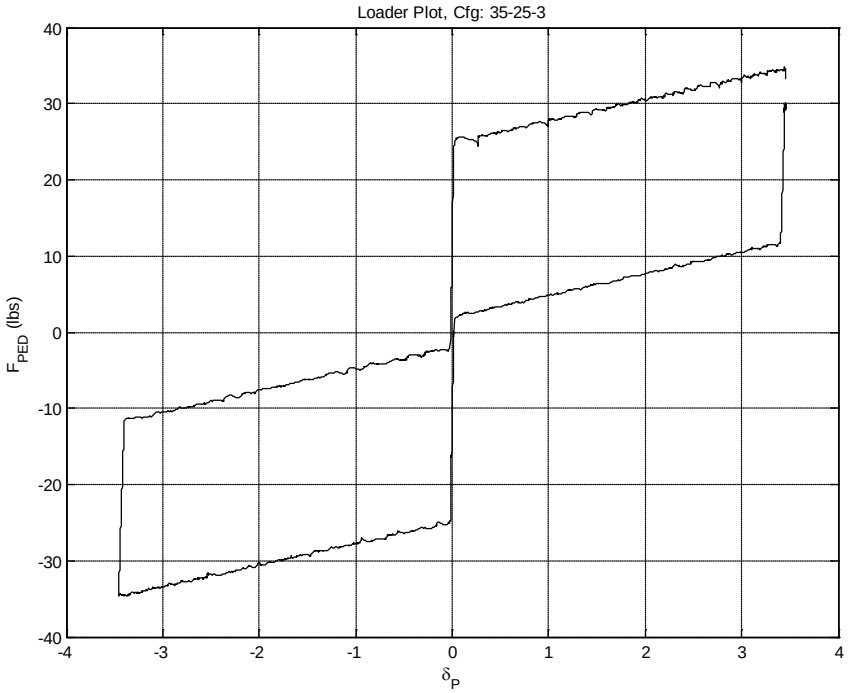

Figure 78. Pedal Control Loader F_{PED} Versus δ_P (35-25-3)

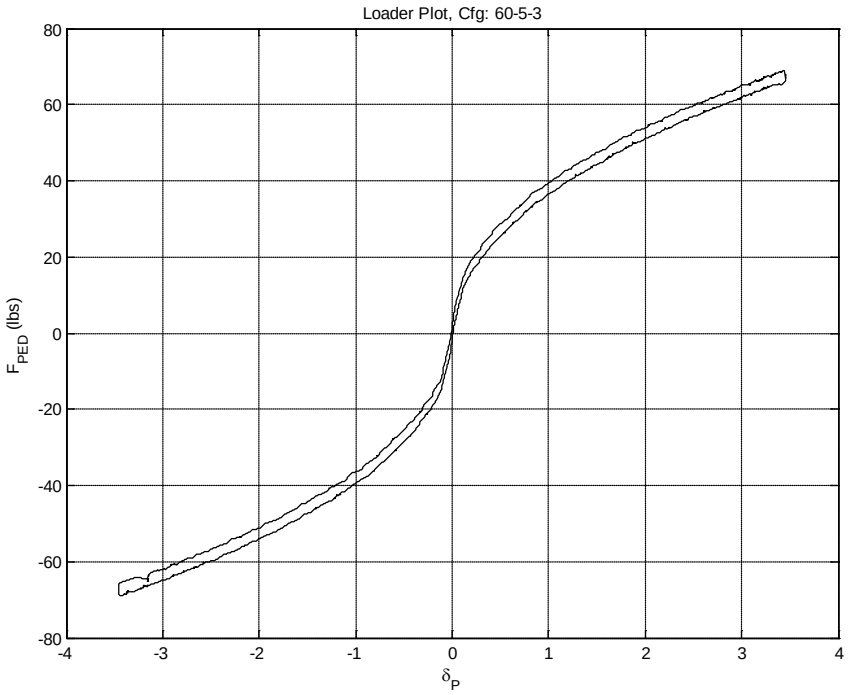

Figure 79. Pedal Control Loader F_{PED} Versus δ_P (60-5-3)

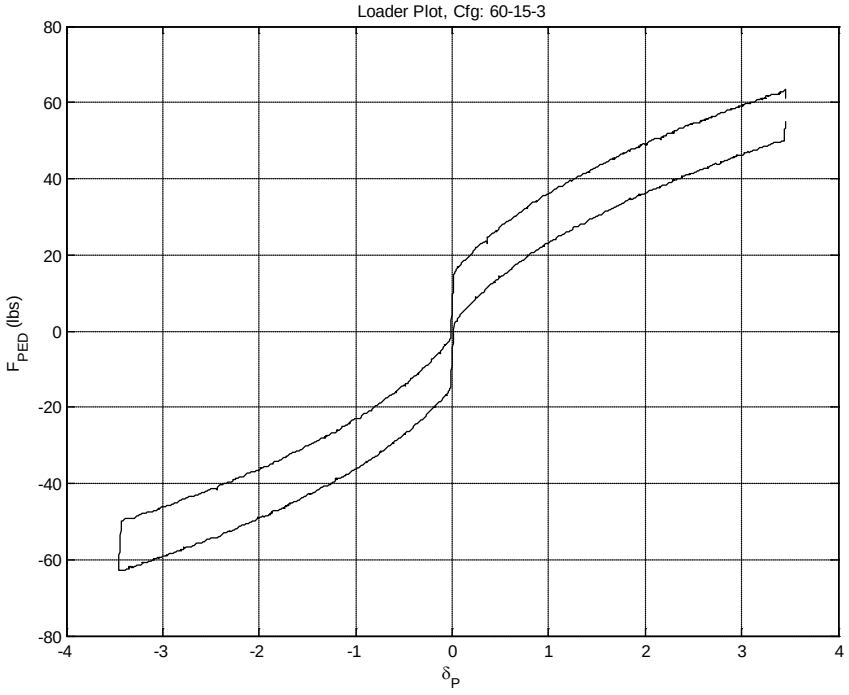

Figure 80. Pedal Control Loader F_{PED} Versus δ_P (60-15-3)

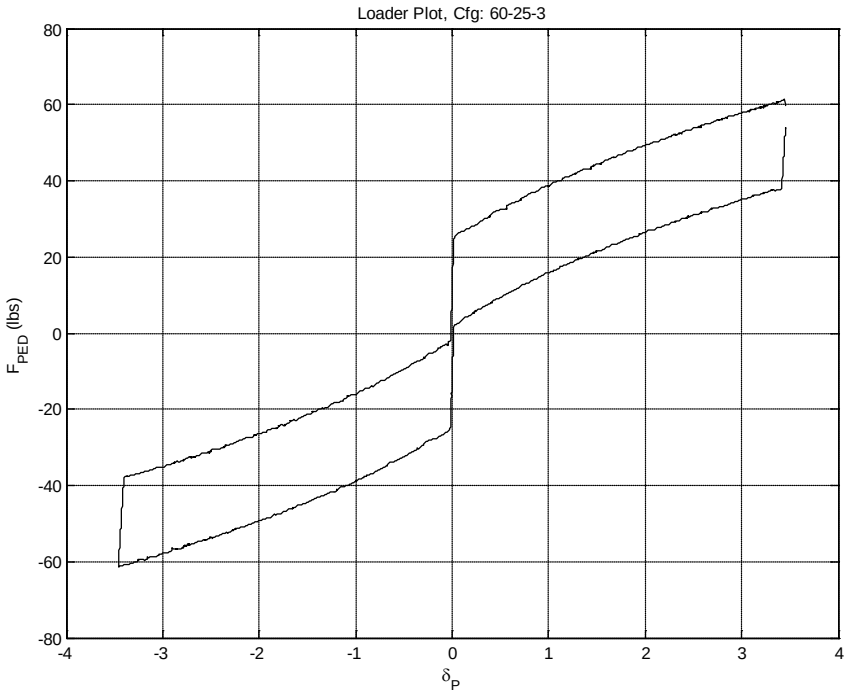

Figure 81. Pedal Control Loader FPED Versus δP (60-25-3)

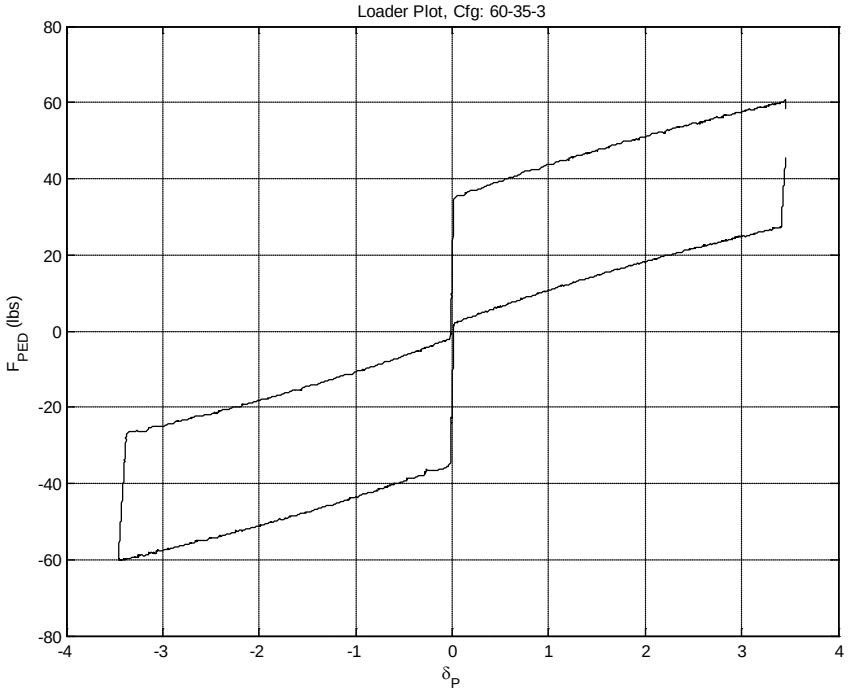

Figure 82. Pedal Control Loader F_{PED} Versus δ_P (60-35-3)

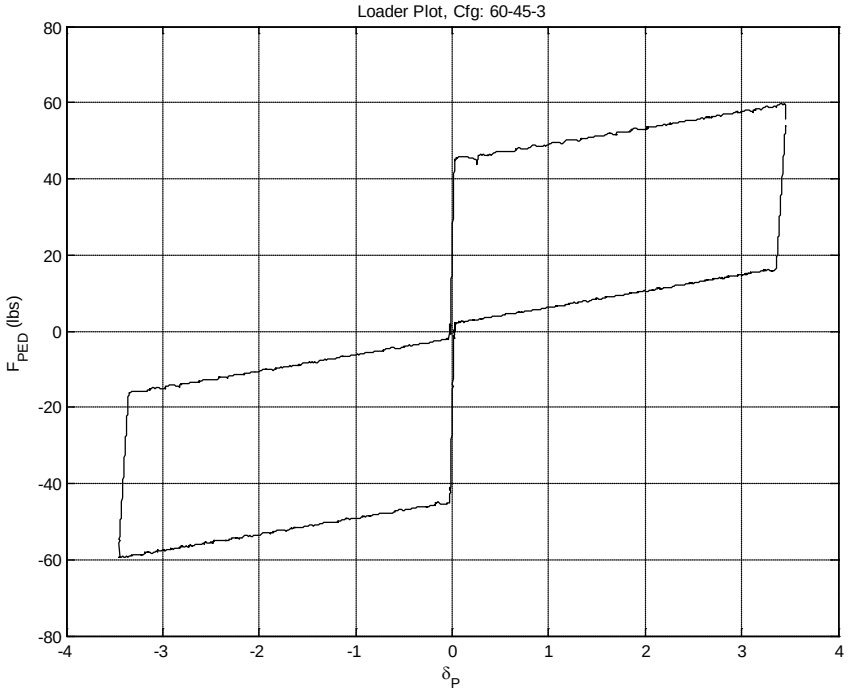

Figure 83. Pedal Control Loader F_{PED} Versus δ_P (60-45-3)

APPENDIX E STATISTICS OF VERTICAL STABILIZER FORCE AND $\left|\beta - \delta_r\right|_{peak}$

Statistical analysis of the simulation data was performed to determine if the peak vertical stabilizer force and $\left|\beta - \delta_r\right|_{peak}$ data are well represented by a normal distribution. This was done to justify the use of 3 standard deviations as representative of the maximum expected value. All first runs were collected for the baseline configurations. The histograms in Figure 84 and Figure 85 were calculated using the Microsoft Excel ® data analysis tool pack.

The Bin range in Figure 84 was selected to cover the minimum through maximum vertical stabilizer force in 2000 lb increments. As can be seen in the histogram, the data is well approximated by a normal distribution with the peak in the vicinity of the mean global average value.

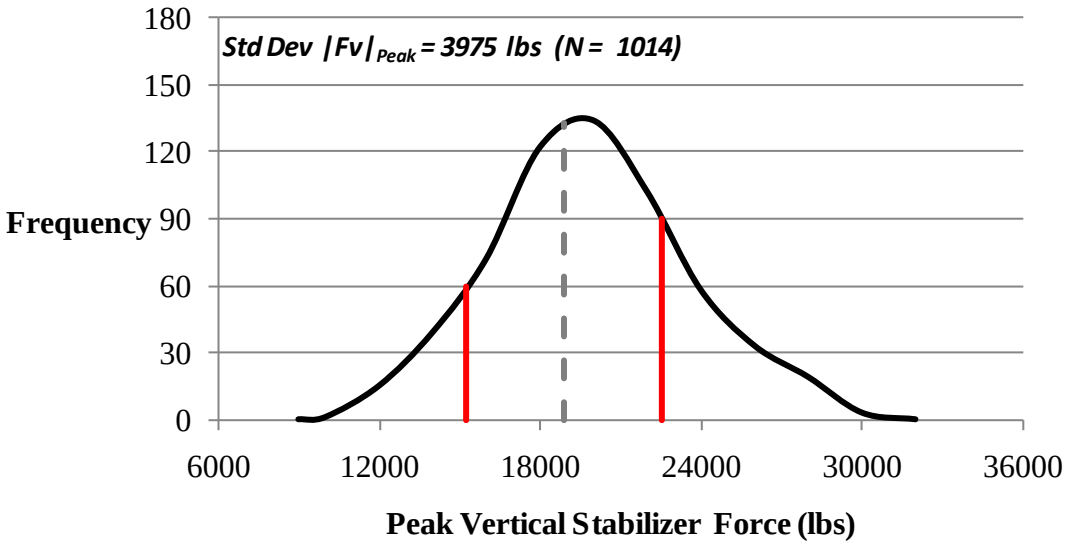

Figure 84. Histogram of Peak Vertical Stabilizer Force

The same analysis was accomplished on the peak values of $|\beta - \delta_r|$ with the result shown in Figure 85.

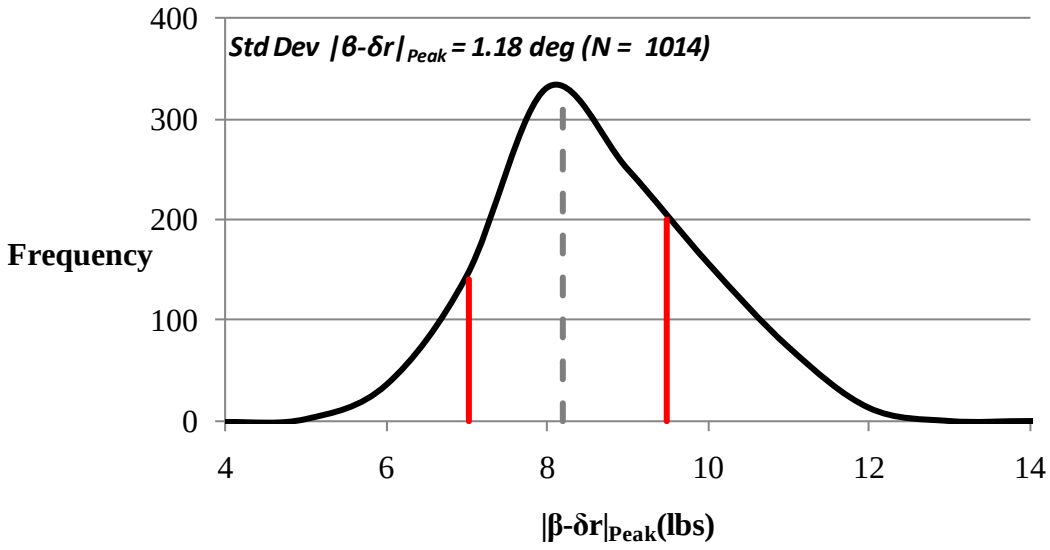

Figure 85 Histogram of $|\beta - \delta_r|_{peak}$

APPENDIX F LINEARITY INDEX

Calculation and Application of the Linear Index to Force Feel Curves

As discussed in references 6 and 7 the Linear Index (LI), is a measure of how "linear" a force-feel system appears to the human operator. The metric is calculated as follows (Figure 86)

$$LI = 1 - \frac{AREA(DAHD) + AREA(JHIJ)}{AREA(DEBFD)}$$ Equation (F-1)

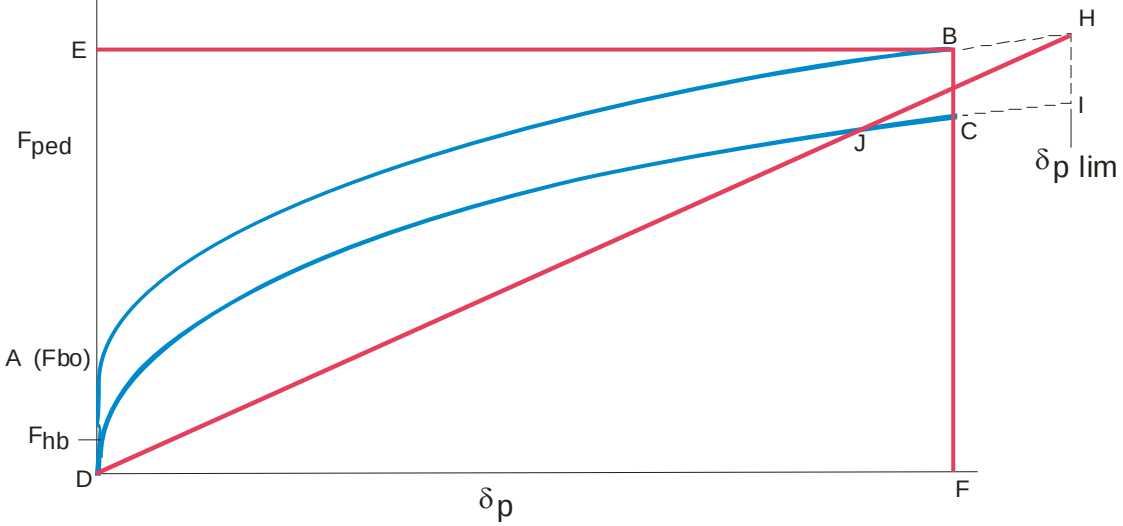

Figure 86. Generic Non-Linear Load-Feel Curve Typical of Transport Aircraft

The bold lines on the force feel curve depicted above (ABCDA) represents the amount of pedal displacement that is used to deflect the control surface. The remaining part of the curve (BHICB) represents a portion of the force-feel curve in which pedal displacement does not result in rudder displacement; analogous to a situation where the rudder limit has been reached, while the control is allowed, either by mechanical means or by deformation of control linkage or cable stretch, to displace further (the scale has been exaggerated for clarity). As shown in Equation (F-1), the LI requires that three separate areas are obtained from the force-feel curve. From the figure, it can be seen that AREA(DAHDA) is the area outlined by connecting the origin (D) to the breakout force (A), following the upstroke of the force-feel curve from point A to point H, and directly back to the origin at point D. The AREA(JHIJ) is outlined by points H, I, and where the line intersects the down stroke of the force-feel curve at point J[1]. The last area, AREA(DEBFD), is simply the rectangle formed by the points corresponding to the control force at maximum surface deflection, and the corresponding control deflection. For clarity these areas are identified and shaded and labeled in Figure 87 , and equation (F-1) becomes LI = [Area (1) + Area(2)]/Area(3)

[1] If the curve representing the downstroke of the pedal does not intersect line DH then J is at the origin (coincident with D).

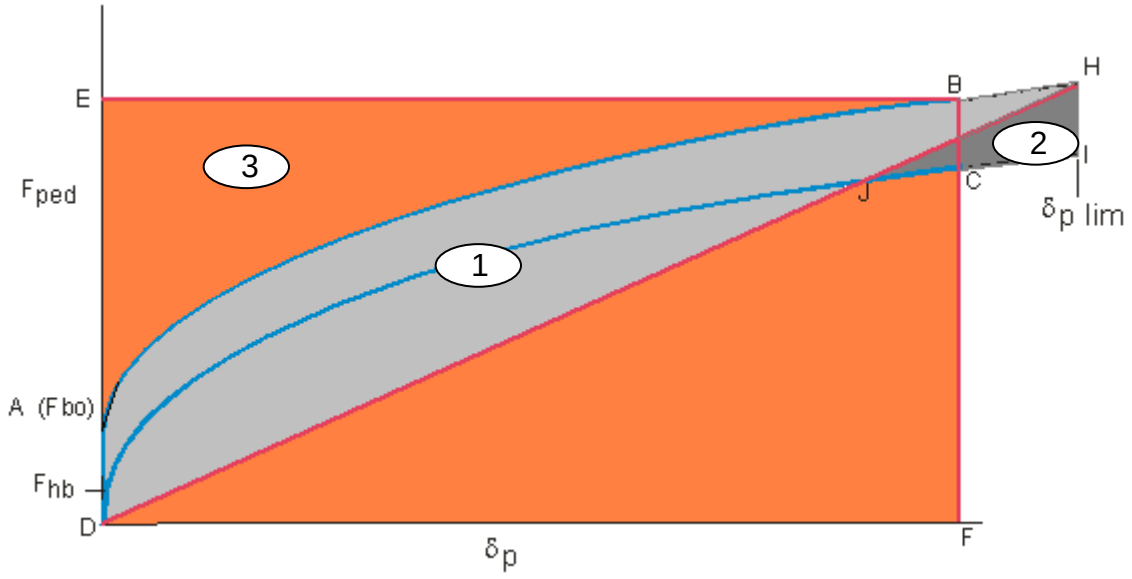

Figure 87. Identification of Linear Index Area Components

This metric has been shown in the above references to delineate differences in force feel system design with pilots performing a closed loop tracking task with some caveats. LI is not an absolute scale. This metric is used to make comparisons of two or more different force-feel systems, and as the author points out an LI value of 1.0 does not necessarily suggest that the force feel system is ideal. For instance, if the control throw is too short or the control force at maximum displacement is too high these factors could contribute to a poor pilot opinion of the force-feel system from a handling qualities perspective regardless of the value of LI. A suggested lower limit of 0.6 is proposed as a criterion boundary in reference 6.

Simulated Load Feel Curves and Area Segment Calculation of Analytical Load-Feel Curves

Application of LI to the analytical pedal displacement curves is rather straight forward, as each area of the curve is defined in terms of known quantities.

AREA(DAHD), or shaded area 1 on Figure 87, is calculated as follows:

$$A_1 = \int_0^{\delta_{p-lim}} \left[\frac{F_{lim} - F_{bo}}{\sqrt{\delta_{p-lim}}} \sqrt{\delta_p} + F_{bo} - \frac{F_{lim}}{\delta_{p-lim}} \delta_p \right] d\delta_p \qquad \text{Equation (F-2)}$$

AREA(DIHD), or shaded area 2 on Figure 87, is calculated as follows:

$$A_2 = \int_{\bar{x}}^{\delta_{p-lim}} \left[\frac{F_{lim}}{\delta_{p-lim}} \delta_p - \frac{F_{lim} - 2F_{cf} - F_{hb}}{\sqrt{\delta_{P-LIM}}} \sqrt{\delta_p} + F_{hb} \right] d\delta_p \qquad \text{Equation (F-3)}$$

Where $\overline{X}$ is the intersection of the down stroke curve and DH (point J in Figure 87), calculated from the quadratic below:

$$0 = \frac{F_{lim}}{\delta_{p-lim}}\overline{X}^2 - \left[\left(\frac{F_{lim}-2F_{cf}-F_{hb}}{\sqrt{\delta_{p-lim}}}\right)^2 + 2F_{hb}\frac{F_{lim}}{\delta_{p-lim}}\right]\overline{X} + F_{hb}{}^2 \qquad \text{Equation (F-4)}$$

Pedal force-feel curves of the current study were of the type that points B and H were coincident, meaning that statically, the rudder was displaced linearly throughout the entire range of pedal motion. Therefore, calculation of AREA(DEBFD) , area 3 on Figure 87, was simply:

$$A_3 = F_{lim}\delta_{p-lim} \qquad \text{Equation (F-5)}$$

Calculation of the area segment 1 for the linear force feel systems was as follows:

$$A_1 = \int_0^{\delta_{p-lim}} \left[\frac{F_{lim}-F_{bo}}{\delta_{p-lim}}(\delta_p) + F_{bo} - \frac{F_{lim}}{\delta_{p-lim}}\delta_p\right] d\delta_p \qquad \text{Equation (F-6)}$$

Calculation of the area segment 2 for the linear force-feel systems was as follows:

$$A_2 = \int_{\overline{X}}^{\delta_{p-lim}} \left[\frac{F_{lim}}{\delta_{p-lim}}\delta_p - \frac{F_{lim}-2F_{cf}-F_{hb}}{\delta_{p-lim}}(\delta_p) + F_{hb}\right] d\delta_p \qquad \text{Equation (F-7)}$$

Where $\overline{X}$ for the linear force-feel systems being calculated as:

$$\overline{X} = \frac{F_{hb}}{\left(\frac{F_{lim}}{\delta_{p-lim}} - \frac{F_{lim}-2F_{cf}-F_{hb}}{\delta_{p-lim}}\right)} \qquad \text{Equation (F-8)}$$

To account for errors between the analytical and actual force-feel curves, the analytical values for F_{lim} were modified with the following changes found in Table 8:

Table 8. Corrected Parameters and Reconciliation of Analytical and Actual RCSR 2 Force-Feel Curves

35-4-1	Analytical	35	60-5-1	Analytical	60
	Recorded	39		Recorded	68
	Error	4		Error	8
35-10-1	Analytical	35	60-15-1	Analytical	60
	Recorded	37		Recorded	64
	Error	2		Error	4
35-20-1	Analytical	35	60-25-1	Analytical	60
	Recorded	35		Recorded	61
	Error	0		Error	1
35-25-1	Analytical	35	60-35-1	Analytical	60
	Recorded	35		Recorded	60
	Error	0		Error	0
			60-45-1	Analytical	60
				Recorded	60
				Error	0
35-4-2	Analytical	35	60-5-2	Analytical	60
	Recorded	39.5		Recorded	71
	Error	4.5		Error	11
35-10-2	Analytical	35	60-15-2	Analytical	60
	Recorded	36		Recorded	63
	Error	1		Error	3
35-20-2	Analytical	35	60-25-2	Analytical	60
	Recorded	35		Recorded	61
	Error	0		Error	1
35-25-2	Analytical	35	60-35-2	Analytical	60
	Recorded	35		Recorded	60
	Error	0		Error	0
			60-45-2	Analytical	60
				Recorded	60
				Error	0
35-4-3	Analytical	35	60-5-3	Analytical	60
	Recorded	39		Recorded	69
	Error	4		Error	9
35-10-3	Analytical	36.5	60-15-3	Analytical	60
	Recorded	36.5		Recorded	63
	Error	0		Error	3
35-20-3	Analytical	35	60-25-3	Analytical	60
	Recorded	35		Recorded	61

	Error	0		Error	1
35-25-3	Analytical	35	60-35-3	Analytical	60
	Recorded	35		Recorded	60
	Error	0		Error	0
			60-45-3	Analytical	60
				Recorded	60
				Error	0

Having made the necessary adjustments to the analytical force-feel curves, the associated areas and LIs were calculated. The results can be found below in Table 9. Example overlays of the analytical and actual pedal force feel curve can be found in Figure 88.

Table 9. Calculated Linear Index Parameters for the RCSR 2 Force-Feel Curves

Force Curve	F_{lim}	F_{bo}	$\delta_{p\text{-}lim}$	F_{cf}	F_{hb}	A^{**}	B^{**}	C^{**}	$\bar{X}$	A1	A2	A3	LI
#	lb	lb	in	lb	lb	Na	Na	Na	in	in-lb	in-lb	in-lb	NA
35-4-1	39	4	1.2	1	2	1056.3	-1168.1	24.8	1.08	8.9	0.1	46.8	0.81
35-10-1	37	10	1.2	4	2	950.7	-741.1	16.4	0.76	10.8	1.7	44.4	0.72
35-20-1	35	20	1.2	9	2	NA	NA	NA	0.12	11.5	9.8	42.0	0.49
35-25-1	35	25	1.2	11.5	2	NA	NA	NA	0.10	14.4	12.8	42.0	0.35
35-4-2	39.5	4	2.4	1	2	270.9	-595.4	14.6	2.17	18.4	0.2	94.8	0.80
35-10-2	36	10	2.4	4	2	225.0	-344.0	9.7	1.50	21.9	3.5	86.4	0.71
35-20-2	35	20	2.4	9	2	NA	NA	NA	0.24	23.5	19.6	84.0	0.49
35-25-2	35	25	2.4	11.5	2	NA	NA	NA	0.19	29.4	25.5	84.0	0.35
35-4-3	39	4	3.5	1	2	124.2	-396.6	11.0	3.17	26.9	0.3	136.5	0.80
35-10-3	36.5	10	3.5	4	2	108.8	-243.5	8.0	2.21	32.4	5.0	127.8	0.71
35-20-3	35	20	3.5	9	2	NA	NA	NA	0.35	34.5	28.5	122.5	0.49
35-25-3	35	25	3.5	11.5	2	NA	NA	NA	0.28	43.2	37.1	122.5	0.34
60-5-1	68	5	1.2	1.5	2	3211.1	-3590.2	71.3	1.10	14.7	0.2	81.6	0.82
60-15-1	64	15	1.2	6.5	2	2844.4	-2248.1	44.7	0.77	17.9	2.7	76.8	0.73
60-25-1	61	25	1.2	11.5	2	NA	NA	NA	0.10	14.2	13.0	73.2	0.63
60-35-1	60	35	1.2	16.5	2	NA	NA	NA	0.07	20.1	18.9	72.0	0.46
60-45-1	60	45	1.2	21.5	2	NA	NA	NA	0.05	26.0	24.8	72.0	0.30
60-5-2	71	5	2.4	1.5	2	875.2	-1948.6	40.6	2.21	31.4	0.3	170.4	0.81
60-15-	63	15	2.4	6.5	2	689.1	-	23.4	1.54	36.3	5.5	151.2	0.72

2							1073.1						
60-25-2	61	25	2.4	11.5	2	NA	NA	NA	0.19	29.1	25.7	146.4	0.63
60-35-2	60	35	2.4	16.5	2	NA	NA	NA	0.14	41.1	37.6	144.0	0.45
60-45-2	60	45	2.4	21.5	2	NA	NA	NA	0.11	53.0	49.4	144.0	0.29
60-5-3	69	5	3.5	1.5	2	388.7	-1255.9	27.5	3.21	45.1	0.4	241.5	0.81
60-15-3	63	15	3.5	6.5	2	324.0	-734.1	17.2	2.24	53.3	8.0	220.5	0.72
60-25-3	61	25	3.5	11.5	2	NA	NA	NA	0.28	42.9	37.3	213.5	0.62
60-35-3	60	35	3.5	16.5	2	NA	NA	NA	0.20	60.3	54.7	210.0	0.45
60-45-3	60	45	3.5	21.5	2	NA	NA	NA	0.16	77.7	72.0	210.0	0.29

** - Note *A*, *B*, and *C* used for quadratic equation not applicable (NA) for linear force-feel curves.

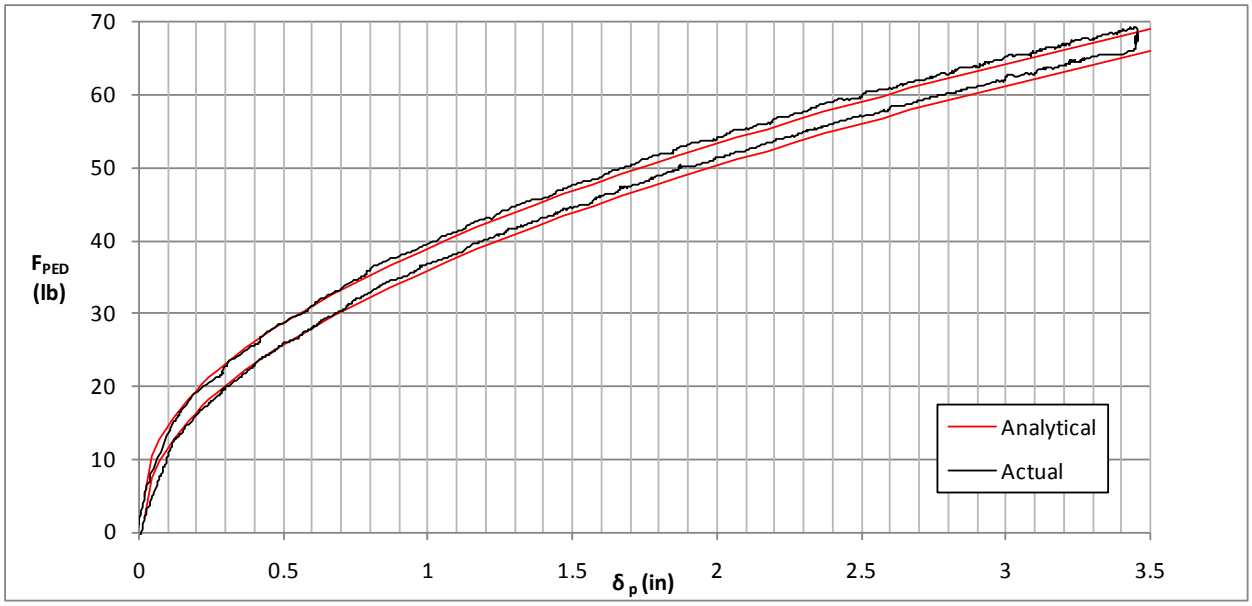

Figure 88. Overlay of Analytical and Actual Force-Feel Curves Used in the RCSR 2 Study

Relationship of Linear Index to F_{bo}/F_{lim}

Another parameter explored in this study was that of the ratio of the breakout force to the limit force $F_{bo} / F_{\lim}$. As it turns out this ratio is closely related to LI. Consider the load-feel curve(60-45-3) shown in Figure 89.

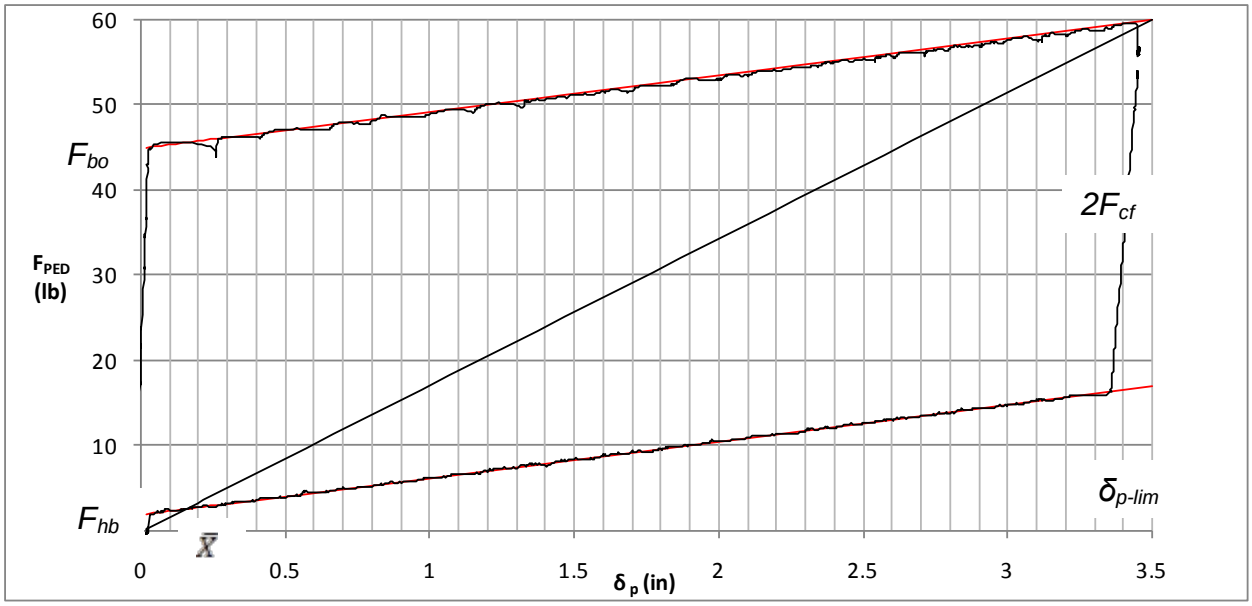

Figure 89. Analytical and Actual Force-Feel Curves of Configuration 60-45-3

Calculation of areas 1, and 2 can be approximated by the areas of a triangle:

$$A_1 = \frac{1}{2} F_{bo} \delta_{p-lim} \qquad \text{Equation (F-9)}$$

$$A_2 = \frac{1}{2}(2F_{cf})(\delta_{p-lim} - \bar{X}) \qquad \text{Equation (F-10)}$$

Area 3 for this configuration is calculated as:

$$A_3 = F_{cf} \delta_{p-lim} \qquad \text{Equation (F-11)}$$

Calculation of LI then becomes:

$$LI = 1 - \frac{\frac{1}{2}F_{bo}\delta_{p-lim} + \frac{1}{2}(2F_{cf})(\delta_{p-lim} - \bar{X})}{F_{lim}\delta_{p-lim}} \qquad \text{Equation (F-12)}$$

For all of the current study configurations the following was true:

$$F_{bo} = 2F_{cf} + F_{hb} \qquad \text{Equation (F-13)}$$

With the approximation of LI becoming:

$$LI = 1 - \frac{\frac{1}{2}F_{bo}\delta_{p-lim} + \frac{1}{2}(F_{bo} - F_{hb})(\delta_{p-lim} - \bar{X})}{F_{lim}\delta_{p-lim}} \qquad \text{Equation (F-14)}$$

Which then reduces to:

$$LI = 1 - \frac{F_{bo}}{F_{lim}} + \frac{F_{hb}}{2F_{lim}} + \frac{\bar{x}}{2\delta_{p-lim}}\left(\frac{F_{bo}}{F_{lim}} - \frac{F_{hb}}{F_{lim}}\right)$$ Equation (F-15)

For the tested configurations in this study the ratio $\frac{F_{bo}}{F_{lim}}$ was the dominant term, resulting in an approximation of LI as:

$$LI \sim 1 - \frac{F_{bo}}{F_{lim}}$$ Equation (F-16)

As can be seen in Figure 90, the calculated and approximated values of LI are in close agreement for all the tested configurations.

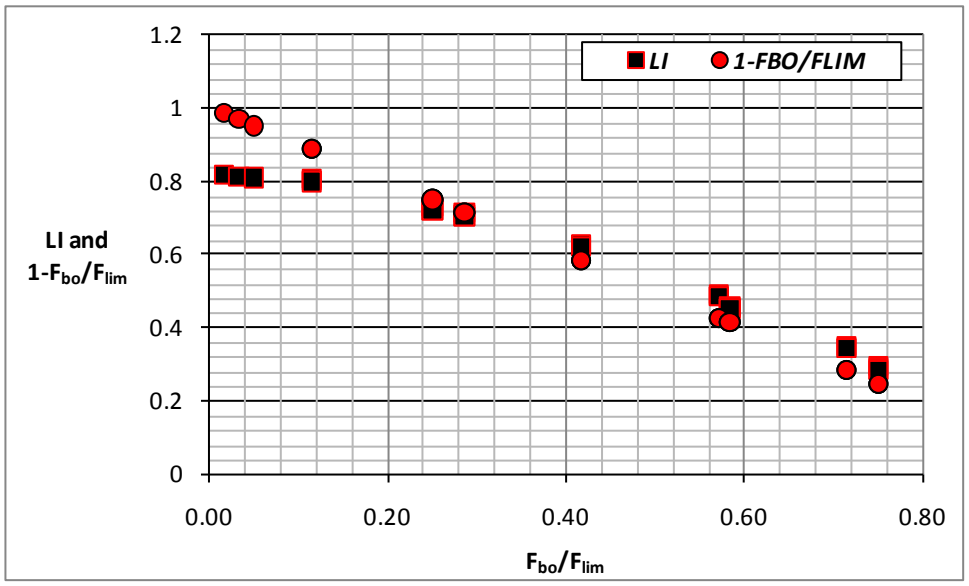

Figure 90. Comparison of LI and Approximation From F_{bo}/F_{lim}

Both $F_{bo} / F_{\lim}$ and LI were considered as candidate metrics for an overcontrol criterion. As shown by equation F-16 and Figure 90, these parameters turn out to be very closely correlated. Nonetheless, both were tested against the simulation data with the results shown in Section 5.3. As expected, both parameters showed essentially identical trends. Neither parameter was sensitive to overcontrol tendency or to maximum force imposed on the vertical stabilizer, and they were therefore rejected as potential criterion parameters.

This analysis shows that for load-feel curves that have the characteristics of those used in this simulation (which is representative of essentially all transport aircraft), $F_{bo} / F_{\lim}$ and LI may be used interchangeably.

APPENDIX G MATLAB SIMULINK MODEL

In order to investigate how changes in yaw damper performance could affect experimental metrics the lateral/directional equations of motion for a transport aircraft were modeled in Simulink®. The transport aircraft model used was the Convair CV-880M (Figure 91). Derivatives and mass properties were obtained from reference *8*. The chosen flight condition was cruise at 23000 ft, M = 0.6 (615 ft/s). The state-space equations of motion can be found in the Code Listing below.

Figure 91. Convair CV-880M Transport

Code Listing

```
% Convair 880M Lateral Directional Derivatives
% From Hefley, pp 205
g       = 32.2;
VT0     = 615;
U0      = VT0*cos(5.3/57.3);
W0      = U0*sin(5.3/57.3);
alpha0  = (5.3)/57.3;
Yv      = -0.115;
Yp      = 0;
Yr      = 0;
Lbeta_p = -5.98;
Lp_p    = -1.14;
Lr_p    = 0.434;
Nbeta_p = 1.42;
Np_p    = -0.0416;
Nr_p    = -0.188;
YdeltaR = 0.0245;
YdeltaA = -0.00458;
LdeltaR = 0.806;
LdeltaA = 2.85;
NdeltaR = -0.926;
NdeltaA = 0.23;

lz      = 0;
lx      = 0;
KTC     = 0.1/57.3;
KAY     = (0.09)/57.3;
KBD     = (1.30);%/57.3;
gct     = g*cos(alpha0);


dplim   = 1.2;
drlim   = 9/57.3;
KPED    = drlim/dplim;
```

```
A = [   Yv                  (W0-Yp)/VT0        (-U0+Yr)/VT0*cos(alpha0)       g*cos(alpha0)/VT0   ;
        Lbeta_p             Lp_p                        Lr_p                          0                 ;
        Nbeta_p             Np_p                        Nr_p                          0                 ;
        0                   1                           tan(alpha0)                   0                ];


B = [   YdeltaA             YdeltaR                     0;
        LdeltaA             LdeltaR                     Lp_p;
        NdeltaA             NdeltaR                     0;
        0                   0                           0];

C = [   1           0           0       0;
        0           1           0       0;
        0           0           1       0;
        0           0           0       1;
        Yv                  (W0-Yp)/VT0                 (-U0+Yr)/VT0*cos(alpha0)       g*cos(alpha0)/VT0 ;
        Lbeta_p             Lp_p                        Lr_p                          0                 ;
        Nbeta_p             Np_p                        Nr_p                          0                ];
D = [   0           0       0;
        0           0       0;
        0           0       0;
        0           0       0;
        YdeltaA             YdeltaR         0;
        LdeltaA             LdeltaR         0;
        NdeltaA             NdeltaR         0];
states = {  'beta';
            'p';
            'r';
            'phi'};
inputs = {  'a';
            'r'
            'pg'};
CON880M = ss(A,B,C,D,'StateName',states,'InputName',inputs);
[num1 den1] = ss2tf(A,B,C,D,1);
[num2 den1] = ss2tf(A,B,C,D,2);

betada = tf(num1(1,:),den1);
pda    = tf(num1(2,:),den1);
rda  = tf(num1(3,:),den1);
phida  = tf(num1(4,:),den1);
frees  = tf([1 0],1);

ayda   = VT0*frees*betada-W0*pda+U0*rda-g*cos(alpha0)*phida;
```

The documented CV-880M model was augmented with an identical yaw damper as used in the simulation trials.

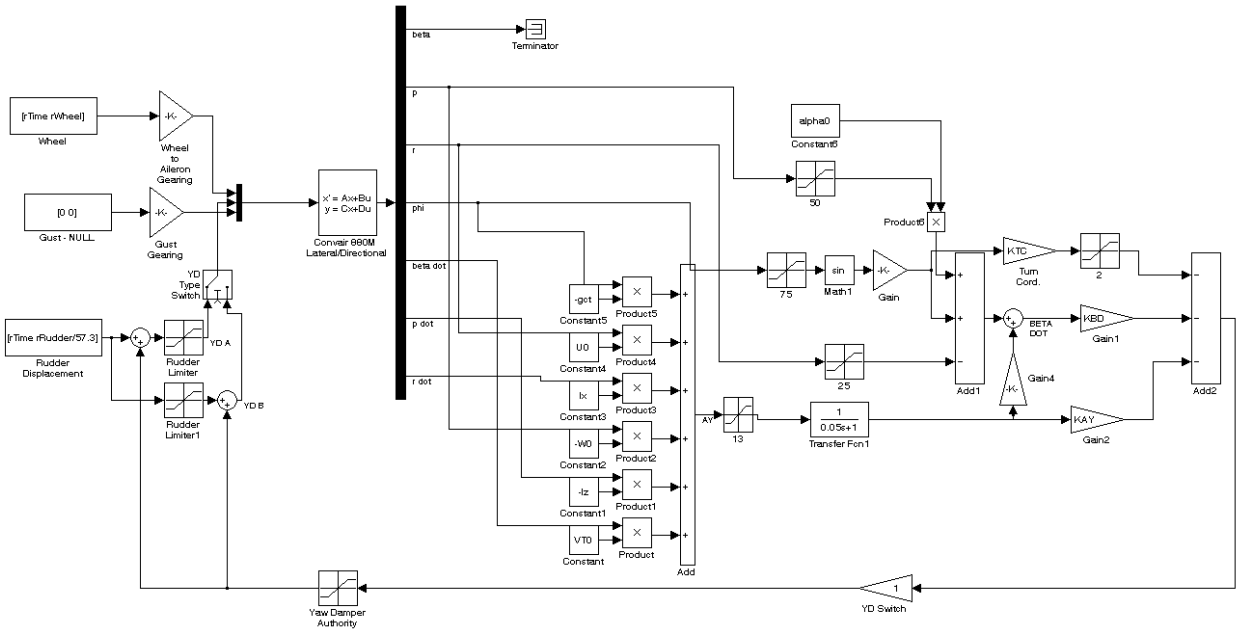

Figure 92. Lateral Directional CV-880M SIMULINK Model

REFERENCES

1 Hoh, Roger H., Thomas K. Nicoll, and Paul Desrochers, "Piloted Simulation Study to Develop Transport Aircraft Rudder Control System Requirements – Phase 1 – Determine Simulator Motion Requirements and Initial Results", HAI Technical Report 1137-1, July 31, 2006.

2 Hoh, Roger H., "Simulation Test Plan to Develop Transport Aircraft Rudder Control System Requirements – Phase 2 – Criteria Development", HAI Technical Report 1137-2, July 31, 2006.

3 Anon, "In-flight Separation of Vertical Stabilizer American Airlines Flight 587 Airbus Industrie A300-605R", N14053 Belle Harbor, New York November 12, 2001, NTSB/AAR-0404, PB2004-910404, Notation 7439B, October 12, 2004

4 Lee, B, and V. Rodchenko, et. al., "Effect of Pedal Feel System Characteristics on Aircraft HQ", Proceedings of AIAA Atmospheric Flight Mechanics Conference, 15–18 August, 2005, San Francisco, CA, AIAA 2005-6034

5 Callaghan, John O, "Flight Control and Wake Turbulence Effects on American Airlines Flight 587", Proceedings of AIAA Modeling and Simulation Technologies Conference, 15- 18 August 2005, San Francisco, CA AIAA 2005-6110

6 Hess, Ronald A. "Rudder Control Strategies and Force/Feel System Designs in Transport Aircraft". *Journal of Guidance, Control, and Dynamics*, Vol 28 Number 6, Pages 1251-1262, Dec 2005

7 Hess, Ronald A. "Preliminary Assessment of Design Metrics for Transport Aircraft Rudder Control Systems". A Presentation at NASA Langley

8 Hefley, Robert K. and Wayne F. Jewell. Aircraft Handling Qualities Data. STI Technical Report 1004-1. May 1972.